Mémoire

Auteur : Verwilghen, Pierrick
Promoteur(s) : Pinçon, Charly; Dupret, Marc-Antoine
Faculté : Faculté des Sciences
Diplôme : Master en sciences spatiales, à finalité approfondie
Année académique : 2020-2021
URI/URL : http://hdl.handle.net/2268.2/12746

AGO

Department of Astrophysics, Geophysics and Oceanography

Modelling the Shear Layer Oscillation and its impact on the rotation of low-mass stars

A thesis carried out in the frame of the Master in Space Sciences 2020-2021

Author: **Pierrick Verwilghen**

Supervisors: **Charly Pinçon** - **Prof. Marc-Antoine Dupret**

Remerciements

Je tiens tout d'abord à remercier sincèrement M. Dupret et Charly Pinçon qui ont pu se rendre extrêmement disponible afin de m'aider à réaliser ce travail. Chaque fois que j'ai eu besoin de leur conseils aussi bien pour les diverses questions que je me suis posées que pour la rédaction du mémoire, ils ont su répondre présents jusqu'au bout malgré les nombreux obstacles qui se sont dressés devant nous durant cette année académique (coronavirus, inondations, etc). J'en profite également pour les remercier une fois de plus (ainsi que tous les professeurs qui m'ont soutenu au travers de leurs lettres de recommandation) de m'avoir encouragé et aidé dans la recherche d'un doctorat que j'ai finalement réussi à décrocher à l'ESO en Allemagne.

Ensuite, mes pensées se tournent vers mes amis et camarades de classe pour qui cette année (et le master en règle générale) aura été loin d'être simple puisqu'il aura fallu qu'on passe tous une bonne partie du temps derrière un écran d'ordinateur pour pouvoir suivre les cours. Je les remercie car malgré la distance, les nombreuses discussions que nous avons pu avoir ainsi que leur réconfort m'a toujours été d'une grande aide tout au long de cette année.

Finalement, je ne peux évidement pas écrire tous ces remerciements sans évoquer ma famille. Elle qui, depuis toutes ces années, me supporte dans mes études et dans mes choix. Voilà pourquoi j'adresse un immense merci à mes parents, mon frère et ma soeur pour le réconfort et le soutien qu'ils ont pu m'apporter tout au long de mon parcours universitaire y compris lors de la rédaction de ce travail.

Contents

Project objectives

Stars are non-static celestial objects constantly evolving and ruled by the hydrodynamics laws. Throughout the last decades, thanks to the satellites SoHO (1995), CoRoT (2006-2014), *Kepler* (2009), etc., the advent of asteroseismology has enabled us to probe their hidden structure for the first time. Asteroseismology is an observational method which studies the interior of stars through analyzing their oscillations. Indeed, the various dynamical phenomena acting within these objects can generate waves whose spectrum depends on the properties of the stellar structure. In particular, the available asteroseismic data have put stringent constraints on the core rotation angular frequencies of the Sun and thousands of distant low-mass stars (i.e. with masses between about 1 and 2 solar masses), as well as raised a lot of questions.

The rotation of stars is a very large subject because it acts during all their life and plays an active role in their evolution. For instance, the rotation can induce chemical elements transport that can supply nuclear regions in hydrogen, and thus significantly impact the main sequence duration. However, several studies have shown that our current stellar evolution models predict core rotation angular frequencies much higher than those measured in low-mass stars. Such discrepancy demonstrates that an efficient process of angular momentum transport is able to extract some angular momentum from the core towards the surface and slow down the core rotation in these stars, and that this process has to be included in stellar models. Today, the issue of the angular momentum transport in stars is one of the hottest topics of stellar physics and remains an open question.

Two main hypotheses have been discussed about the missing transport mechanism. The first one is the transport by internal magnetic fields generated by dynamo effect. This process can reduce the discrepancy between observations and theory on the main sequence, but still remains insufficient to slow down the core rotation of more evolved stars. The second one is the transport by internal gravity waves. Many studies have already been conducted about the angular momentum transport by internal gravity waves and all these works still show nowadays that this process is a serious contender to explain the slowdown of the core rotation rates during the lifetime of stars. Internal gravity waves have buoyancy as the restoring force. They are generated by turbulent motions in the convective zones of stars and can propagate in the radiative layers. There, these waves are damped by radiative diffusion and can not only deposit but also extract angular momentum into the medium; they can thus locally modify the internal rotation. In particular, they can drive an oscillation of the internal rotation profile in a very thin layer at the top of the radiative zone, the so-called Shear Layer Oscillation (SLO). The SLO actually results from the competition between the transport by waves and the instabilities induced by the shear in the rotation profile. The cycle period of the SLO in the Sun is estimated to be of the order of the year, which is much smaller than the time scales of stellar evolution (several billions of years). The difference between these

two time scales makes difficult the inclusion of the transport by waves in stellar evolution codes (e.g., numerical issues concerning the temporal step to use). This mainly explains why most of the previous studies on the transport by internal gravity waves did not properly take the effect of the SLO into account. Currently, the scientific community wonders how the SLO can affect the long-term evolution of the rotation of stars. For instance, it is known that the SLO can filter the wave flux of angular momentum that is transmitted towards the center of stars, but it is not clear how this can influence the evolution of the stellar core rotation.

Within this context, the goal of this work is to study the SLO in more details. To do so, the main task will consist in modelling in a simple way the interaction between internal gravity waves, shear-induced turbulence and rotation in a thin stably-stratified radiative layer. In the considered configuration, internal gravity waves are supposed to be emitted at the upper boundary, corresponding to the interface with an adjacent convective zone. Using a two-dimensional plane parallel assumption, the laws of hydrodynamics will be rewritten according to the mean flow theory. In this approach, the physical quantities are decomposed into an Eulerian mean slowly evolving with time (e.g., the mean flow representing the rotation) and a small perturbation rapidly evolving with time (i.e., the waves), and the evolution equations are deduced for each component. The usual short-wavelength solutions for the linear internal gravity waves propagating in a slowly varying medium will be exploited to express analytically the wave fluxes. These expressions will thus be used in a second step to solve numerically the temporal evolution of the mean flow and the SLO. In order to simplify the physical interpretations of the result, a dimensionless version of the transport equation will be used as well as a unique frequency for the waves. This will allow us to explicitly express the problem as a function of a couple of relevant dimensionless free parameters. By varying these parameters, we will subsequently study the conditions of the appearance and the main properties of the SLO. In addition, a stationary solution will be studied to extract a part of the main properties of the SLO. This work is a preliminary step in the investigation that will permit in the future to propose simple prescriptions easily implementable in stellar evolution codes and describing the effect of the SLO on the rotation of the core on time scales corresponding to the lifetime of stars.

Chapter 1

Introduction

Before getting to the heart of this work, we will first introduce in the next sections fundamental concepts about stellar structure and evolution and the impact of stellar rotation. Then, we will present the different asteroseismic outcomes that have raised the issue of the angular momentum redistribution in stellar interiors. This chapter will end by the introduction of the different studies carried out on the angular momentum transport by internal gravity waves, the SLO and the physical principles hidden behind.

1.1 A brief word about stellar structure and evolution

This section aims at reminding the main characteristics and fundamental concepts of stars and more specifically of Sun-like stars such as their structure equations and their evolution.

Stars stem from the gravitational collapse of molecular clouds. This collapse occurs on a time scale given by the dynamic time (or the free fall time) obtained by keeping only the gravitational force in the Newton's equation (i.e. neglecting the pressure forces of the gas):

$$t_{dyn} \sim \sqrt{\frac{R^3}{GM}} \tag{1.1}$$

where M and R are the initial mass and radius of the molecular cloud, respectively. In the case of a molecular cloud having a mass of 10,000 $M_\odot$ and a radius of 10 parsecs, the corresponding dynamic time is about 4.5 million years. During this collapse, the giant molecular condensate fragments in smaller and smaller clouds until a quasi hydrostatic balance between the gas pressure and the gravitational force is reached: the new celestial object formed is called a protostar. The basic evolution of this celestial object can then be described by the standard model of stellar structure and evolution. In this model, stars are described as non-rotating spheres of plasma in hydrostatic equilibrium. The transport of energy is ensured by radiation and convection. The set of equations

is thus provided by:

$$\text{(Conservation of mass)} : \frac{dm}{dr} = 4\pi r^2 \rho, \tag{1.2a}$$

$$\text{(Hydrostatic equilibrium)} : \frac{dP}{dr} = -\rho \frac{Gm}{r^2}, \tag{1.2b}$$

$$\text{(Energy transport by radiation)} : \frac{dT}{dr} = -\frac{3\kappa\rho L}{16\pi a c r^2 T^3}, \tag{1.2c}$$

$$\text{(Conservation of energy)} : \frac{dL}{dr} = 4\pi r^2 \rho(\epsilon_n - T\frac{ds}{dt}). \tag{1.2d}$$

The transport of energy by convection is much more complicated to model and the approximate Mixing-Length Theory (MLT) is generally used for this purpose. In the latter system, m is the mass of a sphere of gas having a radius r with r the radial coordinate increasing from the center towards the surface. The letter G represents the Cavendish constant [1]. The thermodynamical variables ρ, T and P are the density, the temperature and the pressure, respectively. The specific entropy is given by s. The quantity c is the speed of light in vacuum [2], κ is the Rosseland mean opacity, L is the luminosity, ϵ_n and $-Tds/dt$ (denoted ϵ_{grav}) are the specific nuclear and gravitational energy production rates per unit of time, respectively. This system must be completed by an equation of state linking the thermodynamical variables ρ, T and P, as well as the set of equations describing the temporal evolution of the chemical composition caused by the creation or the destruction of elements during the fusion reactions. It is important to note that the temporal evolution of this system comes either from the thermal disequilibrium ($-Tds/dt$) or from the evolution of the chemical composition due to nuclear reactions when the star is in thermal equilibrium. Finally, appropriate initial and boundary conditions (i.e., at the center and at the surface in connection with stellar atmosphere) have to be applied.

The standard model enables us to describe the general phases of stellar evolution. For the sake of convenience, the stellar evolution is usually represented in the Herzsprung-Russel (HR) diagram. Indeed, celestial objects and more specifically stars can be classified as a function of their surface stellar luminosity $L_\star$ and their surface effective temperature T_{eff}, which continuously evolve during the lifetime of stars. For instance, the evolution track of the Sun in the HR diagram is plotted in the figure 1.1 and we can see that it can be split into several stages. Of course, the evolution track in the HR diagram also depends on the stellar mass. Moreover, it is also possible to plot the stellar radius in this diagram using the relation:

$$L_\star = 4\pi R^2 \sigma T_{eff}^4 \tag{1.3}$$

where R is the stellar radius and σ is the Steffan-Boltzmann constant[3]. The equation of the curves having a constant radius in the HR diagram is obtained by taking the logarithm of the latter equation. This equation is given by the following expression:

$$\log(L_\star) = 4\log(T_{eff}) + 2\log(R) + \log(4\pi\sigma) \tag{1.4}$$

The curves having a constant radius are thus straight lines in the HR diagram, as shown in dotted lines in the figure 1.1.

[1] $G \approx 6.67 \times 10^{-11}\ m^3.kg^{-1}.s^{-2}$
[2] $c = 299,792,458\ m.s^{-1}$
[3] $\sigma \approx 5.670 \times 10^{-8}$ W.m^{-2}.K^{-4}

About 4.5 million years after the beginning of the collapse of the progenitor cloud, the proto-Sun will first start evolving on the Hayashi track in the Hertzsprung-Russell diagram of the figure 1.1 (orange curve). At this stage, the central temperature is too low to trigger the hydrogen fusion and the luminosity of the protostar mainly results from the energy released by the gravitational contraction. The internal structure is totally convective. The time scale on which a star will radiate if the only source of energy is the gravitational energy is called the Kelvin-Helmholtz time and is provided by the ratio between the total content of gravitational energy that can be released during the contraction and the luminosity of the star. According to the Virial theorem, half of the released gravitational potential energy is converted into internal energy and the other half is radiated by the star. This theorem allows us to estimate the Kelvin-Helmholtz time, which is given by:

$$t_{KH} \sim \frac{GM^2}{2RL} \tag{1.5}$$

For instance, the characteristic Kelvin-Helmholtz time for a proto-Sun is of the order of several tens of millions of years. This corresponds to the characteristic time required for a protostar to reach the main sequence. Indeed, during the contraction phase, the pressure and the temperature of the core are progressively increasing. At one moment (purple curve in the figure 1.1), this results in the appearance of a radiative core as well as the ignition of the first nuclear reactions (the little hook just before the beginning of the main sequence). When the core temperature is sufficient ($T_{core} \approx 10^7 K$), the nuclear fusion of the hydrogen into helium via the pp-chain is sustained. The star thus begins its evolution on the main sequence (green curve in the figure 1.1). This phase is the longest in the life of stars and an approximation of the corresponding time duration is given by the nuclear time:

$$t_{nuc} \sim \frac{1}{L_\odot} \frac{0.1 M_\odot}{4 M_H} \Delta E_{reaction} \tag{1.6}$$

where $L_\odot$ [4] is the luminosity of the Sun, $M_\odot$ [5] is the mass of the Sun, M_H [6] is the mass of the hydrogen atom and $\Delta E_{reaction}$ [7] is the amount of energy released by the nuclear fusion of hydrogen into helium. This characteristic time is obtained by the following reasoning: we know that this characteristic time is given by the ratio between the total energy released by the nuclear reactions and the luminosity of the Sun. If we consider that 10% of the mass of the Sun is converted into helium and that one needs four atoms of hydrogen to form one atom of helium, then the total number of reactions is given by $\frac{0.1 M_\odot}{4 M_H}$. Finally, the total energy released is equal to the number of reactions multiplied by the energy released by one reaction $\Delta E_{reaction}$. Replacing the numerical values in this expression gives a characteristic nuclear time of the order of 10^{17} s, which corresponds more or less to 10 billion years. During all this time on the main sequence, the energy released by the nuclear reactions (Eq. 1.2d) in the central layers is carried towards the surface thanks to radiative diffusion in a inner region (Eq. 1.2c) and by convection in the envelope, as shown by the figure 1.2. Furthermore, the dynamics and the thermal times introduced above can also be computed in the case of the Sun. These two characteristic times can be computed as:

$$t_{dyn} \approx 10 \text{ min} \quad \text{and} \quad t_{KH} \approx 10 \text{ million years} \tag{1.7}$$

The dynamical time gives an idea on the time of structural readjustment with respect to the hydrostatic equilibrium. This time scale corresponds to the typical period of an acoustic wave

[4] $L_\odot \approx 3 \times 10^{26}$ W
[5] $M_\odot \approx 2 \times 10^{30}$ Kg
[6] $M_H \approx 1.67 \times 10^{-27}$ Kg
[7] $\Delta E_{reaction} \approx 4.118 \times 10^{-12}$ J

propagating inside the star. In the Sun, we see that:

$$t_{dyn} \lll t_{KH} \ll t_{nuc} \tag{1.8}$$

so that we check that the quasi-static hydrostatic equilibrium is verified. This actually holds true during the whole life of stars, either during gravitational contraction phases (because $t_{dyn} \ll t_{KH}$) or during nuclear phases (because $t_{dyn} \ll t_{nuc}$). Moreover, since $t_{KH} \ll t_{nuc}$, it is also clear that the lifetime of stars strongly depends on the duration of the main sequence and thus, the time during which the nuclear reactions are sustained in the core, which depends on the nuclear reaction rates and the quantity of hydrogen available. The latter relation has also as a consequence that the Sun remains in thermal equilibrium during the main sequence.

After the main sequence, the internal structure is composed of an helium core surrounded by an hydrogen burning shell. From this stage, different fates await stars in function of their masses. In the case of the Sun, its evolution will lead it to climb along the Giant branch (red curve in figure 1.1) and to become larger and brighter. At one moment, it will undergo an helium flash due to the starting of helium burning in a degenerated helium core. Then, when the whole helium in the core will be converted into carbon and oxygen, an helium shell burning will surround the C-O core in addition of the hydrogen shell. Finally, due to instabilites between the H and He shells, the Sun will progressively expel its envelope (through thermal pulses), thus forming a planetary nebulae with in its center a celestial body called white dwarf.

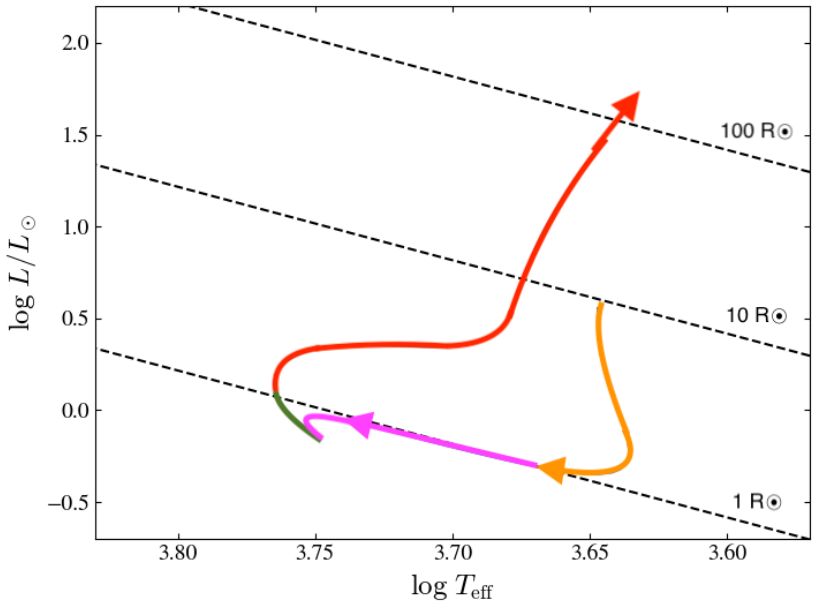

Figure 1.1 – Evolution of the Sun in the Hertzsprung-Russell diagram. The colors represent the different stages of its evolution. The time scale is not included but the range goes from 3 million to 13 billion years. The orange curve shows the Hayashi track (protostar phase). The purple curve represents an adjustment occurring just before the ignition of hydrogen fusion reactions. The green curve represents the main sequence until now (hydrogen burning phase). Finally, the red curve shows the track towards the red giant phase.

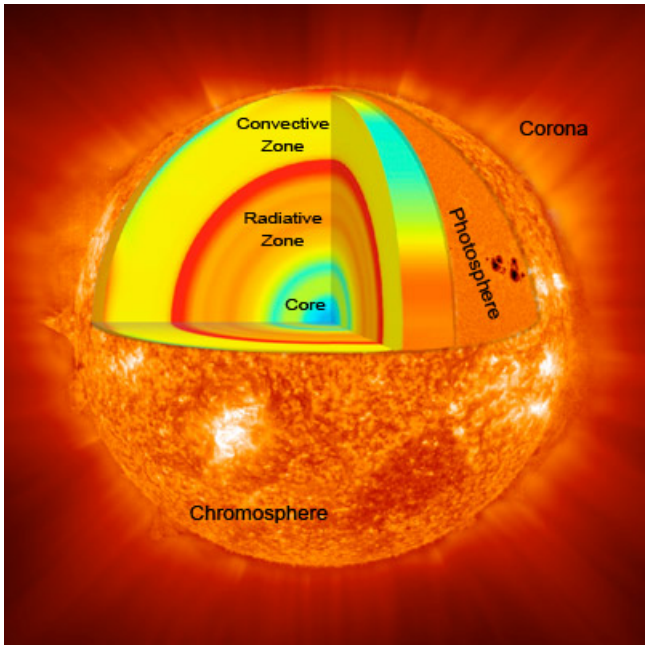

Figure 1.2 – Schematic view of the internal structure of the Sun. Credit: SOHO (ESA & NASA) Site : https://scied.ucar.edu/sun-regions

1.2 What about the rotation?

If we want to describe more precisely what a star is, we have to include rotation in stellar models. Indeed, the initial molecular cloud has already a non-zero angular momentum. During its collapse, the angular momentum of the cloud will be conserved and will be transferred to the newly formed protostar. Then, the protostar will evolve on the Hayashi track and will lose a significant part of its angular momentum through its interaction with its accretion disk. It will finally reach the main sequence with an internal rotation profile resulting from its past history and an induced global internal transport dynamics. It is important to mention that including the rotation in the problem makes it much more complex. Indeed, the set of Eqs. 1.2a - 1.2d considers the spherical symmetry with only one variable which is the radial coordinate r. Nevertheless, taking into account the rotation breaks this symmetry since the centrifugal acceleration deforms the star (i.e., with an oblate shape, flattened at the poles and enlarged at the equator). This new axisymmetric configuration requires to describe the structure in two dimensions as a function of the radial coordinate r and the latitudinal coordinate θ, which makes the set of equations much harder to solve.

Hopefully, for rotating stars having a low rotation frequency such as the Sun, the effects induced by the rotation can be treated as small perturbations with respect to the spherical hydrostatic equilibrium. In such a case, the rotation is said 'shellular' and depends on the radial coordinate r at the dominant order, with small deviations in the latitudinal direction (e.g., Zahn 1992). In fact, it would be more appropriate to say that the problem becomes a 1.5D problem, which can be solved more easily than a 2D one. In such picture, two new transport mechanisms are included in the modelling, which are shear-induced turbulence and meridional circulation. First, the turbulence arises from the instabilities due to strong gradients associated with differential rotation in the flow that generate eddies. The transport and the mixing induced by these eddies are usually modelled by a diffusion process associated with an effective turbulent viscosity. This concept of effective

viscosity will be developed in more details in Chapter 3. Second, the meridional circulation is described as huge current loops crossing the different regions of the star as shown by the figure 1.3. This comes from the fact that a rotating radiative shell cannot be in thermal equilibrium (i.e. the divergence of the heat flux does not vanish). In order to keep the heat conservation, the only solution is to generate current loops that advect the entropy throughout the star in such a way that the energy produced by nuclear reactions is exactly balanced by the energy radiated by the star.

These rotation-induced processes allow to mix the chemical elements in different layers and redistribute angular momentum throughout the star. Therefore, they can significantly modify the properties of stars, as shown by the figure 1.4. In the latter, we see that the evolution track of a Sun-like star during the main sequence well differs with and without rotation in a HR diagram. This observed shift is for instance mainly due to a higher helium abundance in the envelope of stars when considering rotation (Eggenberger 2013). Furthermore, turbulent diffusion and meridional circulation can also supply more hydrogen in the nuclear core of such stars and allows them to stay a longer period on the main sequence by increasing the nuclear time t_{nuc}. This shows that it is of paramount importance to take the effects of the rotation into account, for instance to age stars. The accurate knowledge of the age of stars is crucial to determine the past evolution of certain regions of our galaxy such as the bulb or the galactic disc. Knowing with accuracy the age of stars is also important in exoplanetology because the determination of the age of an exoplanet requires the determination of the age of its host star.

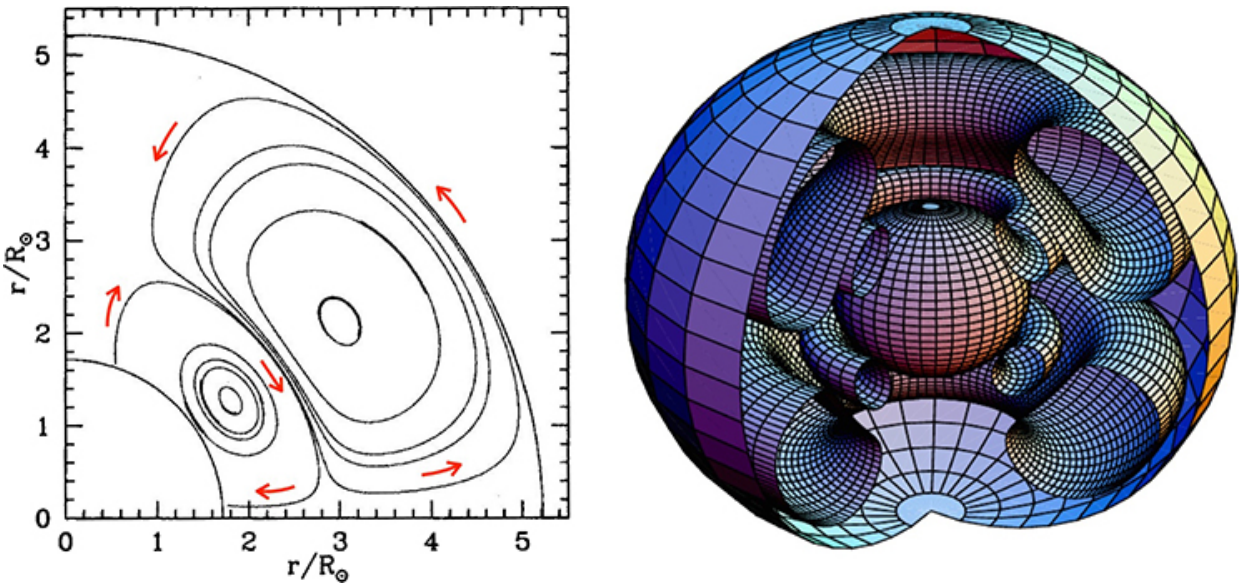

Figure 1.3 – Representation of meridional circulation stream lines in a $20M_{\odot}$ main sequence star (Maeder 2009).

1.3 Issue of the angular momentum redistribution

Seismic data collected by the satellites SoHO, CoRoT and *Kepler* have allowed us to probe with a great accuracy the internal rotation of thousands of stars going from the main sequence to the

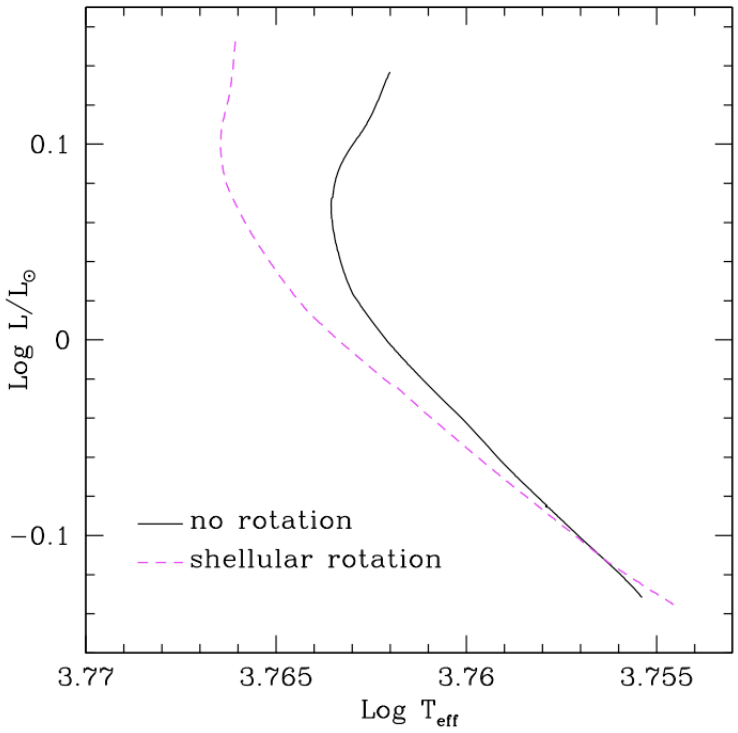

Figure 1.4 – Representation of the evolution on the main sequence of a Sun-like star with and without rotation. We clearly see the difference of the track and the effects on the luminosity and on the effective temperature induced by the rotation (Eggenberger 2013).

red giant branch. In this section, we briefly give an overview of the main results.

First, in the Sun, the observed internal rotation profile is displayed in the figure 1.5 (e.g., García et al. 2007). We see that, in the convective zone ($r \gtrsim 0.7R_\odot$), the rotation frequency depends on the colatitude. The values observed are in line with the observations of the movements of solar spots at the surface of the Sun. In contrast, in the inner radiative zone, we can see that the rotation is almost radially uniform (i.e., for $0.2R_\odot \lesssim r \lesssim 0.6R_\odot$). During the main sequence, the core contracts due to the increase of the mean molecular weight and therefore, the envelope must expand due to the temperature control by nuclear reactions. If the local conservation of the angular momentum was preserved during the past history of the Sun, we should observe a much higher rotation rate in the radiative layers than in the convective envelope, which is not what we observe in the Sun. These observations are thus in disagreement with the local conservation of angular momentum and imply angular momentum redistribution. We note that below this limit, the modes are not able to provide us with information about the rotation profile because the oscillation modes observed in the Sun are pressure modes [8] that mostly propagate in the envelope and thus do not permit to probe deeper than 0.2 $R_\odot$. We mention that gravity modes [9] might help us to probe the deep layers of the Sun (below 0.2 $R_\odot$) since these modes can propagate in the core. However, gravity modes have never been observed yet in the Sun. We note that low rotation contrasts between the core and the surface were also observed in other dozens of main-sequence

[8]Pressure modes are stationary waves with pressure gradient as the restoring force.
[9]Gravity modes are stationary waves with buoyancy as the restoring force.

stars studied by the satellites CoRoT and *Kepler* (e.g., Benomar et al. 2015; Nielsen et al. 2014) demonstrating that the Sun is not an isolated case.

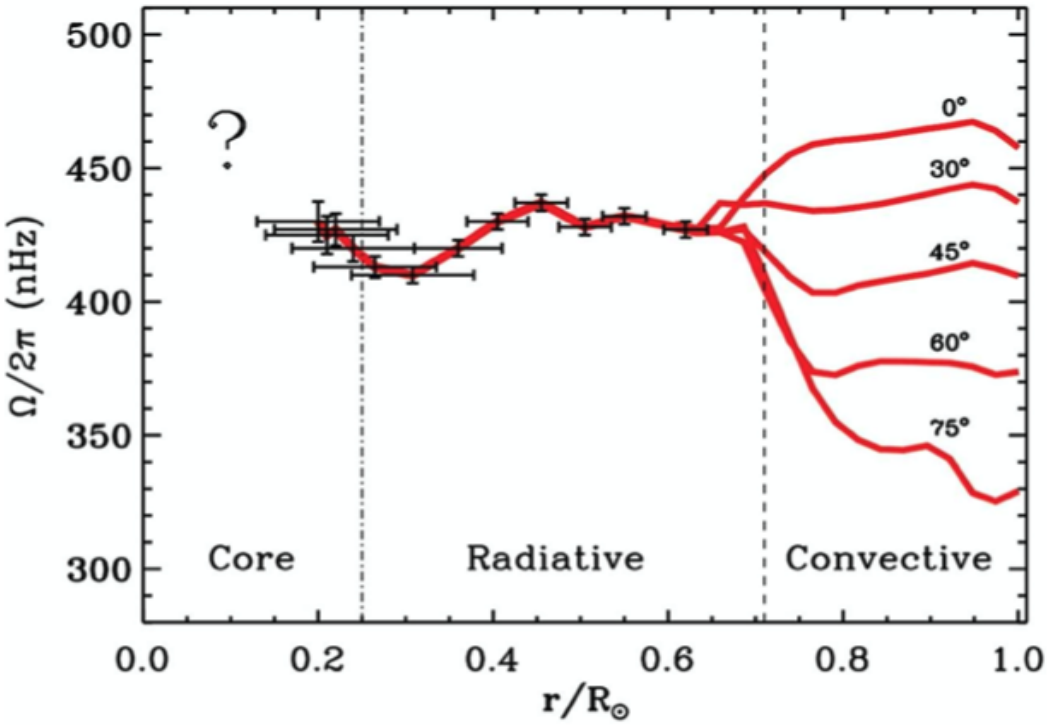

Figure 1.5 – The internal rotation frequency of the Sun as a function of the distance to the center normalized by the solar radius. In the convective zone, the differential rotation depends not only on the distance but also on the colatitude. In the radiative zone, the rotation is mainly radial (García et al. 2007).

Second, the seismic observations also brought a lot of constraints on the evolution of the internal rotation of post-main sequence stars. Indeed, thanks to the precision reached by the satellite *Kepler*, the eigenfrequencies of mixed modes [10] permitted us to probe the deep layers of the core of these evolved stars, whose properties are inaccessible on the main sequence (because mixed modes have not been detected yet in main sequence stars). The study of the mixed modes in red giants carried out by e.g. Mosser et al. (2012) allowed us to obtain for the first time an overview on the evolution of the rotation for the advanced evolving stages as shown in the figure 1.6. This figure shows us the average rotation speed of the central layers for thousands of stars going from the beginning of the giants branch to the red clump (i.e., stars with an helium burning core). During these evolved stages, the central layers are contracting while the envelope expands. In the figure 1.6, the stellar radius in the abscissa thus gives an information on the evolutionary stage. We observe that the rotation frequencies of the core remain quasi constant with evolution while the core is contracting. Once again, this is in disagreement with the local conservation of

[10]Mixed modes can propagate in the core and in the envelope. Their peculiarity is that in the core, they behave as gravity modes and as pressure modes in the envelope. Both cavities communicate through a tunneling effect because they are coupled by an evanescent zone where modes show an exponential behavior. These modes are very important because they have significant amplitudes at the surface and in the core and therefore allow to probe the deep layers of the core.

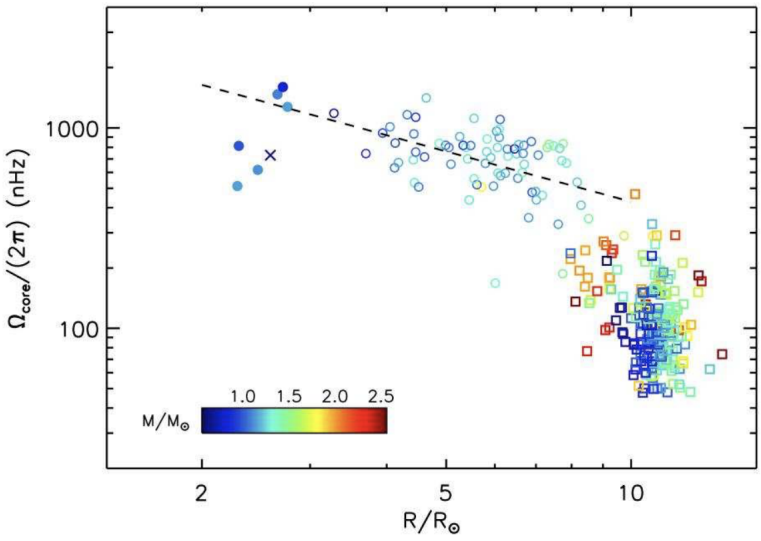

Figure 1.6 – Average core rotation of hundreds of stars located on the subgiants branch (filled circles and crosses), on the red giants branch (empty circles) and on the clump (squares) as a function of the seismic radius and normalized by the solar radius $R_\odot$. The color shows the stellar mass.

angular momentum. According to Mosser et al. (2012), in the case of red clump stars, the slow-down of the core rotation can be partially explained by many structural changes undergone by these stars after the ignition of the helium fusion and, more precisely, by the core radius expansion, but this effect does not seem to be sufficient in order to explain these low rotation frequencies.

Whether it be for main sequence stars or for evolved ones, all these seismic observations show the existence of a process able to extract some angular momentum from the core towards the surface, which could counteract the acceleration of the rotation due to the contraction of the central layers. Nevertheless, previous studies showed that considering only angular momentum transport by the meridional circulation and turbulence is far from being sufficient for main sequence stars (e.g., Amard et al. 2016) and also red giant stars. An idea of the discrepancy between our models and the observations for a red giant star is shown in the figure 1.7. In the latter, we see the result of the modelling of the star rotation profile KIC 7341231 obtained by considering only the meridional circulation as well as the turbulence induced by shearing. Two additional hypotheses were followed during the simulation. The first one is to consider a uniform rotation from the beginning of the evolution until $X_c = 0.1$, where X_c is the hydrogen mass fraction. The second one is to consider the uniform rotation until $X_c = 0$ (the beginning of the subgiant phase). Both cases led to a core rotation frequency one order of magnitude higher than the observed one. As a conclusion, we need to add another process in stellar evolution codes to be able to reproduce the observations and further slowdown the core rotation. Today, many mechanisms are being explored as introduced in the next section.

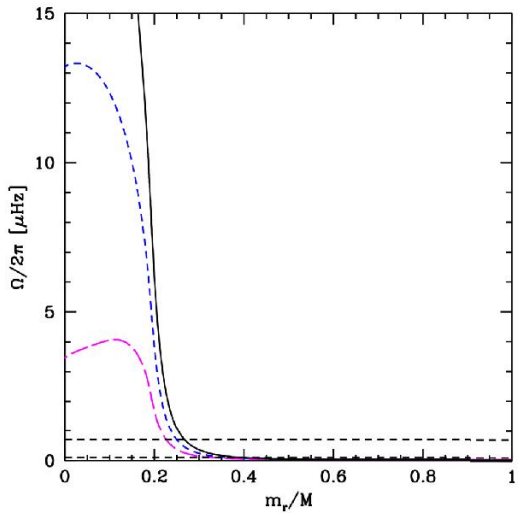

Figure 1.7 – Rotation profile for models of the star KIC 7341231 (Ceillier et al. 2013) including transport by meridional circulation and by turbulence induced by shearing (black). The blue (magenta) dotted line shows the result obtained by assuming a uniform rotation from the beginning of the evolution until $X_c = 0.1$ and ($X_c = 0$), where X_c is the central hydrogen mass fraction. The two black dotted lines are the core and the envelope rotation frequencies observed for this star by Deheuvels et al. (2012)

.

1.4 Solution: Magnetic field or Internal Gravity Waves ?

The previous section has shown the disagreements between the core rotation frequencies predicted by our theoretical models and the observations. Many physical mechanisms acting in the interior of stars could produce an angular momentum transport. A lot of works have been done covering this topic but the two main fields of investigation invoke the effects of a magnetic field generated by a Tayler-Spruit mechanism and the influence of internal gravity waves on the core rotation rate.

1.4.1 The current failure of the Tayler-Spruit mechanism

The first attempts made to explain the disagreement between the theoretical models and the observations involved transport by a magnetic field. The interaction between the mean flow and the magnetic field creates instabilities which transport angular momentum. The most common physical phenomenon able to generate a magnetic field is a Tayler-Spruit mechanism. Such process allows us to reduce successfully the discrepancy (without solving it, though) between the models and the observations for the case of main sequence stars but it is clearly not sufficient to explain the weak core rotation rates observed in red giants as shown in the figure 1.8 (e.g., Cantiello et al. 2014; Eggenberger et al. 2005). However, a recent study (Fuller et al. 2019) has revised the prescriptions of the Tayler-Spruit dynamo and concluded that the theoretical model could be in agreement with the observations for the red giants, but still remain not sufficient for the main sequence and subgiant stars. Therefore, since the Tayler-Spruit dynamo does not provide us with a complete picture of the angular momentum redistribution during the whole life of stars, another mechanism needs to be taken into account.

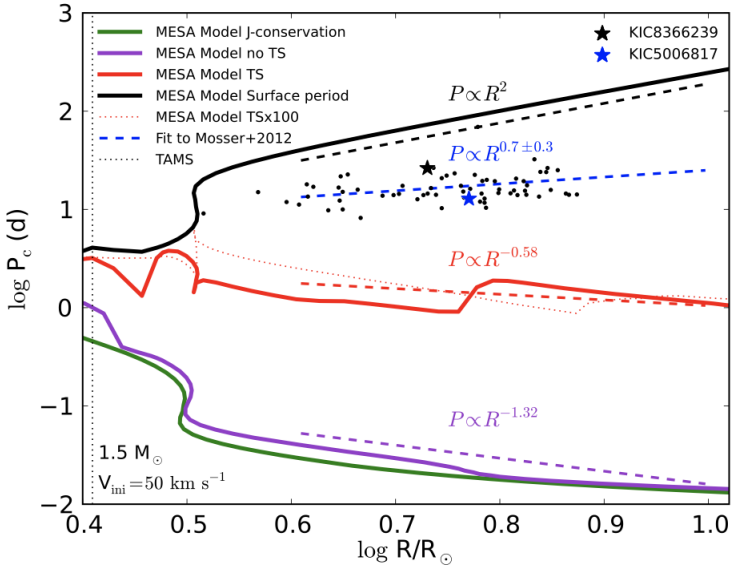

Figure 1.8 – Evolution of the average core rotational period as a function of stellar radius for different assumptions of angular momentum transport in a 1.5M⊙ model initially rotating at 50 km s^{-1}. Models are shown without angular momentum transport (green), including transport of angular momentum due to rotational instabilities (purple) and accounting for magnetic torques in radiative regions (red, Tayler-Spruit magnetic fields). The star symbols and the black dots represent the observed values (Cantiello et al. (2014)).

1.4.2 The promise of Internal Gravity Waves

Internal gravity waves (IGW) are waves having the buoyancy as restoring force and thus propagating in the radiative zone (see Chapter 2). During their travel across the radiative zone, IGW undergo a radiative damping allowing them to deposit their angular momentum into the surrounding medium and therefore can modify the rotation of the medium (see Chapter 3). They are also very likely to play a role in the redistribution of angular momentum in stars. In the case of sun-like stars, these waves are generated at the interface with the external convective zone by turbulent motions (e.g., plumes and eddies). This generation mechanism is well observed in numerical simulations as we can see for instance in the figure 1.9 according to Rogers et al. (2006). We note that internal gravity waves generated by convective penetrations have a typical frequency range between 1 and 10 μHz, which can be considered as low frequency incompressible waves.

Taking into account all angular momentum processes, one can show that the general equation governing the angular momentum transport in stars is given by the horizontal average of the azimuthal component of the momentum equation A.3. In spherical coordinates, this equation can be written within the shellular approximation as follows (Zahn 1992):

$$\rho \frac{d}{dt}(r^2\overline{\Omega}) = \frac{1}{5r^2}\partial_r(\rho r^4 \overline{\Omega} U_r) + \frac{1}{r^2}\partial_r(\rho \nu_v r^4 \partial_r \overline{\Omega}) - \frac{1}{r^2}\partial_r(r^2 \rho r \overline{\mathcal{F}_\mathcal{B}}) - \frac{1}{r^2}\partial_r(r^2 \rho r \overline{\mathcal{F}_\mathcal{W}}) \qquad (1.9)$$

where $\frac{d}{dt}$ is the material derivative, the first and the second term of the right hand side represent

the transport by the meridional circulation[11] and by turbulent diffusion[12], respectively. The quantities $\overline{\mathcal{F}_{\mathcal{W}}}$ and $\overline{\mathcal{F}_{\mathcal{B}}}$ are the horizontally-averaged wave and magnetic fluxes of angular momentum, respectively and the mean rotation is given by $\overline{\Omega} = \frac{\int_0^\pi \Omega \sin^3(\theta) d\theta}{\int_0^\pi \sin^3(\theta) d\theta}$. Many studies have already investigated the effects of the $\overline{\mathcal{F}_{\mathcal{W}}}$ term on the rotation evolution by solving Eq.1.9 during stellar evolutionary sequences. For instance, in the case of the Sun, Talon and Charbonnel (2005) showed that including this term from the beginning of the Hayashi track to the actual age of the Sun could explain the flat rotation profile in our star. Indeed, as we can see in the figure 1.10, IGW induce extraction fronts of angular momentum from the center of the star towards the surface, which prevents the core rotation from drastically increasing due to its contraction. Later, on the subgiant phase, Pinçon et al. (2017) showed that the IGW flux has the appropriate order of magnitude in order to reproduce the observed rotation frequency. Until today, IGW are therefore the only potential solution at this evolutionary stage.

As shown by the previous works, IGW are very promising in order to solve the issue of the angular momentum redistribution in stars. However, all these studies do not take properly into account the whole complex dynamics induced by waves and more particularly what is happening just below the convective zone. Indeed, in this region, the complex interaction between the rotation and the IGW leads to very fast processes difficult to take into account into a stellar evolution code, but potentially with a significant impact on the long term evolution of rotation in stars. This is the so-called problem of the Shear Layer Oscillation (SLO) that we introduce in the next section.

Figure 1.9 – Snapshot of the temperature perturbation, representing the full computational domain. Dark red / white represent cold / hot perturbations with respect to the background temperature. The outer convection region is dominated by descending plumes that overshoot into the inner radiative region, finding themselves hotter than their surroundings (white spots at base of convection zone). Gravity waves are generated by these overshooting plumes.

[11] U_r is the amplitude of the radial component of the meridional circulation's velocity projected on the Legendre Polynomial $P_2(\cos\theta)$.

[12] ν_v is the vertical turbulent viscosity

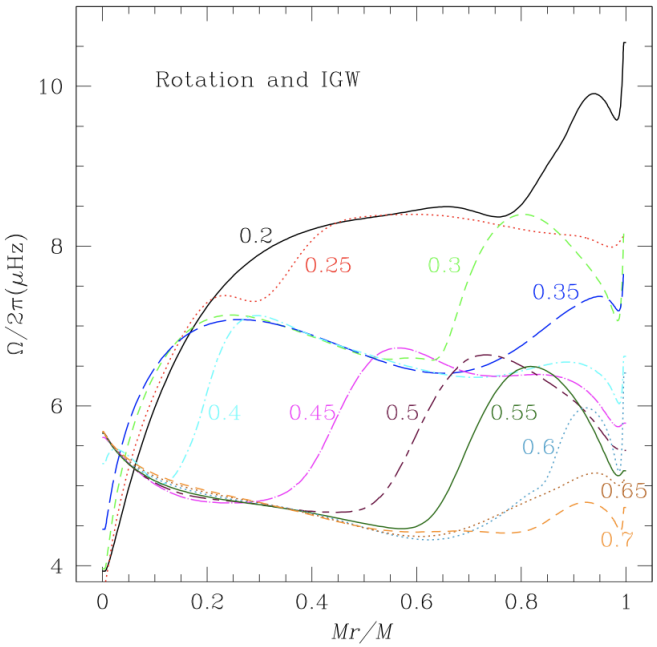

Figure 1.10 – Evolution of the rotation profile in a complete model where the transport of angular momentum is due to internal gravity waves, meridional circulation and turbulence. The model shown is for a 1.2 $M_\odot$ $Z = 0.02$, star with an initial rotation velocity of 50 km s^{-1}. The curves are labeled according to the corresponding ages in Gyr (Talon and Charbonnel 2005).

1.4.3 The Shear Layer Oscillation

The Shear Layer Oscillation (SLO) is a phenomenon extremely localized occurring in stars. It happens just below the convective zone in a thin layer of the radiative zone. More precisely, the SLO is the oscillation of the rotation profile due to its interaction with IGW. We can note that a phenomenon similar to the SLO occurs also on Earth. This is the so-called Quasi Biennal Oscillation (QBO) corresponding to the oscillation of the wind direction in the equatorial stratosphere.

In order to explain how the SLO is established, we need to use the Eq. 1.9 in which we only keep the turbulent as well as the wave flux terms in the right hand side. The meridional circulation and the magnetic flux terms are neglected because they act over time scales much larger than the one of the SLO. Finally, the equation governing the dynamics of the SLO reduces to:

$$\rho \frac{d}{dt}(r^2\bar{\Omega}) = \frac{1}{r^2}\partial_r(\rho\nu_v r^4 \partial_r \bar{\Omega}) - \frac{1}{r^2}\partial_r(r^2 \rho r \overline{\mathcal{F}_\mathcal{W}}). \tag{1.10}$$

On the one hand, we have the first term of the right hand side which stems from hydrodynamical instabilities of the flow. These instabilities are amplified by the shearing profile of the flow and create turbulence with eddies of different sizes. The energy of the flow is then transported from the larger eddies towards the smaller ones. This energy cascade produces a global vertical stress acting against the shear, thus creating an angular momentum transport. As mentioned in section 1.2, this transport is modelled by a diffusion phenomenon through using an effective viscosity (called turbulent viscosity) multiplied by a radial angular momentum gradient. This term tends to rigidify the rotation profile. On the other hand, we have the second wave flux term of the right hand side

that can be obtained by a small wave amplitude analysis. It is written under the following form:

$$\overline{\mathcal{F}_{\mathcal{W}}} = \int_{-\infty}^{+\infty} \sum_m A_m(\omega) \exp\left(- \int_{r_0}^{r} \frac{\gamma_m}{(\omega - m\delta\Omega(r',t))^4} dr' \right) d\omega \tag{1.11}$$

where A_m is an amplitude term having the same sign than m (the azimutal order of spherical harmonics, measuring the horizontal wavenumber), γ_m is the thermal damping coefficient and r_0 is the location of the generation of waves. We can see that the wave flux is composed of a sum of prograde ($m > 0$) and retrograde ($m < 0$) waves having various frequencies exchanging their energy with the flow through a thermal damping mechanism. It is important to understand that prograde (retrograde) waves transport positive (negative) angular momentum flux. In fact, we will see that prograde waves are more rapidly damped than retrograde waves and hence accelerate the rotation profile in the highest layers. The retrograde waves being damped later will decelerate the rotation profile deeper in the radiative zone. This results in a shear of the rotation profile and, under particular conditions, we will show that the balance between the wave flux, which tends to enhance the shear of the profile, and the effective viscosity, which tends to rigidify the profile, may lead to an oscillation, the so-called Shear Layer Oscillation, already studied in stellar physics by Kim and MacGregor (2003) and by Talon et al. (2002) and illustrated in the figure 1.11. In the latter, we can clearly observe an oscillation of the rotation profile. As we will see in Chapter 5, this oscillation can be decomposed in three main parts which are the following:

First, starting from a linear rotation profile with a positive slope, we will observe an equilibrium between the gradient of the prograde waves flux and the turbulent viscosity at the top of the radiative zone (panel 350 yrs). This result is easy to understand, since $\delta\Omega$ is positive. Hence, prograde waves are more rapidly damped than retrograde ones and can deposit a more substantial part of their angular momentum in the flow. This is why, we see a 'hook' in the direction of the positive $\delta\Omega$.

Second, as we go in the deeper layers of the radiative zone, the retrograde waves flux will progressively exceed the prograde waves flux (thanks to the integral in the exponential factor) and will exchange a significant part of their angular momentum with the flow (panel 400 yrs). This is why we will observe a second 'hook' at these depths (but in the opposite direction).

Third, when the shear created between both 'hooks' is sufficiently high, the turbulent viscosity term will act and a kind of a 'wavefront' in the flow will diffuse from the bottom to the top of the radiative zone (panel 450 yrs) resulting in an inversion of the rotation profile for which we will have this time an equilibrium between the gradient of the retrograde waves flux and the turbulent viscosity at the top of the radiative zone (panel 500 yrs).

This process will repeat in a symmetrical way which will lead to a second inversion of the profile bringing it back to its initial equilibrium position, thus creating the so-called Shear Layer Oscillation.

To conclude, it is quite reasonable to expect that this oscillation is able to apply a kind of filtering of the incoming wave flux (generated at the base of the convective zone) or to interact locally with other transport processes, and thus impact the core rotation rate over time scales corresponding to the lifetime of stars (Gy). This is why it is also important to include its effect in a stellar evolution code. Nevertheless, the typical time scale of the SLO is of the order of the year

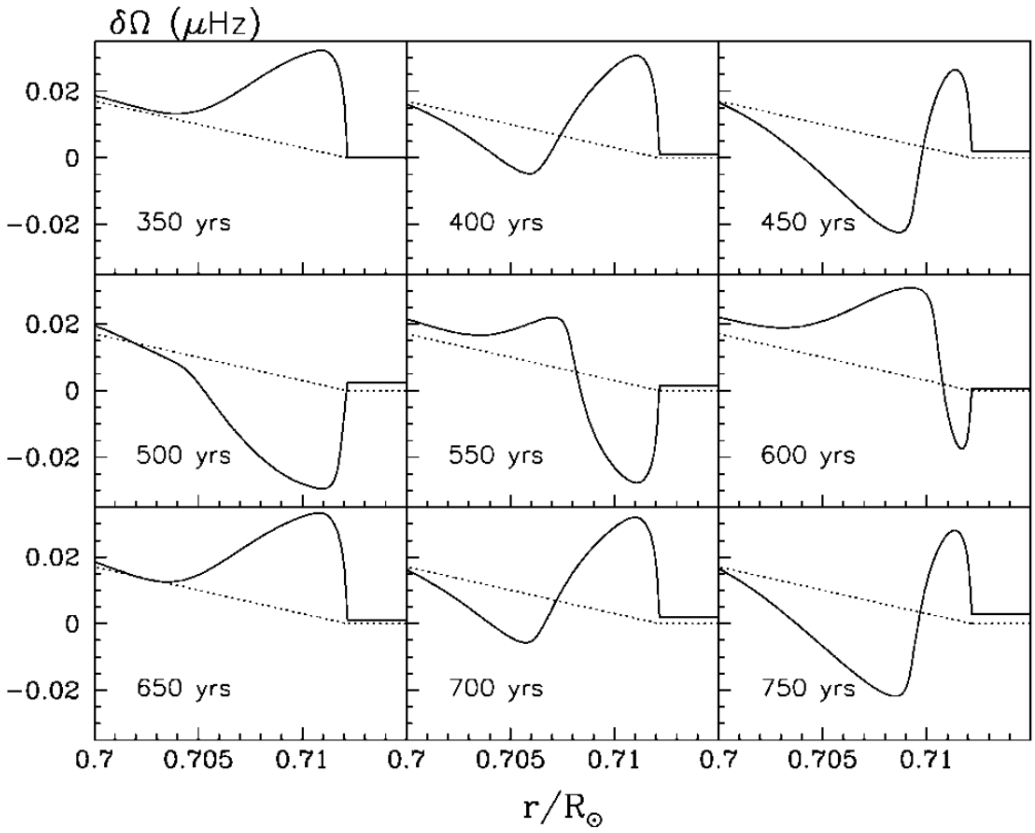

Figure 1.11 – Representation of the SLO in a solar model from 350 to 750 yrs (Talon et al. 2002). The dotted lines represent the initial rotation profile.

which is much smaller than the typical time scale corresponding to the evolution of stars. This explains why it is very difficult to include properly its effects over large time scales. This is what this work is about and more particularly it will consist in studying the physical characteristics of the SLO in a simple configuration, considering the fast SLO only in a small region at the top of the radiative zone, but with the aim to express the results in a convenient way easily implementable in global rotating stellar models. To do so, in the next chapters, we will introduce the concept of IGW in more details as well as the interaction between them and a mean flow in the frame of a simple 2D plan parallel model.

Chapter 2

Internal gravity waves in a static medium

Internal gravity waves (IGW) are waves propagating through media stably stratified in density and having the buoyancy as restoring force. Such kind of waves are ubiquitous in the Earth's atmosphere and oceans where the density varies with depth due to temperature variations as we can see in the figures 2.1 and 2.2. Similarly, they can also propagate in the radiative layers of stars. These waves show a certain behaviour and possess some properties which will be developed in the next sections in the frame of a simple theoretical model.

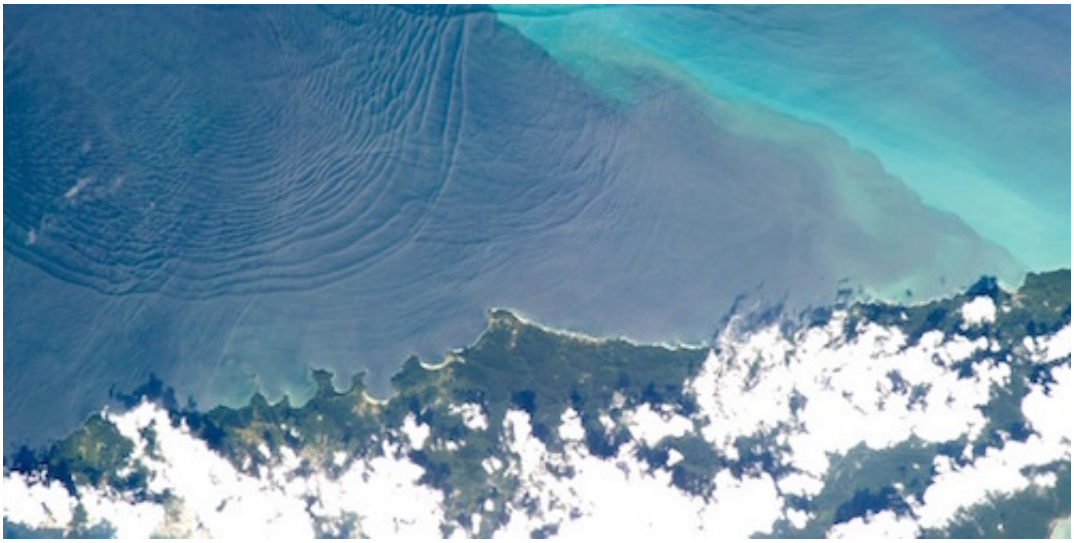

Figure 2.1 – Surface manifestation of oceanic internal waves. The upward energy propagation of internal waves modifies the properties of surface waves making them visible from space. Source : https://physics.aps.org/articles/v9/s50 (Internal Wave trains around Trinidad, as seen from space)

Figure 2.2 – The effect of internal gravity waves on clouds. Tualatin, United States. Source : https://fyfluiddynamics.com/2019/07/striped-clouds/

2.1 Small amplitude wave equation

In this section, we consider an infinite medium in hydrostatic equilibrium in which waves can freely propagate. We also assume that wave amplitudes are small and there are neither ambient rotation nor dissipative mechanisms. Within this hypothesis, the velocity, density and pressure fields are decomposed as:

$$\vec{v} = \vec{v}\,' = u'(x,y,z,t)\vec{e}_x + v'(x,y,z,t)\vec{e}_y + w'(x,y,z,t)\vec{e}_z, \tag{2.1a}$$

$$\rho(x,y,z,t) = \rho_0(z) + \rho'(x,y,z,t), \tag{2.1b}$$

$$p(x,y,z,t) = p_0(z) + p'(x,y,z,t). \tag{2.1c}$$

where the quantities X' (Eulerian perturbations) are supposed to be small compared to the reference state X_0. At the hydrostatic equilibrium, we have:

$$\vec{\nabla} p_0 = \rho_0 \vec{g} = -\rho_0 g \vec{e}_z, \tag{2.2}$$

with g the gravitational acceleration. It is important to note that the perturbations are such that any product between them is considered as much smaller than any perturbation and will be neglected in the equations.

2.1.1 The momentum equation

The momentum equation for a perfect fluid is provided in Eq. A.3 with a negligible viscosity and reads:

$$\frac{\partial \vec{v}}{\partial t} + (\vec{v}.\vec{\nabla})\vec{v} = -\frac{1}{\rho}\vec{\nabla} p + \vec{g} \tag{2.3}$$

where $\vec{\nabla}$ is the nabla operator. The latter equation can be written following Eqs. 2.1

$$(\rho_0 + \rho') \left(\frac{\partial \vec{v}\,'}{\partial t} + (\vec{v}\,'.\vec{\nabla})\vec{v}\,' \right) = -\vec{\nabla}(p_0 + p') + (\rho_0 + \rho')\vec{g}.$$

Neglecting terms of order higher than one and using the hydrostatic equilibrium, we can finally write:

$$\rho_0 \frac{\partial \vec{v}\,'}{\partial t} = -\vec{\nabla}p' + \rho'\vec{g} \tag{2.4}$$

2.1.2 The continuity equation

The continuity equation in Eq. A.2 is written:

$$\frac{\partial \rho}{\partial t} + \vec{v}.(\vec{\nabla}\rho) + \rho(\vec{\nabla}.\vec{v}) = 0 \tag{2.5}$$

Using Eq. 2.1, we have:

$$\frac{\partial \rho'}{\partial t} + \vec{v}\,'.(\vec{\nabla}[\rho_0 + \rho']) + (\rho_0 + \rho')(\vec{\nabla}.\vec{v}\,') = 0.$$

Once again, neglecting terms of order higher than one, we finally write:

$$\frac{\partial \rho'}{\partial t} + \vec{v}\,'.\vec{\nabla}\rho_0 + \rho_0(\vec{\nabla}.\vec{v}\,') = 0 \tag{2.6}$$

2.1.3 The state equation

In order to close the problem, we have to add the relation linking the density and pressure perturbations. To do so, we will use the adiabatic approximation ($\delta S = 0$, with δS the Lagrangian perturbation of the entropy), so that the state equation reads:

$$\frac{\delta p}{p_0} = \Gamma_1 \frac{\delta \rho}{\rho_0} \tag{2.7}$$

where Γ_1 is the adiabatic exponent. We note that the Lagrangian perturbation (δX) and the Eulerian perturbation (X') of a quantity X are related by:

$$\delta X = X' + \delta\vec{r}.\vec{\nabla}X_0 \tag{2.8}$$

where $\delta\vec{r}$ represents the small displacement of particles relatively to their equilibrium position and is such that $\vec{v}\,' = \partial_t \delta\vec{r}$. Using the Eq. 2.8, we can write:

$$\begin{aligned} \frac{p'}{p_0} + \delta\vec{r}.\vec{\nabla}\ln(p_0) &= \Gamma_1 \left(\frac{\rho'}{\rho_0} + \delta\vec{r}.\vec{\nabla}\ln(\rho_0) \right) \\ \Leftrightarrow \rho' &= \frac{\rho_0}{\Gamma_1 p_0} p' + \left(\frac{1}{\Gamma_1} \frac{d\ln(p_0)}{dz} - \frac{d\ln(\rho_0)}{dz} \right) \rho_0 \xi_z \end{aligned}$$

where ξ_z is the z component of the vector $\delta\vec{r}$. Noting that the sound speed in the medium and the Brunt-Väisälä frequency[1] are given by:

$$c^2 = \frac{\Gamma_1 p_0}{\rho_0} \tag{2.9a}$$

$$N^2 = g\left(\frac{1}{\Gamma_1}\frac{d\ln(p_0)}{dz} - \frac{d\ln(\rho_0)}{dz}\right) \tag{2.9b}$$

we can finally write:

$$\rho' = \frac{1}{c^2}p' + \frac{N^2}{g}\rho_0\xi_z \tag{2.10}$$

2.1.4 Set of equations governing IGW

Considering what we have done for the momentum, continuity and state equations, the set of equations we need to solve is the following:

$$\rho_0\frac{\partial u'}{\partial t} = -\frac{\partial p'}{\partial x} \tag{2.11a}$$

$$\rho_0\frac{\partial v'}{\partial t} = -\frac{\partial p'}{\partial y} \tag{2.11b}$$

$$\rho_0\frac{\partial w'}{\partial t} = -\frac{\partial p'}{\partial z} - g\rho' \tag{2.11c}$$

$$\frac{\partial \rho'}{\partial t} + w'\frac{d\rho_0}{dz} + \rho_0(\vec{\nabla}.\vec{v}\,') = 0 \tag{2.11d}$$

$$\rho' = \frac{1}{c^2}p' + \frac{N^2}{g}\rho_0\xi_z \tag{2.11e}$$

where all the components have been written explicitly. We can see that we have five equations for five unknowns (u', v', w', p' and ρ') since $w' = \partial_t\xi_z$. However, we can rewrite it under a more convenient form. Indeed, we can replace Eq. 2.11e in Eq. 2.11c and we can rewrite $\partial_t\rho' + w'\frac{d\rho_0}{dz} = \partial_t\delta\rho = \partial_t(\delta p/c^2)$. Finally, the system can be rewritten as:

$$\rho_0\frac{\partial u'}{\partial t} = -\frac{\partial p'}{\partial x} \tag{2.12a}$$

$$\rho_0\frac{\partial v'}{\partial t} = -\frac{\partial p'}{\partial y} \tag{2.12b}$$

$$\rho_0\frac{\partial w'}{\partial t} = -\frac{\partial p'}{\partial z} - \frac{g}{c^2}p' - N^2\rho_0\xi_z \tag{2.12c}$$

$$\frac{1}{c^2}\frac{\partial p'}{\partial t} - \frac{\rho_0 g}{c^2}w' + \rho_0(\vec{\nabla}.\vec{v}\,') = 0 \tag{2.12d}$$

which is totally equivalent to the above result. Nonetheless, this time, we have four equations for four unknowns (u', v', w' and p'), which makes it easier to solve.

[1] This frequency represents the characteristic oscillation frequency of a buoyant bubble in a medium stably stratified in density (see appendix B for more details).

2.2 Plan wave solution

By assuming a solution of the type $e^{i(k_x x+k_y y+k_z z-\omega t)}$ for each quantity (u', v', w' and p'), where ω is the angular frequency and k_i is the wavenumber in the direction $\vec{e}_i$, the previous Eqs. 2.12 can be written as:

$$\begin{cases} \omega\rho_0 u'_0 - k_x p'_0 = 0 \\ \omega\rho_0 v'_0 - k_y p'_0 = 0 \\ \omega\rho_0 \left(1 - \dfrac{N^2}{\omega^2}\right) w'_0 + \left(\dfrac{ig}{c^2} - k_z\right) p'_0 = 0 \\ \rho_0 k_x u'_0 + \rho_0 k_y v'_0 + \rho_0 \left(\dfrac{ig}{c^2} + k_z\right) w'_0 - \dfrac{\omega}{c^2} p'_0 = 0 \end{cases} \tag{2.13}$$

where u'_0, v'_0, w'_0, p'_0 are the amplitudes of the quantites u', v', w' and p', respectively. We can see that the latter system can be considered as a matrix equation. Indeed, this system can be written as:

$$\begin{pmatrix} \omega\rho_0 & 0 & 0 & -k_x \\ 0 & \omega\rho_0 & 0 & -k_y \\ 0 & 0 & \omega\rho_0 \left(1 - \dfrac{N^2}{\omega^2}\right) & \left(i\dfrac{g}{c^2} - k_z\right) \\ \rho_0 k_x & \rho_0 k_y & \rho_0 \left(i\dfrac{g}{c^2} + k_z\right) & -\dfrac{\omega}{c^2} \end{pmatrix} \begin{pmatrix} u'_0 \\ v'_0 \\ w'_0 \\ p'_0 \end{pmatrix} = 0$$

This matrix equation admits a non trivial solution if, and only if the determinant of the matrix vanishes. This condition leads directly to the following dispersion relation:

$$\left(\frac{N^2}{\omega^2} - 1\right)\left(\frac{\omega^2}{c^2} - k_h^2\right) + k_z^2 + \frac{g^2}{c^4} = 0 \tag{2.14}$$

where k_h is the horizontal wave number ($k_h^2 = k_x^2 + k_y^2$). We can notice that this expression is very similar to the one obtained for the non-radial adiabatic oscillations of stars. As a matter of fact, here the 'traditional' Lamb frequency ($L_l^2 = \frac{l(l+1)c^2}{r^2}$, with l the angular degree of spherical harmonics and r the radial coordinate) can be identified as $k_h^2 c^2$. IGW correspond to the low frequency branch (i.e. $\omega^2 \ll N^2$ and $\omega^2 \ll c^2 k_h^2$) so that the dispersion relation reduces to:

$$k_z^2 \approx \left(\frac{N^2}{\omega^2} - 1\right)(k_x^2 + k_y^2),$$

in which we have neglected the term g^2/c^4 since according to the hydrostatic equilibrium and the low-frequency hypothesis, it is equal to $1/(\Gamma_1 H_p)^2 \ll |\vec{k}|^2 = \left(\frac{2\pi}{\lambda}\right)^2$, where H_p is the pressure scale height and λ is the wavelength. We can rewrite the latter expression under the form:

$$\omega^2 \approx N^2 \frac{k_x^2 + k_y^2}{k_x^2 + k_y^2 + k_z^2}. \tag{2.15}$$

Since we have assumed a plane wave solution, we directly see that the wave propagates when k_z^2 is positive and the wave is evanescent (shows an exponential behaviour) when k_z^2 is negative. It is therefore clear that the wave propagates for the low-frequency branch when $\omega^2 \ll N^2$ ($k_z^2 \gg k_h^2$).

A very important point is that within this low-frequency approximation, one can show that it is exactly the same as assuming that $\vec{\nabla}.\vec{v}\,' \approx 0$. Indeed, thanks to Eqs. 2.13, where we neglect again the terms proportional to g/c^2, we have:

$$\begin{aligned}\vec{\nabla}.\vec{v}\,' &= i\ \vec{k}.\vec{v}\,' \\ &= i(k_x u' + k_y v' + k_z w') \\ &\approx \frac{i}{\omega\rho_0}\left(\underbrace{(k_x^2+k_y^2) - \frac{k_z^2}{(N^2/\omega^2-1)}}_{=0}\right) p' \approx 0.\end{aligned}$$

This is why we can assume that (to leading order approximation for $\omega^2 \ll N^2$):

$$\vec{\nabla}.\vec{v}\,' \approx 0 \tag{2.16}$$

meaning that these waves are incompressible. We can also note that taking the horizontal laplacian of the partial time derivative of Eq. 2.11c and replacing the different terms through the momentum equation and the continuity equation reduced to $\vec{\nabla}v' \approx 0$ (still within the low-frequency regime), we obtain the following wave equation:

$$\frac{\partial^2}{\partial t^2}(\nabla^2 w') + N^2(\nabla_h^2 w') = 0 \tag{2.17}$$

which also leads to the dispersion relation 2.15 assuming a plane wave solution. It is then straightforward to show that by substituting in Eqs. 2.11a-2.11c and Eq. 2.16 a real solution for the density in the form of:

$$\rho' = +A\rho_0 \cos(k_x x + k_y y + k_z z - \omega t) \tag{2.18}$$

we find:

$$u' = -A\ \frac{g\omega k_z k_x}{N^2(k_x^2+k_y^2)}\ \sin(k_x x + k_y y + k_z z - \omega t), \tag{2.19a}$$

$$v' = -A\ \frac{g\omega k_z k_y}{N^2(k_x^2+k_y^2)}\ \sin(k_x x + k_y y + k_z z - \omega t), \tag{2.19b}$$

$$w' = +A\ \frac{g\omega}{N^2}\ \sin(k_x x + k_y + k_z z - \omega t) \tag{2.19c}$$

$$p' = -A\ \frac{\rho_0 g k_z}{k_x^2+k_y^2+k_z^2}\ \sin(k_x x + k_y y + k_z z - \omega t) \tag{2.19d}$$

for which we directly verify the incompressibility condition in Eq. 2.16 since $k_x u' + k_y v' + k_z w' = 0$. Moreover, we see that the magnitude of the horizontal velocity is equal to:

$$v_h' = \sqrt{u'^2 + v'^2} = \frac{k_z}{\sqrt{k_x^2+k_y^2}}|w'| = \sqrt{\left(\frac{N^2}{\omega^2}-1\right)}|w'|. \tag{2.20}$$

Since $\omega \ll N$ for propagative internal gravity waves in the low-frequency regime, we see that the horizontal velocity is larger than the vertical velocity.

2.3 Phase and group velocity of IGW

In the following, we set $k_y = 0$. This is actually always possible with an appropriate choice of frame of reference. In this case, Eq. 2.19b shows that the y component of the wave velocity vanishes. Furthermore, the dispersion relation in Eq. 2.15 can be rewritten as:

$$\omega^2 \approx N^2 \frac{k_x^2}{k_x^2 + k_z^2} = N^2 \cos^2(\theta) \leqslant N^2 \tag{2.21}$$

where we recall the norm of the wavevector $\vec{k} = (k_x, k_z)$ given by $k = \sqrt{k_x^2 + k_z^2}$. This vector indicates the direction of the propagation of the wave phase, which is rotated by an angle θ from the x axis. The phase velocity thus points in this direction and is given by:

$$\vec{v}_\phi = \frac{\omega}{k^2}\vec{k}. \tag{2.22}$$

In the limiting case where $\omega \ll N$, $k_z \gg k_x$ so that the phase velocity is mostly vertical, internal gravity waves are thus transverse waves (indeed, $\vec{v}'.\vec{v}_\phi = 0$). In contrast, the group velocity representing the propagation velocity of the energy carried by the wave is given according to Eq. 2.15 by:

$$\begin{aligned} \vec{v}_g = \vec{\nabla}_{\vec{k}}\, \omega = \frac{\omega k_z^2}{k_x k^2}\, \vec{e}_x - \frac{\omega k_z}{k^2}\, \vec{e}_z, \\ \Rightarrow |\vec{v}_g| = \frac{k_z}{k_x}\frac{\omega}{k} = \frac{k_z}{k_x}|\vec{v}_\phi|. \end{aligned} \tag{2.23}$$

This relation shows that the gravity waves are dispersive waves because the phase and the group velocity have not the same expression. Equations 2.22 and 2.23 show that for the phase and the energy, the horizontal directions of propagation are the same but the vertical direction of propagation are opposite. We can also see that the propagation direction of the wave is perpendicular to its group velocity since $\vec{k}.\vec{v}_g = 0$. A convenient representation of the phase and group velocity as well as an illustration of the layout of internal gravity waves with respect to these velocities is shown in the figure 2.3 .

2.4 Thermal damping of IGW

In the last sections, we have neglected all the dissipative mechanisms so that the oscillations have been considered adiabatic with a constant amplitude over time. However, IGW obviously generate temperature perturbations that can in turn be countered by any thermal diffusion mechanism. The wave amplitude is thus progressively damped by thermal diffusion. Here, we aim to study and quantify this phenomenon in a simple way.

To do so, we have to consider in addition the heat equation that is given by:

$$\rho \frac{dq}{dt} = -\vec{\nabla}.\vec{q} \tag{2.24}$$

where $dq = Tds$ is the specific heat, s is the specific entropy and $\vec{q}$ is the heat flux. In stably stratified radiative zone in stars, the heat transport is ensured by photons radiation so that:

$$\rho T \frac{ds}{dt} = -\vec{\nabla}.\vec{F}_R \tag{2.25}$$

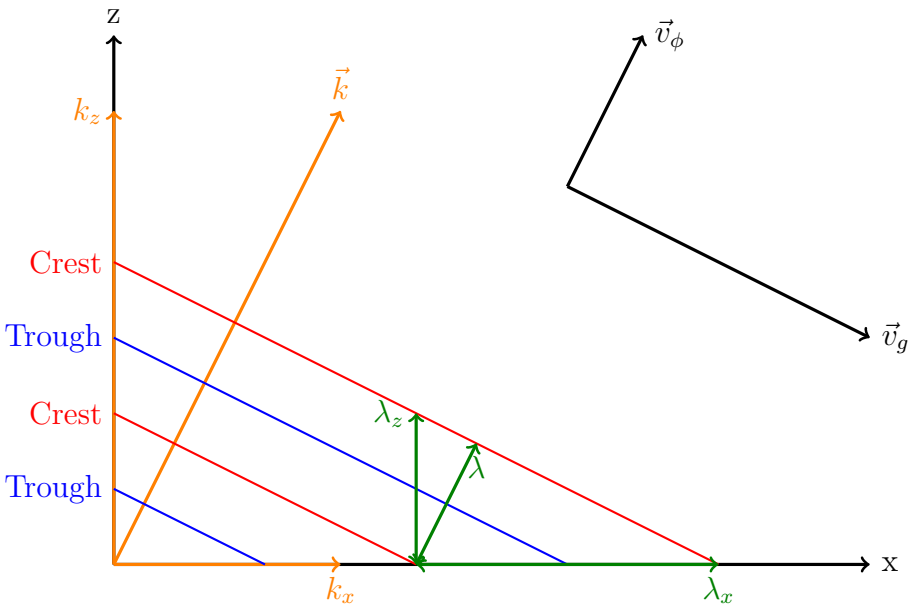

Figure 2.3 – Representation of IGW. Here, there is no scale for the axis but the scheme is such that $k_z = 2k_x$ and thus, $v_g = 2\ v_\phi$. The different wavelengths are also represented and we can see that they are inversely proportional to the wave numbers

where the flux of radiative energy can be written in the diffusion approximation:

$$\vec{F_R} = -K_{rad}\vec{\nabla}T \tag{2.26}$$

with $K_{rad} = \frac{16\sigma T^3}{3\kappa\rho}$ the thermal conductivity, σ the steffan-Boltzmann constant and κ the opacity. At the equilibrium, the radiative flux is assumed vertical and conserved so that:

$$K_{rad}\frac{dT_0}{dz} = \text{constant} \tag{2.27}$$

where $T_0(z)$ is the equilibrium temperature. In presence of internal gravity waves, Eq. 2.25 is perturbed. In order to keep the problem simple, we make the following assumptions. First, in case of incompressible gravity waves, we can neglect the Lagrangian perturbation of pressure to good approximation (Dintrans and Rieutord 2001) so that we have the relation:

$$\frac{\delta s}{c_p} \approx \frac{\delta T}{T} \tag{2.28}$$

where δs and δT is the Lagrangian perturbation of specific entropy and temperature respectively. Second, we assume the vertical wavelength is much smaller than the variation scale height of the structure and the horizontal wavelength so that the Lagrangian perturbation of the energy flux divergence is dominated by the vertical gradient of the temperature perturbation. Within these approximations, linearizing the energy equation leads to:

$$\frac{d\delta T}{dt} \approx +\chi_{rad}\partial_z^2\delta T = -\chi_{rad}k_z^2\delta T \tag{2.29}$$

where $\chi_{rad} = K_{rad}/\rho c_p$ is the radiative diffusivity. This latter equation shows that the wave amplitude is progressively damped over a time at a rate $1/t_{damp}$ with:

$$t_{damp} = \frac{1}{k_z^2 \chi_{rad}} \tag{2.30}$$

Of course, in addition to this damping, the variations of temperature is also ruled by the momentum equation and thus oscillates with the frequency ω of the wave. Therefore, the general solution takes the form of an exponentially-damped harmonic oscillator which is given to good approximation by:

$$\delta T(t) \approx \delta T(t_0)\ e^{-\int_{t_0}^{t} \frac{dt'}{t_{damp}}} e^{-i\omega t} \tag{2.31}$$

It is also interesting to convert this expression for the damping of the oscillation at one point with the damping of an energy ray that propagates at the group velocity in the z direction. During a time interval dt, the wave amplitude decreases by a factor dt/t_{damp}. During this lapse of time, the energy ray moves over a distance $dz = v_{g,z}\ dt$ in the vertical direction. Therefore, the amplitude of the energy ray decreases by a factor $dt/t_{damp} = dz/(v_{g,z} t_{damp})$, where $v_{g,z}$ is the vertical group velocity. Using Eq. 2.23, it is thus straightforward to show that the total damping of the energy ray between z_0 and z can be described to good approximation by a factor $e^{-\tau}$, where τ is given by:

$$\tau(z) \approx k_x^3 \int_{z_0}^{z} \chi_{rad} \frac{N^3}{\omega^4} dz' \tag{2.32}$$

where we consider that $z_0 < z$. This approximate expression is actually very close to the rigorous expression that will be derived in more details in the Chapter 3. Since gravity waves are damped, they deposit energy and momentum and interact with the medium, for example a mean flow. This is what happens for the SLO, as we discussed earlier. In particular, when an horizontal flow $\overline{U}(z,t)$ is considered in the direction $\vec{e}_x$ the wave frequency is doppler-shifted in Eq. 2.32 so that ω has to be replaced by $\hat{\omega} = (\omega - k_x \overline{U}(z,t))$, meaning that prograde waves, that is propagating in the same direction as the flow ($k_x \overline{U} > 0$), is more rapidly damped than the retrograde ones, that is propagating in the opposite direction of the flow ($k_x \overline{U} < 0$). This asymmetry can create a net transport of angular momentum in the medium as we will see in the next chapter.

To conclude this chapter, we can say that IGW are low frequency transverse waves having buoyancy as restoring force and with an incompressible nature. Their phase velocity is perpendicular to their group velocity which is also the propagation direction of the energy carried by the waves. They propagate in media stably stratified in density and undergo a radiative damping mechanism during their travel across the medium. We can therefore see that these waves can interact with a surrounding medium (by exchanging angular momentum), for instance with a mean flow as developed in the next chapter.

Chapter 3

Modelling the Shear Layer Oscillation

3.1 Description of the problem

This chapter is aiming at modelling the interaction between a mean flow and internal gravity waves generated at the interface between the convective and the radiative zones. The mean flow lies just below the bottom of the convective zone, on the top of the radiative zone on a depth much smaller than the characteristic radius of the star R. We assume that L, the largest horizontal spatial scale of the problem, is much smaller than R. This configuration allows us to make an approximation on the dimensions of the problem. Indeed, we focus on a small part of the radiative zone and we assume that we place ourselves in a two dimensional plan parallel model, as shown in the figure (3.1), to study the behavior of the mean flow interacting with internal gravity waves.

In order to achieve this, we work with a cartesian plan $(\vec{e}_x, \vec{e}_z)$. The medium is stably stratified (radiative zone), at the hydrostatic equilibrium in the $\vec{e}_z$ direction and moves at an horizontal velocity $\vec{u} = U(z)\vec{e}_x$ (the vertical component of the velocity is neglected since the contraction velocity is very small and negligible over the timescales of interest). We also neglect the microscopic viscosity of the bulk and the heating due to friction.

Figure 3.1 – Illustration of the physical situation of the flow inside a small box at the interface between the convective and radiative zones.

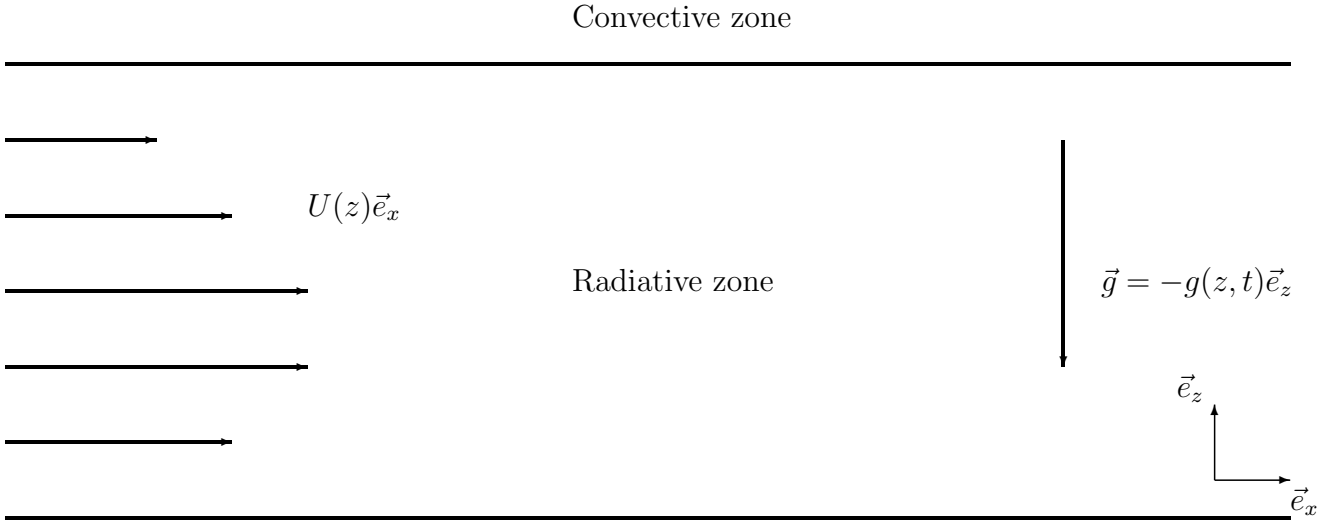

We consider now that we disturb this equilibrium. All physical quantities can be decomposed as follows:

$$X(x,z,t) = \overline{X}(z,t) + X'(x,z,t) \tag{3.1}$$

where t is the time, $X'(x,z,t)$ is the fluctuating part and $\overline{X}(z,t)$ is the horizontal Eulerian mean defined by:

$$\overline{X}(z,t) = \frac{1}{L}\int_{-L/2}^{+L/2} X(x,z,t)dx \tag{3.2}$$

We note for later purposes that the following properties are valid for any quantity X an Y:

$$\begin{gathered}\overline{X'} = 0,\ \overline{\partial_t X} = \partial_t \overline{X},\ \overline{\partial_z X} = \partial_z \overline{X},\ \overline{\partial_x X} = \partial_x \overline{X} = 0 \\ \overline{XY} = \overline{X}\ \overline{Y} + \overline{X'Y'}\end{gathered} \tag{3.3}$$

Assuming periodical boundary conditions in the $\vec{e}_x$ direction, L corresponds to the spatial period such as $X(x+L,z,t) = X(x,z,t)$. In this context, the fields $\rho,\ p$ and $\vec{v}$ are written:

$$\begin{aligned}\rho(x,z,t) &= \overline{\rho}(z,t) + \rho'(x,z,t), \\ p(x,z,t) &= \overline{p}(z,t) + p'(x,z,t), \\ \vec{v}(x,z,t) &= \left[\overline{U}(z,t) + u'(x,z,t)\right]\vec{e}_x + w'(x,z,t)\vec{e}_z\end{aligned} \tag{3.4}$$

The gravity field is governed by the Poisson equation $\vec{\nabla}.\vec{g} = -4\pi G\rho$ with G, the gravitational constant and $\vec{g}$ is the gravitational acceleration vector. We adopt the Cowling approximation (Cowling 1941), which allows us to neglect the fluctuations of $\vec{g}$. We can write:

$$\vec{g}(x,z,t) \approx -\overline{g}(z,t)\vec{e}_z \tag{3.5}$$

This approximation implicitly assumes that the fluctuations have weak amplitudes and oscillate on spatial scales smaller than L. Indeed, in this case, the fluctuations of $\vec{g}$ induced by the fluctuations of ρ over all the plane vanish by mean effect. This condition will be satisfied for the low frequencies gravity waves (Dintrans and Rieutord 2001).

3.2 Eulerian mean of conservation equations

In this section, we are going to derive the Eulerian mean of balance equations by using the continuity equation A.2 and the two components of the momentum equation A.4 along the $\vec{e}_x$ and $\vec{e}_z$ directions. For the sake of clarity, one replaces the expressions of the density ρ, the pressure p and the velocity field $\vec{v}$ by the relations 3.4 in the continuity and momentum equations, while neglecting the viscous term which is always valid in stars. Then, we take the horizontal Eulerian mean of these equations and only the terms up to the second order in the perturbations are kept in the disturbances because we assume that their amplitudes are much smaller than the amplitudes of the undisturbed variables. Finally, we simplify the expressions by using the relations given by equations 3.3.

Replacing ρ, p and $\vec{v}$ by the equations 3.4, the continuity and the two momentum equations are written:

$$\partial_t[\overline{\rho}+\rho'] + \partial_x[(\overline{\rho}+\rho')(\overline{U}+u')] + \partial_z[\overline{\rho}w'] + \partial_z[\rho'w'] = 0$$
$$\partial_t[\rho w'] + \partial_x[\rho(\overline{U}+u')w'] + \partial_z[\rho w'^2] = -\partial_z p - \rho g$$
$$\partial_t[\rho(\overline{U}+u')] + \partial_x[\rho(\overline{U}+u')^2] + \partial_z[\rho(\overline{U}+u')w'] = -\partial_x p$$

and taking the Eulerian mean while using the relations 3.3, we obtain:

$$\partial_t\overline{\rho} = -\partial_z\left(\ \overline{\rho'w'}\ \right) = C \tag{3.6a}$$
$$-\partial_z\overline{p} - \overline{\rho}g = \partial_t(\overline{\rho'w'}) + \partial_z(\overline{\rho}\overline{w'^2} + \overline{\rho'w'^2}) = V \tag{3.6b}$$
$$\partial_t(\overline{\rho}\overline{U}) = \partial_z(\overline{\rho}\overline{u'w'}) - \partial_t(\overline{\rho'u'}) - \partial_z(\overline{U}\ \overline{\rho'w'}) = H \tag{3.6c}$$

where we have used the periodic boundary conditions in the x direction to remove the partial derivatives with respect to x. At this stage, it is the equation 3.6c which will allow us to describe the interactions between the mean flow $\overline{U}$ and the wave terms. To go further, we thus have to express the evolution of the perturbations as a function of t and z. To do so, we will consider two cases. First, we will consider the case of small amplitude waves oscillating in a stable way around the equilibrium state: these are the IGW. Second, we will address the case where the level of shear in the star can lead to instabilities and the perturbations cannot be considered as small amplitude waves anymore. In this last case, we will derive the instability criterions and will propose a simple modelling to describe the induced turbulence and mixing.

3.3 Case 1: Stable linear fluctuation analysis (IGW)

3.3.1 Small wave amplitude assumption

In this section, we are going to derive the fluctuations equations by using, once again, the continuity equation A.2, but this time, instead of working with equation A.4, we are going to use equation A.3 in order to derive the two components of the momentum equation. In a similar way to the previous section, we will use the equation 3.4 to develop the mathematical expressions of these equations without applying the Eulerian mean but by keeping only the first order terms in disturbances because, in our case, we assume that these fluctuations are small with respect to the Eulerian mean : $\overline{X} \gg X'$ for all variable X, which justifies the linear approximation for the fluctuations.

The continuity and the two momentum equations are written:

$$\partial_t[\overline{\rho}+\rho'] + \partial_x[(\overline{\rho}+\rho')(\overline{U}+u')] + \partial_z[(\overline{\rho}+\rho')w'] = 0$$
$$(\overline{\rho}+\rho')[\partial_t w' + (\overline{U}+u')\partial_x w' + w'\partial_z w'] = -\partial_z[\overline{p}+p'] - (\overline{\rho}+\rho')g$$
$$(\overline{\rho}+\rho')[\partial_t(\overline{U}+u') + (\overline{U}+u')\partial_x(\overline{U}+u') + w'\partial_z(\overline{U}+u')] = -\partial_x[\overline{p}+p']$$

and keeping only the first order terms in disturbances, we obtain:

$$\partial_t\rho' + \overline{U}\partial_x\rho' + \vec{\nabla}.(\overline{\rho}\vec{v}\,') = -\partial_t\overline{\rho} = -C \approx 0 \tag{3.7a}$$
$$\overline{\rho}\partial_t w' + \overline{\rho}\overline{U}\partial_x w' + \partial_z p' + \rho' g = -\partial_z\overline{p} - \overline{\rho}g = V \approx 0 \tag{3.7b}$$
$$\overline{\rho}\partial_t u' + \overline{\rho}\overline{U}\partial_x u' + \overline{\rho}w'\partial_z\overline{U} + \partial_x p' = -(\overline{\rho}+\rho')\partial_t\overline{U} \approx 0 \tag{3.7c}$$

In these equations, the right hand side vanishes because it is straightforward to show, thanks to equations 3.6a, 3.6b and 3.6c, that these terms are of order two in disturbances. Moreover, we assume that:

$$|u'|, |w'| \ll \overline{U} \ll c \tag{3.8}$$

where $c^2 = \Gamma_1 \overline{p}/\overline{\rho}$ is the sound velocity, with Γ_1 the first adiabatic exponent. In other words, in order to study the interaction between the fluctuations and $\overline{U}$, the mean of the other variables $\overline{\rho}$ and $\overline{p}$ can be considered as independent of time in good approximation, which means that the variation of the mean structure with respect to the hydrostatic equilibrium is totally negligible. Indeed, by taking $C \approx 0$ and $V \approx 0$ for equations 3.6a and 3.6b we find:

$$\partial_t \overline{\rho} \approx 0 \Rightarrow \overline{\rho} \approx \rho(z) \Rightarrow \vec{g} \approx -g(z)\vec{e}_z \tag{3.9}$$

$$\partial_z \overline{p} \approx -\overline{\rho} g \Rightarrow \overline{p} \approx p(z) \tag{3.10}$$

where the second mathematical implication in equation 3.9 comes from the Poisson equation $\vec{\nabla}.\vec{g} = -4\pi G\overline{\rho}$. The Eulerian mean of the structure variables therefore depends only on the altitude z, except for $\overline{U}$, which is also time dependent. In the following, the notation is simplified by omitting the bar (the overline) on Eulerian mean, corresponding by hypothesis to the quantities at the hydrostatic equilibrium of ρ, p and the other variables such as the temperature T or the specific entropy s (entropy per unit mass). However, there are also two other equations that we need to take into account: the state equation for ρ and the heat equation.

First, the state equation for the variable $\rho \equiv \rho(p, T)$, assuming that the gradient of chemical composition is weak, is given by:

$$\frac{\rho'}{\rho} = \alpha \frac{p'}{p} - \delta \frac{T'}{T} \tag{3.11}$$

where $\alpha = \left(\frac{\partial \ln \rho}{\partial \ln p}\right)_T$ and $\delta = -\left(\frac{\partial \ln \rho}{\partial \ln T}\right)_p$. Indeed, we can always write this state equation for any gas having a relation between the pressure and the temperature. For instance, in the case of a perfect gas, we have $\alpha = \delta = 1$ since $\rho \propto \frac{p}{T}$.

Second, the heat equation is given by:

$$\rho \frac{dq}{dt} = -\vec{\nabla}.\vec{q}$$

where $dq = Tds$ is the heat and $\vec{q} = \vec{F}_R$ is the radiative flux. This equation can be written:

$$\rho T \frac{ds}{dt} = -\vec{\nabla}.\vec{F}_R$$

Now, by replacing $\rho, T, s, \vec{F}_R$ by their averaged plus a perturbation (eq 3.1), developing the total derivative with respect to time and getting rid of the bar for the mean quantities, keeping only the first order perturbations and assuming the equilibrium such that $\partial_t \overline{s} = -\vec{\nabla}.\overrightarrow{\overline{F}}_R$, we obtain the following equation:

$$\rho T(\partial_t s' + \overline{U}\partial_x s' + w' \frac{ds}{dz}) = -\vec{\nabla}.\vec{F}'_R$$

where the term $\frac{ds}{dz}$ can be expressed as a function of the Brunt-Väisälä frequency $N^2 = \frac{g\delta}{c_p}\frac{ds}{dz}$ thanks to the state equation for the density. We obtain:

$$\rho T(\partial_t s' + \overline{U}\partial_x s' + w'\frac{c_p N^2}{g\delta}) = -\vec{\nabla}.\vec{F}'_R \tag{3.12}$$

where c_p is the heat capacity at constant pressure.

Finally, at this stage, we have the following set of equations to solve for the linear IGW:

$$\partial_t \rho' + \overline{U}\partial_x \rho' + \vec{\nabla}.(\rho\vec{v}\,') = 0 \tag{3.13a}$$

$$\rho(\partial_t u' + \overline{U}\partial_x u' + w'\partial_z \overline{U}) + \partial_x p' = 0 \tag{3.13b}$$

$$\rho(\partial_t w' + \overline{U}\partial_x w') + \partial_z p' + \rho' g = 0 \tag{3.13c}$$

$$\rho T(\partial_t s' + \overline{U}\partial_x s' + w'\frac{c_p N^2}{g\delta}) = -\vec{\nabla}.\vec{F}'_R \tag{3.13d}$$

3.3.2 Low frequency fluctuations

Now we suppose that the fluctuations belong to low frequency regime as seen in the chapter 2 meaning that the characteristic frequency ω verifies that $\omega^2 \ll N^2$ as well as $\omega^2 \ll c^2/H_p^2$, where $H_p \equiv -(d\ln p/dr)^{-1}$ corresponds to the pressure height scale. Under these hypotheses, the deviation with respect to the hydrostatic equilibrium induced by the fluctuations is almost instantaneously rebalanced (on the fluctuations time scale). Fluctuations may be considered as nearly incompressible meaning that the terms with ρ' can be neglected in Eq. 3.13a and $p'/p \ll \rho'/\rho$ in Eq. 3.11. Although frequencies are considered to be low, we assume that $1/\omega$ is much smaller than the evolution time scale of the mean flow ($\frac{\partial \ln \overline{U}}{\partial t} \equiv \frac{1}{\tau_U} \ll \omega$). This hypothesis allows us to state that the flow $\overline{U}$ in fluctuation Eqs. 3.13a-3.13d may be considered time independent, meaning:

$$\overline{U}(z,t) \approx \tilde{U}(z). \tag{3.14}$$

We can therefore rewrite the fluctuation equations under the following form:

$$\vec{\nabla}.(\rho\vec{v}\,') = 0 \tag{3.15a}$$

$$\rho(\partial_t u' + \tilde{U}\partial_x u' + w'\partial_z \tilde{U}) + \partial_x p' = 0 \tag{3.15b}$$

$$\rho(\partial_t w' + \tilde{U}\partial_x w') + \partial_z p' + \rho' g = 0 \tag{3.15c}$$

$$\frac{\rho'}{\rho} = -\delta\frac{T'}{T} = -\frac{\delta}{c_p}s' \tag{3.15d}$$

$$\rho T(\partial_t s' + \tilde{U}\partial_x s' + w'\frac{c_p N^2}{g\delta}) = -\vec{\nabla}.\vec{F}'_R \tag{3.15e}$$

where Eqs. 3.15a and 3.15d come from the incompressible nature of the low-frequency waves.

The latter system consisting of 6 equations with 6 unknowns (u', w', p', ρ', s' and T') represents the oscillation equations for internal gravity waves damped in an horizontal flow having the buoyancy force ($\rho' g$) as main restoring force. We can note that this system is quite similar to the system 2.12 developed in the previous chapter. Thus, we expect to find some similarities for the solution but keeping in mind that this system is much more complex since we have taken into account the thermal damping of the waves as well as an horizontal non-vanishing mean flow.

3.3.3 Solution of the system

The system of Eqs. 3.15 is quite complex and has already been solved by Press (1981). The idea is to find an evolution equation for the variable $\rho w'$ and then expand the solution as a Fourier series and express it within the low-frequency approximation using an asymptotic JWKB analysis. The different steps of the development are presented hereafter.

The following developments are quite heavy and can be skipped by the reader until the part 3.3.3 where we make a little synthesis of the most important results obtained hereunder.

Equation for $\rho w'$

The first step is to take the horizontal divergence of the momentum conservation represented by Eqs. 3.15b and 3.15c, and so that using Eq.3.15a we obtain:

$$\Delta p' = -\partial_z(\rho' g) - 2\partial_z \tilde{U}(\partial_x \rho w') \tag{3.16}$$

where Δ is the Laplacian operator. Then, we take the Laplacian of Eq. 3.15c to get:

$$\begin{aligned} \partial_\tau \Delta(\rho w') &= -\partial_z \Delta p' - \Delta(\rho' g) - \partial_z^2 \tilde{U}(\partial_x \rho w') - 2\partial_z \tilde{U}(\partial_{zx}^2 \rho w') \\ &= \partial_z^2(\rho' g) - \Delta(\rho' g) + \partial_z^2 \tilde{U}(\partial_x \rho w') \\ &= -g\partial_x^2 \rho' + \partial_z^2 \tilde{U}(\partial_x \rho w') \end{aligned} \tag{3.17}$$

where the second equality has been obtained by using Eq. 3.16 and for which we have defined the operator $\partial_\tau = \partial_t + \tilde{U}\partial_x$ representing the derivative with respect to time in the frame of reference moving with the mean flow in the horizontal direction.

The second step is to express the density perturbation thanks to the heat flux in Eq.3.15e. In the diffusion approximation, the flux of radiative energy can generally be written:

$$\vec{F}_R = -K_{rad}\vec{\nabla}T$$

where $K_{rad} = \frac{16\sigma T^3}{3\kappa\rho}$ is the thermal conductivity, with σ the steffan-Boltzmann constant and κ the opacity. The Eulerian perturbation of the flux is therefore given by:

$$\vec{F'}_R = -K'_{rad}\vec{\nabla}T - K_{rad}\vec{\nabla}T'$$

In the case of internal gravity waves having low frequencies, one can show that the vertical wavelength is very small compared to the height scale of the equilibrium variation (of the pressure). It will be verified later thanks to the dispersion relation (see chapter 2). Using the latter equation and Eq. 3.15d, the leading order gives:

$$\vec{\nabla}.\vec{F'}_R \approx -K_{rad}\Delta T' \approx \frac{TK_{rad}}{\delta\ \rho}\Delta\rho'$$

Inserting this result in Eq. 3.15e and using Eq.3.15d, we obtain:

$$\partial_\tau \rho' - \chi_{rad}\Delta\rho' = \frac{N^2}{g}\rho w' \tag{3.18}$$

where $\chi_{rad} = K_{rad}/\rho c_p$ is the radiative diffusivity. Then, we take the derivative ∂_τ of Eq. 3.17 and we replace $\partial_\tau \rho'$ by the latter equation in order to find:

$$\partial_\tau^2 \Delta(\rho w') = -g\chi_{rad}\Delta\partial_x^2\rho' - N^2\partial_x^2(\rho w') + \partial_z^2\tilde{U}(\partial_{x\tau}\rho w')$$

and replacing $\partial_x^2\rho'$ by Eq.3.17, we finally get:

$$\partial_\tau^2 \Delta(\rho w') = g\chi_{rad}\Delta\left(\frac{1}{g}\left[\partial_\tau\Delta(\rho w') - \partial_z^2\tilde{U}(\partial_x\rho w')\right]\right) - N^2\partial_x^2(\rho w') + \partial_z^2\tilde{U}(\partial_{x\tau}\rho w') \tag{3.19}$$

Before going further, we expand the dependent variable as a Fourier series in the horizontal direction. One assumes that the length scale L is the largest horizontal wavelength of the considered spectrum. In this case, the perturbation of the quantity X can be written:

$$X'(x,z,t) = \sum_{l=-\infty}^{l=+\infty} X'_l(z,t)e^{ik_l x} \tag{3.20}$$

where $k_l = 2\pi l/L$ with l, an integer and

$$X'_l(z,t) = \frac{1}{L}\int_{-L/2}^{+L/2} X'(x,z,t)e^{-ik_l x}dx \tag{3.21}$$

in such a way that ∂_x can be substituted by ik_l in the equation Eq. 3.19. In the same way, one also introduces the temporal Fourier transform of any variable $X(t)$ by:

$$TF_\omega[X(t)] \equiv \hat{X}(\omega) = \int_{-\infty}^{+\infty} X(t)e^{i\omega t}dt \tag{3.22}$$

where ω is the angular frequency of the wave in a Galilean frame. Of course, we can write $TF_\omega(\partial_t X) = -i\omega\hat{X}(\omega)$.

All these conventions have been introduced in order to write Eq.3.19 in the Fourier's space under the following form:

$$\left[-\hat{\omega}^2(\partial_z^2 - k_l^2) - N^2k_l^2 - k_l\hat{\omega}\partial_z^2\tilde{U}\right](\rho\hat{w}'_l) = g\chi_{rad}(\partial_z^2 - k_l^2)\left(\frac{1}{g}\left[-i\hat{\omega}(\partial_z^2 - k_l^2) - ik_l\partial_z^2\tilde{U}\right]\right)(\rho\hat{w}'_l) \tag{3.23}$$

where we have defined $\hat{\omega} = \omega - k_l\tilde{U}(z)$ which is the intrinsic frequency of the wave in the co-moving frame of reference following the horizontal flow. A prograde wave whose phase propagates in the same horizontal direction than $\overline{U}$ (such as $l\overline{U} > 0$) will have an intrinsic frequency lower than the one in the considered Galilean frame. It will be exactly the opposite for a retrograde wave (such as $l\overline{U} < 0$). It is also convenient to be careful to the definition of the Fourier transform. Indeed, the link between the sign of l and the property prograde/retrograde depends on the convention of the Fourier transform. The case where $l > 0$ will refer to a prograde wave because we have used $e^{i\omega t}$ instead of $e^{-i\omega t}$ when we have passed into the frequency space through the Fourier transform in Eq.3.22.

Short wavelength JWKB analysis

The Eq. 3.23 does not posses analytical solution. However, a quite good approximation is to neglect the velocity gradient acting on the waves. This approximation is only done here in order to simplify the mathematical resolution of the problem but will be relaxed in section 3.4. In other words, we consider that the flow only acts on the waves through Doppler effect on their frequencies (included in $\hat{\omega}$). We therefore neglect the derivatives of $\tilde{U}$ in Eq. 3.23 which becomes:

$$\left\{ \left([\partial_z^2 - k_l^2] + \frac{k_l^2 N^2}{\hat{\omega}^2} \right) - i \frac{g}{\hat{\omega}} \chi_{rad} [\partial_z^2 - k_l^2] \left(\frac{1}{g} [\partial_z^2 - k_l^2] \right) \right\} (\rho \hat{w}_l') = 0 \tag{3.24}$$

As already mentioned, we expect that internal gravity waves having low frequencies ($\hat{\omega} \ll N$) have their wavelength much smaller than the pressure height scale. Thus, we search for solution in the WKB approximation such as:

$$\rho \hat{w}_l' = A(z) e^{i\Phi(z)} \tag{3.25}$$

where $A(z)$ and $\Phi(z)$ are an amplitude slowly varying and a phase rapidly varying with z meaning that:

$$(\partial_z \Phi)^2 \equiv k_z^2(z) \gg (\partial_z \ln A)^2, \partial_z^2 \ln g$$

where we have defined the local radial (vertical) wave number $k_z(z)$. Moreover, we consider the quasi-adiabatic hypothesis. We therefore suppose that the losses by radiative diffusion are associated with time scales much longer than the wave period. Thus, we suppose that:

$$\epsilon_{nad} \equiv \frac{\chi_{rad} k_z^2}{\hat{\omega}} \ll 1$$

Physically, ϵ_{nad} measures the radiative diffusion efficiency with respect to the restoring force. To the dominant order in ϵ_{nad}, Eq. 3.24 can be written:

$$\partial_z^2 (\rho \hat{w}_l') + \left(\frac{N^2}{\hat{\omega}^2} - 1 \right) k_l^2 (\rho \hat{w}_l') = 0 \tag{3.26}$$

By replacing Eq. 3.25 in the latter equation and gathering the dominant terms in k_z, the WKB solution is written:

$$k_z = \pm \sqrt{\left(\frac{N^2}{\hat{\omega}^2} - 1 \right) k_l^2} \tag{3.27}$$

$$\partial_z \ln A = -\frac{1}{2} \partial_z \ln(k_z) \Rightarrow A(z) = |k_z|^{-1/2} \tag{3.28}$$

where the + and - represent the case of a progressive and a regressive wave in the z direction, respectively. We also note that the leading-order dispersion relation we have just found has the same expression than the one obtained in the chapter 2. Now we consider the first order disruption in ϵ_{nad} of the solution. We search for the perturbation of the wave number k_z by writing:

$$\partial_z \Phi = k_z^{(0)} + \epsilon_{nad} k_z^{(1)} = \pm \sqrt{\left(\frac{N^2}{\hat{\omega}^2} - 1 \right) k_l^2} + \epsilon_{nad} k_z^{(1)} \tag{3.29}$$

where $k_z^{(0)}$ is the solution of the non-disrupted case. Inserting the latter relation in Eq.3.25 and Eq. 3.24, we can identify the first order terms in ϵ_{nad} giving:

$$\epsilon_{nad} k_z^{(1)} = \mp \frac{i}{2} |k_l|^3 \chi_{rad} \frac{N^3}{\hat{\omega}^4} \left(\frac{N^2}{N^2 - \hat{\omega}^2} \right)^{1/2} \tag{3.30}$$

which is similar to the expression founded by Press (1981). Finally, the general expression of the wave function in the frame of the WKB approximation can be expressed as a linear combination of the progressive and regressive solutions, which can be written as follows:

$$\rho \hat{w}_l' \approx \frac{1}{|k_z^{(0)}|^{1/2}} (A_l e^{i\phi(z)+\tau(z)} + B_l e^{-i\phi(z)-\tau(z)}) \tag{3.31}$$

where A_l and B_l are two complex constants entirely determined by the excitation mechanism. The functions $\phi(z)$ and $\tau(z)$ are given by:

$$\phi(z) = \int_{z_0}^{z} |k_z^{(0)}| dz \tag{3.32}$$

and

$$\tau(z) = \frac{1}{2} |k_l|^3 \int_{z_0}^{z} \chi_{rad} \frac{N^3}{\hat{\omega}^4} \left(\frac{N^2}{N^2 - \hat{\omega}^2} \right) dz \tag{3.33}$$

representing the damping rate of the waves (z_0 is the location of the waves generation on the bottom of the convective zone). Since we have considered that $\hat{\omega} \ll N$, the latter expression for the damping wave can be written:

$$\tau(z) = \frac{1}{2} |k_l|^3 \int_{z_0}^{z} \chi_{rad} \frac{N^3}{\hat{\omega}^4} dz \tag{3.34}$$

and we conclude that prograde waves are much rapidly damped than retrograde ones. We can also note that this expression is quite similar to the expression 2.32 obtained with a simpler reasoning in the previous chapter. Once one comes back to the time space, the more general expression for the variable $\rho w'$ can therefore be expressed as follows:

$$\rho w' = \int \sum_l \frac{1}{|k_z^{(0)}|^{1/2}} (A_l \ e^{i\phi+\tau} + B_l \ e^{-i\phi-\tau}) e^{ik_l x} e^{-i\omega t} d\omega \tag{3.35}$$

Flux expression

The last step is to find the expressions for the various fluxes in Eq. 3.6c. In order to achieve this, we need to extract u' and ρ' from the system of Eq.3.15. By using Eq. 3.15a and Eq.3.18, we find the following expressions:

$$u' = -\frac{1}{\rho} \frac{k_z}{k_l} (\rho w') \tag{3.36}$$

and

$$\rho' = \frac{N^2}{g} \frac{1}{(\chi_{rad}(k_l^2 + k_z^2) - i\hat{\omega})} (\rho w') \tag{3.37}$$

However, the flux of the second term of the left hand side of Eq. 3.6c has the following expression:

$$\begin{aligned}\overline{u'w'} &= \frac{1}{L}\int_{-L/2}^{+L/2} u'w'dx \\ &\approx \int\int \sum_l \hat{u}'_l(\omega)\hat{w}'_{-l}(\omega')e^{-i(\omega+\omega')t}d\omega\ d\omega'\end{aligned} \tag{3.38}$$

which is an expression very difficult to compute. In fact, the latter double integral cannot be computed because we have not taken into account the whole wave excitation process in our previous developments. The study of the convective excitation of waves is well beyond the scope of this work and will not be tackled with in what follows. Nevertheless, we can find an analytical expression for the wave flux if we assume an equality between the spatial and temporal mean (on the characteristic time for convective excitation) as shown in appendix C. Its expression is given by:

$$\begin{aligned}\overline{u'w'} &= \frac{1}{2\pi}\int \frac{1}{\tau_c}\hat{u}'\hat{w}'^* d\omega \\ &= \frac{1}{2\pi}\frac{1}{\tau_c}\int -\frac{1}{\rho^2}\sum_l \frac{1}{k_l}|A_l|^2 e^{2\tau(z)}d\omega \\ &= -\int \sum_l F_J(l,\omega)e^{2\tau(z)}d\omega\end{aligned} \tag{3.39}$$

where τ_c is the characteristic time for the convection and F_J is the wave flux computed at $z = z_0$.

Synthesis of the important results

In the next parts of this work, we will only keep in Eq.3.6c the flux term $\overline{u'w'}$ giving the following equation and neglect the mass flux, as usually done in previous works (Kim and MacGregor 2003):

$$\partial_t(\rho\overline{U}) = -\partial_z(\rho\ \overline{u'w'}) \tag{3.40}$$

for which the linear analysis has just given this expression for the flux term:

$$\overline{u'w'} = -\int \sum_l F_J(l,\omega)e^{2\tau(z)}d\omega \tag{3.41}$$

where F_J is the wave flux computed at the top of the radiative zone where the waves are generated. Moreover, the following expression for the damping rate of waves is given by this expression:

$$\tau(z) = \frac{1}{2}|k_l|^3\int_{z_0}^{z}\chi_{rad}\frac{N^3}{\hat{\omega}^4}dz \tag{3.42}$$

where $z_0 > z$ is the vertical coordinate where waves are generated, χ_{rad} is the radiative coefficient and finally, the symbol $\hat{\omega}$ has the following expression:

$$\hat{\omega} = (\omega - k_l\overline{U}) \tag{3.43}$$

with ω the frequency of the wave. Finally, we can note that the relation 3.42 tells us that the prograde waves will be more rapidly damped that the retrograde ones (through the Doppler shifted frequency $\hat{\omega}$) meaning that retrograde waves will exchange more momentum with the mean flow.

3.4 Case 2 : Unstable shear profile

The entire developments we have done until now are only based on the fact that the perturbations u', w', p' and ρ' are small compared to the corresponding mean quantities for any time t. This hypothesis is true since we have considered IGW, but becomes invalid when the amplitude of the small fluctuations increases in function of time. As a matter of fact, there is an important quantity that we have intentionally forgotten in the linear analysis. This quantity is the vertical variation of the mean flow itself, or in other words, its vertical gradient. In the next parts of this chapter, we are going to demonstrate the link between the vertical shearing of the mean flow and the growing or not growing of the fluctuations, as well as proposing a simple prescription to express the term $\overline{u'w'}$ seen through a stability analysis as developed in the chapter 14 of the reference book Roisin and Beckers (2010).

3.4.1 The Richardson criterion

An important quantity needed to know the degree of instability of a shear flow is the Richardson number that we are introducing here. We still consider a two dimensional flow with the same decomposition 3.1 for the quantities of the problem. The linearized [1] momentum and continuity equations are (assuming $\vec{\nabla}.\vec{v} = 0$):

$$\partial_t(u') + \overline{U}\partial_x(u') + w'\frac{d\overline{U}}{dz} = -\frac{1}{\rho_0}\partial_x p' \tag{3.44a}$$

$$\partial_t(w') + \overline{U}\partial_x(w') = -\frac{1}{\rho_0}\partial_z p' - \frac{\rho'}{\rho_0}g \tag{3.44b}$$

$$\partial_x(u') + \partial_z(w') = 0 \tag{3.44c}$$

$$\partial_t(\rho') + \overline{U}\partial_x(\rho') + w'\frac{d\overline{\rho}}{dz} = 0 \tag{3.44d}$$

with the boundary conditions : $w'(0) = w'(H) = 0$ (H is the height of the domain). The fact that the velocity field has a vanishing divergence allows us to introduce a new variable $\psi(x, z, t)$ called current function such as: $\partial_x\psi = w'$ and $\partial_z\psi = u'$ ($\psi(x, 0, t) = \psi(x, H, t) = 0$). We can show that the two components of the momentum equation can be combined and written under the following form:

$$[\partial_t + \overline{U}\partial_x]\Delta\psi - \partial_x(\psi)\frac{d^2\overline{U}}{dz^2} - \frac{g}{\rho_0}\partial_x(\rho') = 0 \tag{3.45}$$

By introducing the plane wave solutions: $\psi(x, z, t) = \Psi(z)e^{ik(x-ct)}$ and $\rho'(x, z, t) = R(z)e^{ik(x-ct)}$ (c is the phase velocity) it is possible to write, thanks to the continuity equation, the following Taylor-Goldstein equation:

$$(\overline{U} - c)\left[\frac{d^2\Psi}{dz^2} - k^2\Psi\right] + \left[\frac{N^2}{(\overline{U} - c)} - \frac{d^2\overline{U}}{dz^2}\right]\Psi = 0 \tag{3.46}$$

with $\Psi(0) = \Psi(H) = 0$. We can note that if c and Ψ are solutions of the latter equation, then c^* and Ψ^* are also solutions (thanks to the properties of the complex conjugate operator on the derivative).

[1] This is the only step for which we have to linearize the equations and what follows is a linear stability analysis.

Let us consider now that $\Psi(z)$ can be decomposed as : $\Psi = \sqrt{\overline{U} - c}\ \phi$. The Eq. 3.46 can therefore be written:

$$\frac{d}{dz}\left[(\overline{U}-c)\frac{d\phi}{dz}\right] - \left[k^2(\overline{U}-c) + \frac{1}{2}\frac{d^2\overline{U}}{dz^2} + \frac{1}{(\overline{U}-c)}\left\{\frac{1}{4}\left(\frac{d\overline{U}}{dz}\right)^2 - N^2\right\}\right]\phi = 0 \tag{3.47}$$

with $\phi(0) = \phi(H) = 0$. Multiplying the latter equation by ϕ^*, integrating over the whole domain and assuming a decomposition for the velocity c: $c = c_r + ic_i$, the imaginary part of the result is given by:

$$c_i \int_0^H \left(N^2 - \frac{1}{4}\left(\frac{d\overline{U}}{dz}\right)^2\right)\frac{|\phi|^2}{|\overline{U}-c|^2}dz = -c_i \int_0^H \left(\left|\frac{d\phi}{dz}\right|^2 + k^2|\phi|^2\right)dz \tag{3.48}$$

We directly see that if $N^2 - \frac{1}{4}\left(\frac{d\overline{U}}{dz}\right)^2 > 0$ everywhere in the domain, then c_i must be equal to zero to satisfy the latter relation. However, the fact that $c_i = 0$ makes the system stable. Thus, the stability criterion is given by a condition on the Richardson number (Ri) taking the form:

$$Ri = \frac{N^2}{\left(\frac{d\overline{U}}{dz}\right)^2} > \frac{1}{4} \tag{3.49}$$

where $N^2 = -\frac{g}{\rho_0}\frac{d\overline{\rho}}{dz}$ and $M^2 \equiv \left(\frac{d\overline{U}}{dz}\right)^2$ is the Prandtl frequency. A local indicator of instability is therefore given by:

$$Ri < \frac{1}{4} \tag{3.50}$$

To conclude this discussion about the Richardson number it is interesting to consider the case of two fluids with densities and velocities ρ_1, U_1 and ρ_2, U_2 each on a height $H/2$ one above the other which by instability will be mixed into a new fluid having a density $\rho = (\rho_1 + \rho_2)/2$ and a velocity $U = (U_1 + U_2)/2$. It can be shown that the ratio between the variation of the potential energy and the variation of the kinetic energy of the flow is approximatively given by the Richardson number and is written:

$$Ri \sim \frac{gH(\rho_2 - \rho_1)}{\rho_0(U_2 - U_1)^2} \tag{3.51}$$

and the instability criterion can be interpreted as follows. If the loss in kinetic energy is at least as large as the gain in potential energy, then the flow will be unstable.

3.4.2 The eddy viscosity

Once the Richardson criterion has been established, it could be interesting to model these instabilities. In fact, these instabilities take the shape of eddies with different sizes and rotation speeds. The flow of energy goes from the larger eddies towards the smaller eddies where the viscosity starts to act (because the friction becomes as large as the inertia) and extracts the energy of the mean flow by damping these eddies. This phenomenon is called Kolmogorov cascade. The idea is to introduce an effective viscosity ν_{eff} in order to model the damping of the larger eddies (i.e. the macro-scale eddies) since it is not possible to model each eddy scales. This situation is very similar to the one of a perfect gas for which its accurate description requests the temporal evolution of a huge amount of particles and becomes immeasurably difficult to model. This is why we introduce the thermodynamical variable such as the temperature or the pressure of the gas. We can show by

a dimension analysis that the eddy scale and velocity for the macro-scale L_m, U_m and the effective viscosity ν_{eff} are related by: $\nu_{eff} \sim U_m L_m$ and thus, the Reynolds number (Re) at the macroscopic dissipation scale can be written:

$$Re \sim \frac{U_m L_m}{\nu_{eff}} \sim 1 \tag{3.52}$$

However, the Reynolds number is the ratio between the advection term and the viscosity term in the momentum equation. We can therefore say that the advection term ($\rho\ \overline{u'w'}$) of Eq. 3.40 can be modelled the same way that a viscous term. This is why we will use the following relation in order to model the advection term:

$$\overline{u'w'} = -\nu_{eff}\partial_z(\overline{U}) \tag{3.53}$$

which can be interpreted as a Fick law. Another way to see that is to write the first component of the momentum equation as follows (by keeping explicitly the viscous term):

$$\begin{aligned}
&\partial_t(\rho u) + \partial_x(\rho u u) + \partial_z(\rho u w) = \partial_x p + \eta\Delta u \\
\Leftrightarrow\ &\partial_t(\overline{\rho}\overline{U}) + \partial_z(\overline{\rho}\ \overline{u'w'}) \approx \eta\Delta\overline{U} = \eta\partial_z^2\overline{U} \\
&\overline{\rho} \to \rho \\
\Leftrightarrow\ &\partial_t(\rho\overline{U}) = \partial_z[\eta\partial_z\overline{U} - (\rho\overline{u'w'})]
\end{aligned}$$

and we directly see the meaning of the term ($\rho\overline{u'w'}$) which can be seen as a viscous term and, in some way, justifies the relation 3.53 . Finally, we mention that this term is just one component of a mathematical entity called Reynolds stress tensor having the form $R_{ij} = \rho v_i' v_j'$ where v_i' and v_j' are the ith and jth component of the velocity field $\vec{v}\,'$.

3.5 The transport equation

Once the linear and turbulent analysis have been done, we can write the final form of the transport equation. The first component of the momentum equation is written:

$$\begin{aligned}
\frac{\partial(\rho\overline{U})}{\partial t} &= -\frac{\partial}{\partial z}[(\rho\ \overline{u'w'})_{lin} + (\rho\ \overline{u'w'})_{turb}] \\
&= \frac{\partial}{\partial z}\left(\nu_{eff}\frac{\partial(\rho\overline{U})}{\partial z}\right) - \frac{\partial}{\partial z}[(\rho\ \overline{u'w'})_{lin}] \\
&= \frac{\partial}{\partial z}\left(\nu_{eff}\frac{\partial(\rho\overline{U})}{\partial z}\right) + \frac{\partial}{\partial z}\left(\frac{1}{2\pi}\frac{1}{\tau_c}\int_{-\infty}^{+\infty}\frac{1}{\rho}\sum_l\frac{1}{k_l}|A_l|^2 e^{2\tau(z,\omega)}d\omega\right)
\end{aligned}$$

If ρ (i.e. $\overline{\rho}(z)$) varies slower with z than the mean flow $\overline{U}(z,t)$, we can write:

$$\begin{aligned}
\frac{\partial\overline{U}}{\partial t} &= \frac{\partial}{\partial z}\left(\nu_{eff}\frac{\partial\overline{U}}{\partial z}\right) + \frac{\partial}{\partial z}\left(\frac{1}{2\pi}\frac{1}{\tau_c}\int_{-\infty}^{+\infty}\frac{1}{\rho^2}\sum_l\frac{1}{k_l}|A_l|^2 e^{2\tau(z,\omega)}d\omega\right) \\
&= \frac{\partial}{\partial z}\left(\nu_{eff}\frac{\partial\overline{U}}{\partial z}\right) + \frac{\partial}{\partial z}\left(\sum_l F_J(l,\omega)\int_{-\infty}^{+\infty} e^{2\tau(z,\omega)}d\omega\right)
\end{aligned}$$

Moreover, we can write the damping rate as follows:

$$\begin{aligned}\tau(z) &= \frac{\gamma_l}{2}\int_{z_0}^{z}\frac{1}{\hat{\omega}^4(z')}dz' \\ &= \frac{\gamma_l}{2}\int_{z_0}^{z}\frac{1}{\left[\omega - k_l\overline{U}(z',t)\right]^4}dz'\end{aligned}$$

and the final transport equation takes the following shape:

$$\frac{\partial\overline{U}}{\partial t} = \frac{\partial}{\partial z}\left(\nu_{eff}\frac{\partial\overline{U}}{\partial z}\right) + \frac{\partial}{\partial z}\left(\sum_l F_J\int_{-\infty}^{+\infty}\exp\left[\gamma_l\int_{z_0}^{z}\frac{1}{\left[\omega - k_l\overline{U}(z',t)\right]^4}dz'\right]d\omega\right) \tag{3.54}$$

where F_J has the dimensions of a viscosity ($m^2.s^{-1}$) and γ_l is expressed in ($m^{-1}.s^{-4}$). Making the change of variable $z \to -z$, removing the overline for the velocity and keeping only one frequency and one l, we get:

$$\boxed{\frac{\partial U(z,t)}{\partial t} = \nu_{eff}\frac{\partial^2 U(z,t)}{\partial z^2} - F_J\frac{\partial}{\partial z}\left(\exp\left[-\int_{z_0}^{z}\frac{\gamma_l}{\left[\omega - k_l U(z',t)\right]^4}dz'\right]\right)} \tag{3.55}$$

where we also have assumed that the viscosity is independent of the z coordinate. Furthermore, it is important to note that since we have considered one and only one frequency, the $d\omega$ of the integral is absorbed in the F_J which has now the dimensions of a squared velocity ($m^2.s^{-2}$). **It is very important to understand that the coordinate z in Eq. 3.55 has been inverted compared to the z in Eq. 3.54.**

This transport equation has to be completed with appropriate initial and boundary conditions. Since the higher order for the time derivative is equal to one and the higher order for the spatial derivative is two, we need one initial condition and two boundary conditions. As an initial condition, we have to impose an initial rotation profile that we can write in the following way:

$$U(z,0) = f(z) \tag{3.56}$$

where f is any analytical function of z (straight line, sine function, ...). The boundary conditions are a bit tricky to determine. We assume that we are in the frame following the location where the waves are generated. In such a case, we set the parameter z_0 to 0 (the origin of the coordinate system). We can therefore write as a first condition:

$$U(0,t) = 0. \tag{3.57}$$

Finally, we want the bottom of the SLO to be free to move. This condition is satisfied if we impose as a second condition:

$$\partial_z U(H,t) = 0 \tag{3.58}$$

It is important to mention that Eq. 3.55 is not exactly the equation describing the problem. Indeed, we have to add in the second term of the right hand side another term for the flux taking into account the retrograde waves flux (same expression than for the prograde waves flux but with a negative k_l and thus, a negative F_J). However, for the sake of simplicity, we intentionally neglect this term here and in chapter 4, but will have to take it into account when solving the whole problem in Chapter 5.

Chapter 4

Numerical resolution of the transport equation

4.1 Nondimensionalization

In order to simplify the numerical resolution of Eq. 3.55 and to have a physical interpretation of the results, we are going to nondimensionalize the problem. To do so, we will define two characteristic physical quantities which are the characteristic height L_p and time t_c as:

$$z = L_p \, \tilde{z} \tag{4.1}$$

$$t = t_c \, \tilde{t} \tag{4.2}$$

where $L_p = \omega^4/\gamma_l$ is the wave damping depth and $t_c = L_p^2/\nu_{eff} = \omega^8/(\gamma_l^2 \nu_{eff})$ is the characteristic viscous time of the problem. It is important to note that the tilde variables are dimensionless. We also define a dimensionless velocity $\tilde{U}$ as:

$$U = U_0 \, \tilde{U} \tag{4.3}$$

where U_0 is the characteristic velocity (for example, we can choose its maximum at $t = 0$). We can therefore rewrite Eq. 3.55 under the following form:

$$\left(\frac{U_0}{t_c}\right)\frac{\partial \tilde{U}(\tilde{z},\tilde{t})}{\partial \tilde{t}} = \left(\frac{\nu_{eff} U_0}{L_p^2}\right)\frac{\partial^2 \tilde{U}(\tilde{z},\tilde{t})}{\partial \tilde{z}^2} - \left(\frac{F_J}{L_p}\right)\frac{\partial}{\partial \tilde{z}}\left(\exp\left[-\int_0^{\tilde{z}} \frac{\gamma_l L_p}{[\omega - k_l U_0 \, \tilde{U}(\tilde{z}',\tilde{t})]^4} d\tilde{z}'\right]\right)$$

$$\Leftrightarrow \frac{\partial \tilde{U}(\tilde{z},\tilde{t})}{\partial \tilde{t}} = \left(\frac{\nu_{eff} t_c}{L_p^2}\right)\frac{\partial^2 \tilde{U}(\tilde{z},\tilde{t})}{\partial \tilde{z}^2} - \left(\frac{F_J t_c}{U_0 L_p}\right)\frac{\partial}{\partial \tilde{z}}\left(\exp\left[-\int_0^{\tilde{z}} \frac{\gamma_l L_p}{\omega^4}\frac{1}{[1 - \frac{k_l U_0}{\omega}\tilde{U}(\tilde{z}',\tilde{t})]^4} d\tilde{z}'\right]\right)$$

and we can express R and D as a function of the wave damping depth L_p

$$R = \frac{F_J L_p}{U_0 \nu_{eff}} = \frac{F_J \omega^4}{\gamma_l U_0 \nu_{eff}}, \tag{4.4a}$$

$$D = \frac{k_l U_0}{\omega}. \tag{4.4b}$$

We can see that R represents the ratio between the wave flux magnitude to the turbulent diffusion intensity while D is the ratio between the mean horizontal velocity to the horizontal phase velocity

of the waves. The dimensionless transport equation is thus written as:

$$\frac{\partial \tilde{U}(\tilde{z},\tilde{t})}{\partial \tilde{t}} = \frac{\partial^2 \tilde{U}(\tilde{z},\tilde{t})}{\partial \tilde{z}^2} - R\frac{\partial}{\partial \tilde{z}}\left(\exp\left[-\int_0^{\tilde{z}} \frac{1}{[1-D\tilde{U}(\tilde{z}',\tilde{t})]^4} d\tilde{z}'\right]\right)$$

and making the substitutions $\tilde{z} \to z$, $\tilde{t} \to t$ and $\tilde{U} \to U$ (to simplify the reading), we finally obtain the following dimensionless transport equation:

$$\boxed{\frac{\partial U(z,t)}{\partial t} = \frac{\partial^2 U(z,t)}{\partial z^2} - R\frac{\partial}{\partial z}\left(\exp\left[-\int_0^{z} \frac{1}{[1-DU(z',t)]^4} dz'\right]\right)} \tag{4.5}$$

where the only parameters of the problem are R and D, which will simplify a bit the code implementation as well as the physical interpretation of the results.

4.2 Code Implementation

4.2.1 Discretization

In order to solve the problem numerically, we have to use a scheme of integration based on the discretization of the wave flux as well as the partial derivatives of the dimensionless transport equation 4.5. The discretization of the temporal step Δt and spatial step Δz can be done in the following way (see, e.g., Press et al. 2007, for a reference book).

- Discretization:

$$\begin{aligned} \alpha &= M\Delta t \\ \beta &= N\Delta z \\ U(z,t) = U(n\Delta z, m\Delta t) &\to U_n^m \\ m &= 0,1,2,...,M \\ n &= 0,1,2,...,N \end{aligned} \tag{4.6}$$

  where m and n are referred to the time and space, respectively, and where α and β are real numbers of the order of unity (they are generally chosen as equal to one in the following). Moreover, the '$\to$' means the transition between the continue physical variable and its discretized version.

- Initial condition:

$$\begin{aligned} U(z,0) &= \frac{f(z)}{U_0} \\ \to U_n^0 &= \frac{f(\Delta z)}{U_0} \\ &\text{(f is an arbitrary function)} \end{aligned} \tag{4.7}$$

- Boundary conditions:

$$\begin{aligned} U(0,t) = 0 &\to U_0^m = 0 \\ \partial_z(U)(H,t) = 0 &\to U_{N-1}^m = U_N^m \end{aligned} \tag{4.8}$$

- Time derivative:

$$\begin{aligned}\frac{\partial U(z,t)}{\partial t} &= \lim_{\Delta t\to 0}\frac{U(z,t+\Delta t)-U(z,t)}{\Delta t}\\ &\to \frac{1}{\Delta t}(U_n^{m+1}-U_n^m)\ \text{(Forward)}\end{aligned} \tag{4.9}$$

- First spatial derivative:

$$\begin{aligned}\frac{\partial U(z,t)}{\partial z} &= \lim_{\Delta z\to 0}\frac{U(z+\Delta z,t)-U(z,t)}{\Delta z} \to \frac{1}{\Delta z}(U_{n+1}^m-U_n^m)\ \text{(Forward)}\\ &= \lim_{\Delta z\to 0}\frac{U(z,t)-U(z-\Delta z,t)}{\Delta z} \to \frac{1}{\Delta z}(U_n^m-U_{n-1}^m)\ \text{(Backward)}\end{aligned} \tag{4.10}$$

- Second spatial derivative:

$$\begin{aligned}\frac{\partial^2 U(z,t)}{\partial z^2} &= \lim_{\Delta z\to 0}\frac{1}{(\Delta z)^2}[U(z+\Delta z,t)-2U(z,t)+U(z-\Delta z,t)]\\ &\to \frac{1}{(\Delta z)^2}[U_{n+1}^m-2U_n^m+U_{n-1}^m]\ \text{(Centered)}\end{aligned} \tag{4.11}$$

  In the following, we will use the forward scheme for the partial time derivative and the centered scheme for the second partial spatial derivative because we can show that in such case the error is proportional to Δz^2. The second spatial derivative is obtained by applying successfully a forward and a backward scheme on the first spatial derivative.

- Matrix form:

$$\begin{pmatrix} U_0^0 & U_1^0 & U_2^0 & ... & U_n^0 & ... & U_{N-2}^0 & U_{N-1}^0 & U_N^0\\ U_0^1 & & & & & & & & U_N^1\\ U_0^2 & & & & & & & & U_N^2\\ . & & & & & & & & .\\ . & & & & & & & & .\\ U_0^m & & & & & & & & U_N^m\\ . & & & & & & & & .\\ . & & & & & & & & .\\ U_0^{M-2} & & & & & & & & U_N^{M-2}\\ U_0^{M-1} & & & & & & & & U_N^{M-1}\\ U_0^M & & & & & & & & U_N^M \end{pmatrix} \tag{4.12}$$

This matrix is a $(M+1)\times(N+1)$ matrix representing the whole spatial and temporal domain of integration. The first line represents the initial condition ($U_n^0 = f(\Delta z)/U_0$) and the first column represents the boundary condition ($U_0^m = 0$) at the top of the radiative zone where the waves are generated. The second boundary condition ($U_N^m = U_{N-1}^m$) will be satisfied during the integration. Indeed, for each temporal step, we will explicitly impose that $U_N^m = U_{N-1}^m$. The algorithm will consist in computing what is left of the matrix in order to know the flow for each temporal and spatial step. An extract of the code is available in appendix D.

4.2.2 Integration scheme

The integration scheme is given by the discretized version of Eq. 4.5. Its expression is the following:

$$\frac{1}{\Delta t}(U_n^{m+1} - U_n^m) = \frac{1}{\Delta z^2}(U_{n+1}^m - 2U_n^m + U_{n-1}^m) + \frac{R}{(1 - DU_n^m)^4} \exp\left(-\int_0^z \frac{1}{(1 - DU(z', t))^4} dz'\right) \tag{4.13}$$

where we have already derived the expression of the wave flux and the integral is computed thanks to the trapeze method whose expression is given by:

$$\int_0^z \frac{1}{(1 - DU(z', t))^4} dz' \to \sum_{j=0}^{n-1} \frac{\Delta z}{2} \left[\frac{1}{(1 - DU_j^m)^4} + \frac{1}{(1 - DU_{j+1}^m)^4}\right].$$

In the following, we will write the prograde wave flux term as $(F_{pW})_n^m$. It is interesting to note that the only term in Eq. 4.13 allowing us to compute the next temporal step of the flow is U_n^{m+1}, meaning that we are using an explicit method[1] to solve the problem. As a matter of fact, we can rewrite the latter equation as:

$$U_n^{m+1} = (1 - 2\alpha)U_n^m + \alpha(U_{n+1}^m + U_{n-1}^m) - \Delta t \frac{1}{(1 - DU_n^m)^4}(F_{WP})_n^m \tag{4.14}$$

where $\alpha = \frac{\Delta t}{\Delta z^2}$. We directly see in Eq. 4.14 that the line $m + 1$ of the matrix 4.12 is computed on the basis of the line m (the previous one). It is then clear that implementing a first loop going from $m = 0$ to $m = M$ containing a second loop going from $n = 1$ to $n = N - 1$ will allow us to compute the entire matrix 4.12.

4.3 Numerical stability

A significant problem for the numerical resolution of transport equations is the stability of the integration regarding our choice for the temporal and spatial steps. Indeed, in a general way, we can write a diffusion equation under the following form:

$$\frac{\partial F(x, t)}{\partial t} = \kappa \frac{\partial^2 F(x, t)}{\partial x^2} \tag{4.15}$$

which gives under its discretized form (following the same notations as in the previous section):

$$F_n^{m+1} = (1 - 2\sigma)F_n^m + \sigma(F_{n+1}^m + F_{n-1}^m) \tag{4.16}$$

where $\sigma = \frac{\kappa \Delta t}{\Delta z^2}$. The stability of the numerical integration depends on the ratio σ as we are going to show now. Using the Fourier decomposition into eigen modes, we can write:

$$F_n^m = \sum_k f_k^m e^{ikn\Delta x} \tag{4.17}$$

where k is the wave number of the mode f_k^m. We can see that from one temporal step to another, we have:

$$f_k^{m+1} = g(k) f_k^m$$

[1] Another method for solving differential and partial differential equations is the implicit method involving the resolution of a system of equations for each time step. This is why implicit methods are more complex that explicit ones.

for which the stability criterion is given by:

$$||g(k)|| < 1 \tag{4.18}$$

where the expression of $g(k)$ is found by inserting Eq. 4.17 in Eq. 4.16, giving:

$$\begin{aligned}
\sum_k f_k^{m+1} e^{ikn\Delta x} &= (1-2\sigma)\sum_k f_k^m e^{ikn\Delta x} + \sigma \sum_k \left[f_k^m e^{ik(n+1)\Delta x} + f_k^m e^{ik(n-1)\Delta x} \right] \\
&= (1-2\sigma)\sum_k f_k^m e^{ikn\Delta x} + \sigma \sum_k \left[f_k^m \left(eik\Delta x + e^{-ik\Delta x} \right) e^{ikn\Delta x} \right] \\
&= (1-2\sigma)\sum_k f_k^m e^{ikn\Delta x} + 2\sigma \sum_k \left[f_k^m \cos(k\Delta x) e^{ikn\Delta x} \right]
\end{aligned}$$

and projecting this expression on one mode k we get:

$$\begin{aligned}
f_k^{m+1} &= (1-2\sigma) f_k^m + 2\sigma f_k^m \cos(k\Delta x) \\
&= [1 - 2\sigma + 2\sigma\cos(k\Delta x)] f_k^m \\
&= [1 - 2\sigma(1 - \cos(k\Delta x))] f_k^m \\
&= \left[1 - 4\sigma \sin^2\left(\frac{k\Delta x}{2} \right) \right] f_k^m
\end{aligned}$$

and since $g(k) = \frac{f_k^{m+1}}{f_k^m}$, we obtain:

$$g(k) = 1 - 4\sigma \sin^2\left(\frac{k\Delta x}{2} \right) \tag{4.19}$$

and the condition 4.18 leads directly to:

$$\sigma = \frac{\kappa \Delta t}{\Delta z^2} < \frac{1}{2}. \tag{4.20}$$

This condition means that the chosen time step Δt must be at least smaller than half of the characteristic diffusion time $\Delta z^2/\kappa$ over a mesh space of Δz, which can be seen as the characteristic time needed for the information transmission. If we consider Eq. 4.14, we clearly see that it has not exactly the same shape as Eq. 4.16 because we see another term coming from the wave flux. Nevertheless, this wave flux term is highly non-linear and the decomposition 4.17 does not work anymore. Neglecting the last term of the right hand side in Eq. 4.14 allows us to find the following stability condition:

$$\alpha = \frac{\Delta t}{\Delta z^2} < \frac{1}{2}. \tag{4.21}$$

Experimentally, we find that the real stability condition is very close to this value meaning that the flux term is stable under the integration scheme we have chosen. This condition imposes quite strong constraints on the temporal step since the spatial step is squared. For instance, if we want a precision of 0.01 for the spatial step, then we must have at least a precision of $0.01^2/2 = 1/20000 = 0.00005$ meaning that the dimensions of the matrix will be $101 \times 20001 = 2020101$. In other words, if we want a spatial step two times more precise, we have to divide the temporal step by a factor four. In a more general way, if we want a spatial step $\mathcal{N}$ times more precise, we have to divide the temporal step by a factor $\mathcal{N}^2$.

Chapter 5

Analysis of the results

5.1 Occurrence conditions and detailed visualization

As we have just seen in the previous chapter, the problem of the SLO can be reduced to only two control parameters. Nevertheless, there is an ambiguity concerning the characteristic velocity U_0 defined in Eq. 4.3. Indeed, this characteristic velocity seems completely arbitrary. However, we can show that there is a judicious choice to make on this velocity. Indeed, the prograde wave flux is written:

$$F_{WP} = -R \exp\left[-\int_0^z \frac{1}{(1-DU(z,t))^4} dz'\right] \tag{5.1}$$

and considering a positive linear profile as initial condition, since $D = k_l U_0/\omega = U_0/v_{\phi,h}$ (where $v_{\phi,h}$ is the horizontal phase velocity of waves, see Sect. 2.3), we can see that the prograde wave flux will be negligible when $U_0 U = v_{\phi,h}$ (i.e., the prograde waves will be rapidly damped compared to retrograde waves and will accelerate the rotation profile until $UU_0 = v_{\phi,h}$). We can thus consider that $U_{max} U_0 = v_{\phi,h}$. Hence, as a characteristic velocity we can choose $U_0 = v_{\phi,h}$. We will see in the following that this choice is judicious and physically-grounded to scale the problem. Moreover, adopting this velocity for U_0 allows us to reduce the problem to only one parameter (R) since D is equal to one for any value of k_l and ω. It is important to note that making this choice for D includes each physical parameter ($F_J, \omega, \nu_{eff}, \gamma_l$ and k_l) in R. Indeed, R is now written:

$$R = \frac{F_J \omega^4}{\gamma_l \nu_{eff} U_0} = \frac{F_J \omega^3 k_l}{\gamma_l \nu_{eff}}. \tag{5.2}$$

Now that the problem is reduced to only one control parameter, we can explore several regimes.

5.1.1 The diffusion regime ($R \leq 1$)

When we consider that $R \leq 1$, it is the diffusion that dominates and there is no SLO. As a matter of fact, as we can see in the figure 5.1, we start from an initial rotation profile (e.g., for instance, an hyperbolic tangent function) with a control parameter R equal to 0.5 and we clearly see the large contribution of the diffusion term compared to the contribution of the wave flux terms. The question is: why can the SLO not be established? The answer is that the wave flux terms are still acting but the diffusion is so efficient that it rapidly smoothes the rotation profile and makes U tend towards zero for all z. Therefore, when U is equal to zero for all z, the two wave fluxes have

opposite values and cancel each other out and there is no possibility for the SLO to be established.

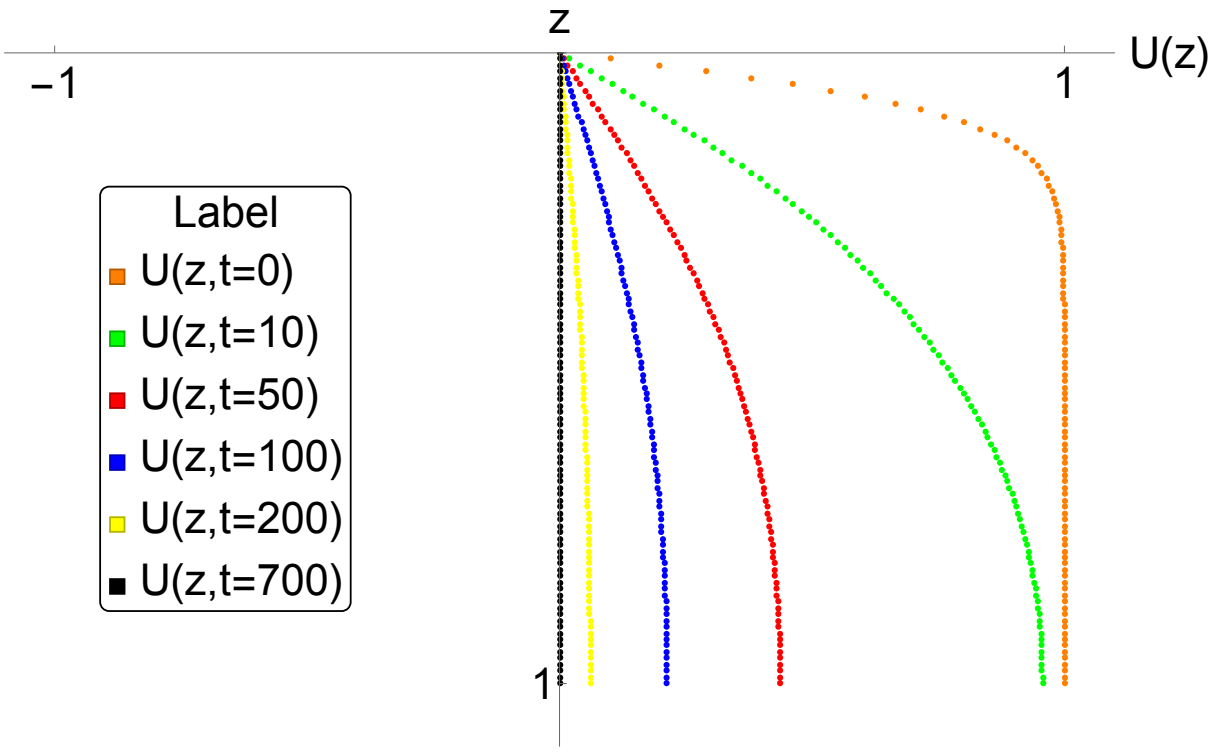

Figure 5.1 – Representation of the diffusion phenomenon of the rotation profile U as a function of the depth at different times ($R = 0.5$).

5.1.2 The SLO regime ($R > 1$)

If we consider regimes with $R > 1$, then a SLO can be established because the competition between the wave fluxes and the diffusion phenomenon is no more dominated by the latter. An example of a SLO (computed for $R = 20$[1]) is given in the figures 5.2 and 5.3. As you can see in these figures, we start from an initial linear rotation profile ($t = (0)$). Then, an equilibrium is established between the gradient of the prograde wave flux ($\partial_z F_P$) and the diffusion term ($\partial_z^2 U$) taking the shape of a 'hook' ($t = (172)$). After that, in the deeper layers, the gradient of the retrograde wave flux ($\partial_z F_R$) acts and tends to decelerate the rotation profile thus creating a second 'hook' but in the opposite direction ($t = (198)$) until the shear between the two 'hooks' becomes sufficiently strong to make the second 'hook' diffuse (a kind of wavefront is created) towards the top layers ($t = (210)$). After that, a new equilibrium between the gradient of the retrograde wave flux and the diffusion term is established and the whole process repeats in a symmetrical way to come back to the initial equilibrium between the gradient of the prograde wave flux and the diffusion term ($t = (234) - (405)$). All these steps constitute the so-called Shear Layer Oscillation and, in the following sections, we will study its behaviour and properties as a function of R.

[1]Two additional videos showing the SLO as well as the wave fluxes for $R = 5$ and $R = 20$ are available as supporting documents (SLO_R=5.avi and SLO_R=20.avi).

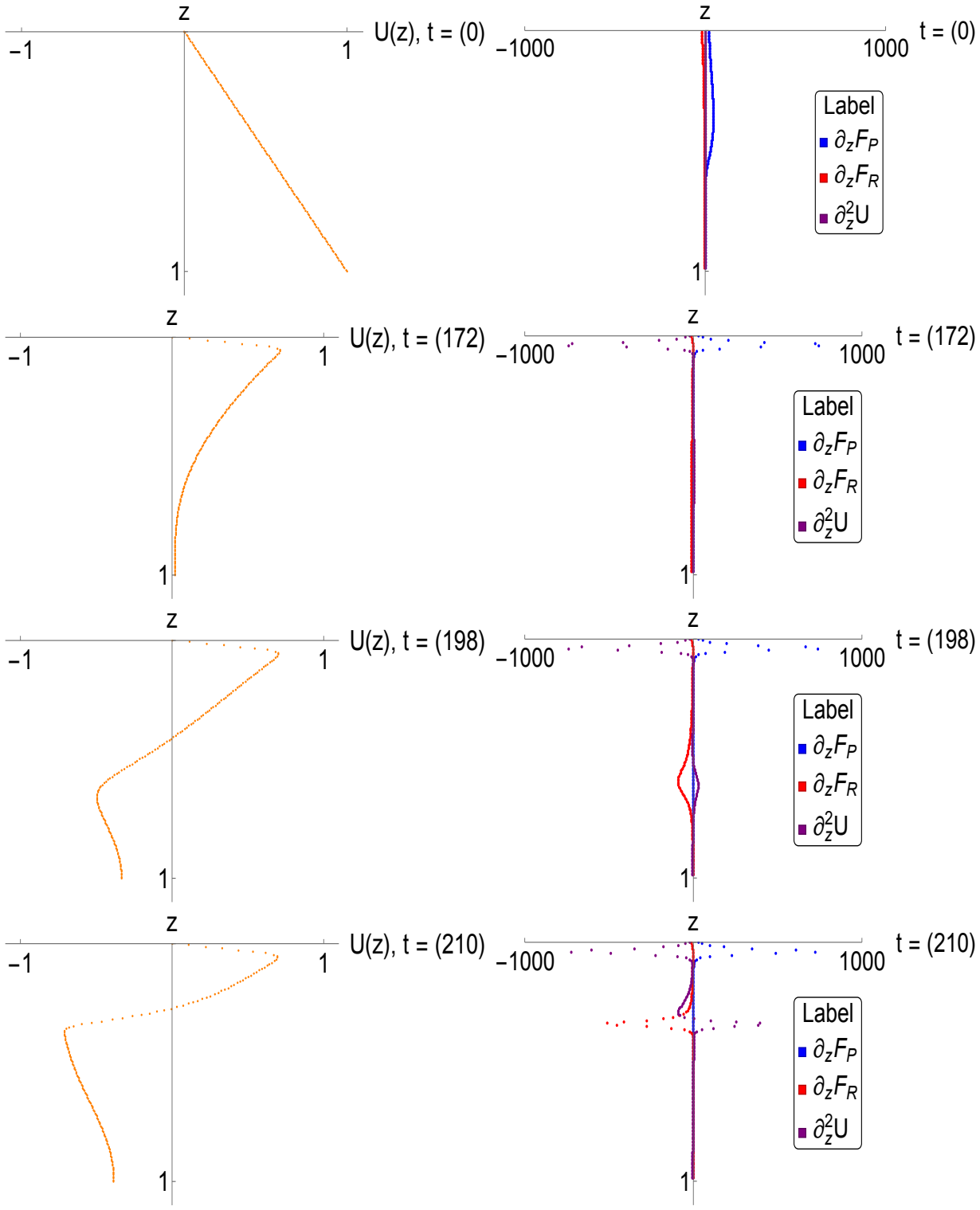

Figure 5.2 – Representation of one cycle of the SLO (computed for $R = 20$) and the different terms of the rhs in Eq.4.5. The abscissa axis (value of the rotation profile) is located at the boundary between the bottom of the convective zone (above the axis) and the beginning of the radiative zone (bellow the axis).

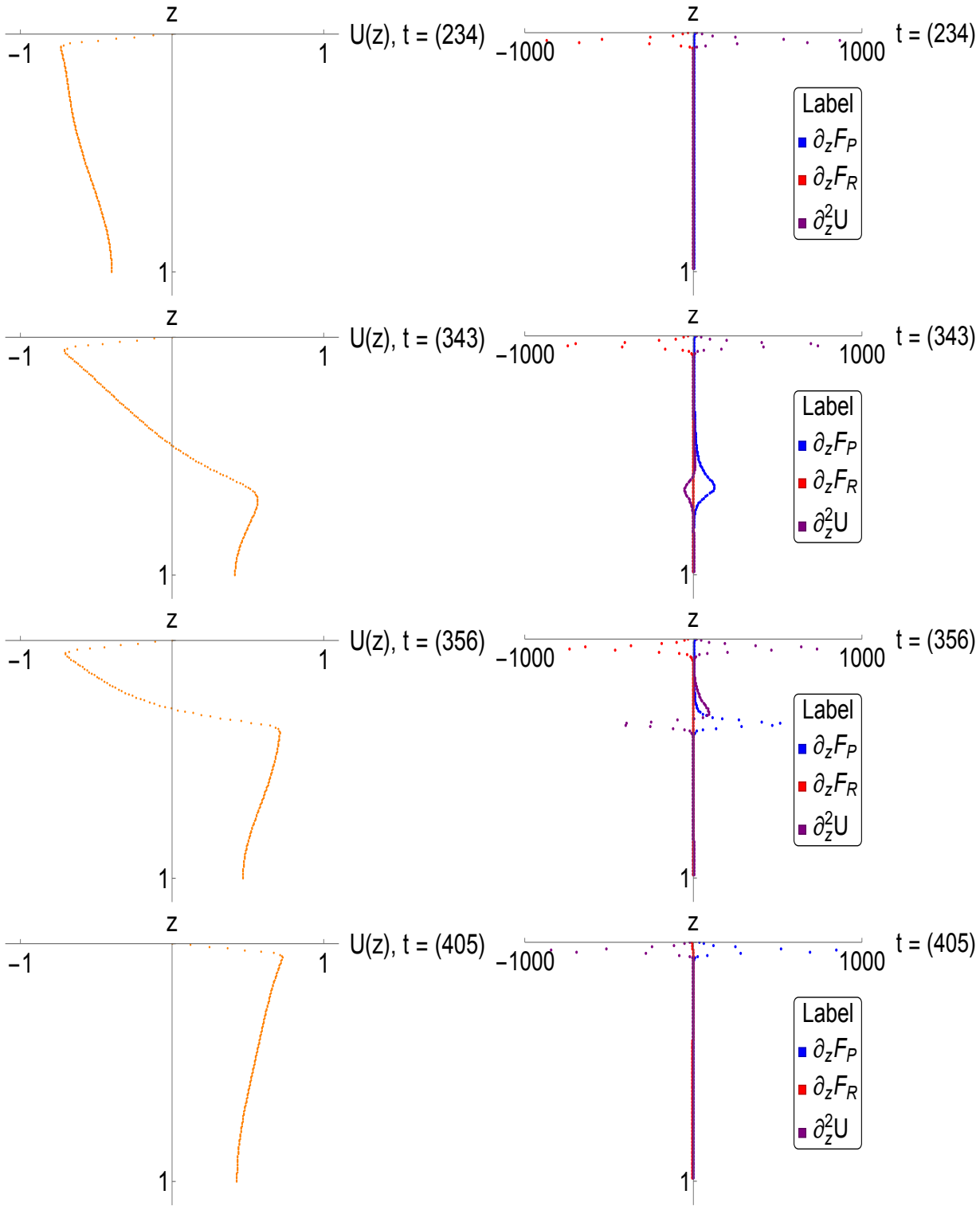

Figure 5.3 – See figure 5.2 for more details.

5.2 Oscillations as a function of the depth

The figure 5.4 shows the evolution as a function of time of a point located at three different depths. First, the depth $z = (0.06)$ corresponds to the location of the upper hook created by the balance between the gradient of the prograde wave flux and the diffusion term. At this depth, we can see that the oscillations are sharp. This is due to the action of prograde waves. Second, the depth $z = (0.5)$ is interesting to observe because the passage of the wavefront occurs around this depth and is clearly visible in the figure. In addition, we can observe that the oscillations are smoother than for the hook. Finally, the depth $z = (1.)$ corresponds to the bottom of the SLO and we can see that the oscillations look like a sine function (the smoothest oscillations). We can say that the deeper we go, the smoother the oscillations are. This is due to the fact that the dynamics of the upper layers is created by the prograde waves while the dynamics of the lower layers results from the action of the retrograde waves. The prograde waves are more rapidly damped and thus act more rapidly than the retrograde waves. Once the equilibrium with the diffusion term is established, the prograde waves have to wait the action in the deeper layers of the retrograde waves in order to create a sufficiently high shear which will 'trigger' the SLO. Hence, we see that the period of the SLO is ruled by the characteristic time over which the retrograde waves act (the kind of plateau). Moreover, we see that there is a short initial phase to make the transition from the initial velocity profile to the final velocity profile of the oscillation cycle. Once this cycle begins, we clearly see that the SLO has three main properties: amplitude, period and position of the upper hook. We observe that the amplitude is close to one, meaning that the choice for the scaling is smart. Nevertheless, we can wonder if this fact can result from the choice of the amplitude of the initial rotation profile. Finally, we can see that the oscillation cylce is of the order of a few tenths of t_c. What is the origin of this feature? What is its relation with the control parameters of the problem? These questions will be addressed in the next sections.

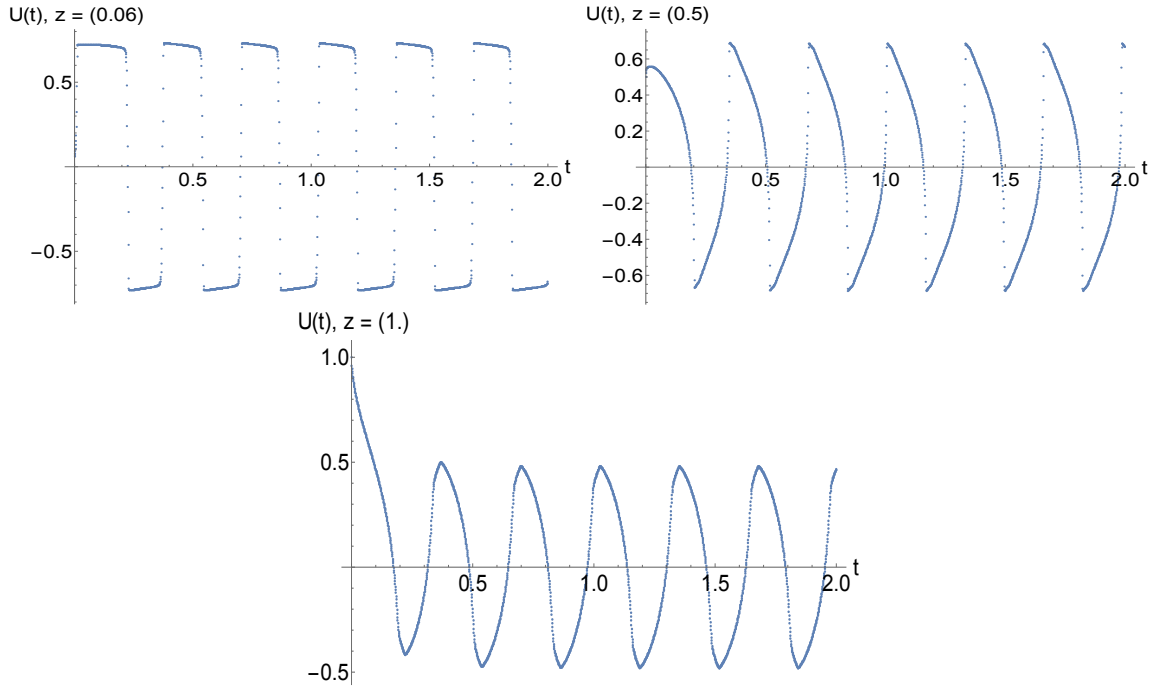

Figure 5.4 – Evolution of the oscillations over time for three different depths corresponding to the first hook ($z = (0.06)$), the middle of the SLO ($z = (0.5)$) and the bottom of the SLO ($z = (1.)$).

5.3 The impact of the initial profile on the solution

In this section, we study how the characteristics of the initial rotation profile can impact the dynamics and the properties of the SLO.

5.3.1 Impact of the amplitude

In order to show whether the amplitude of the initial rotation profile could impact or not the SLO, we have to choose an appropriate initial profile. To do so, we can choose a hyperbolic tangent. The figure 5.5 shows the results of the impact of the amplitude on the SLO. In this figure, we see that the only effect the amplitude has on the SLO is the equilibration time of the hook and that the final dimensionless amplitude of the SLO remains close to $U \sim 1$, which means close to $v_{\phi,h}$.

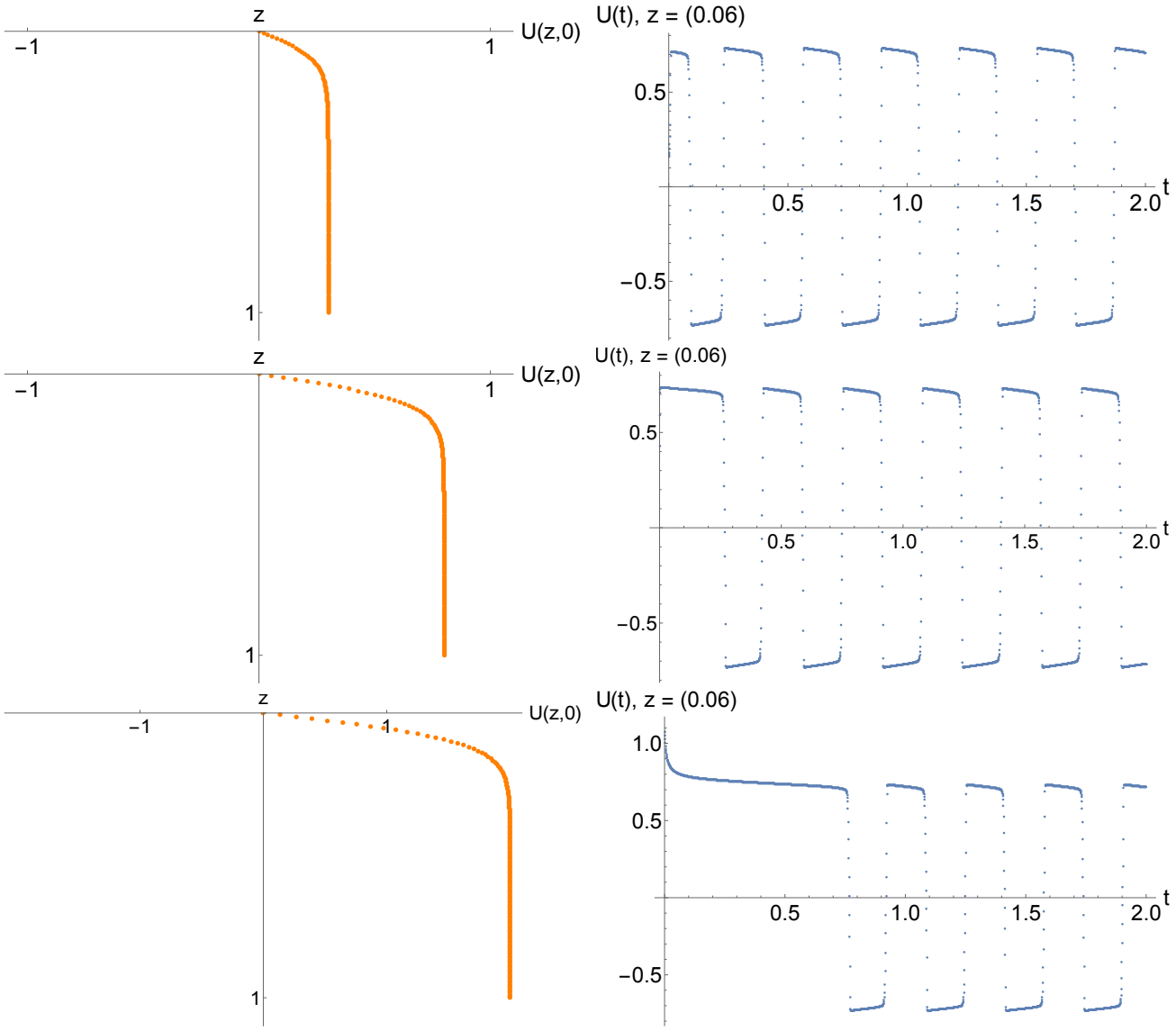

Figure 5.5 – Impact of the initial amplitude of the rotation profile on the SLO. The initial function is the following: $f(z) = A\tanh(10z)$, where $A = 0.3,\ 0.8$ and 2.

5.3.2 Impact of the shape

In order to show whether the shape of the initial profile impacts or not the SLO, we need to test several profiles given by different functions. In the figure 5.6, we can see the impact of the initial shape of the profile on the SLO. As we can observe, the behaviour of the SLO is not disrupted and the equilibration is quite fast in each case (i.e., the final cycle is obtained after one first oscillation). Once again, we can see that the amplitude is close to one, which justifies the choice of $U_{max} \approx v_{\phi,h}$ and thus the choice to put $D = 1$ in the following.

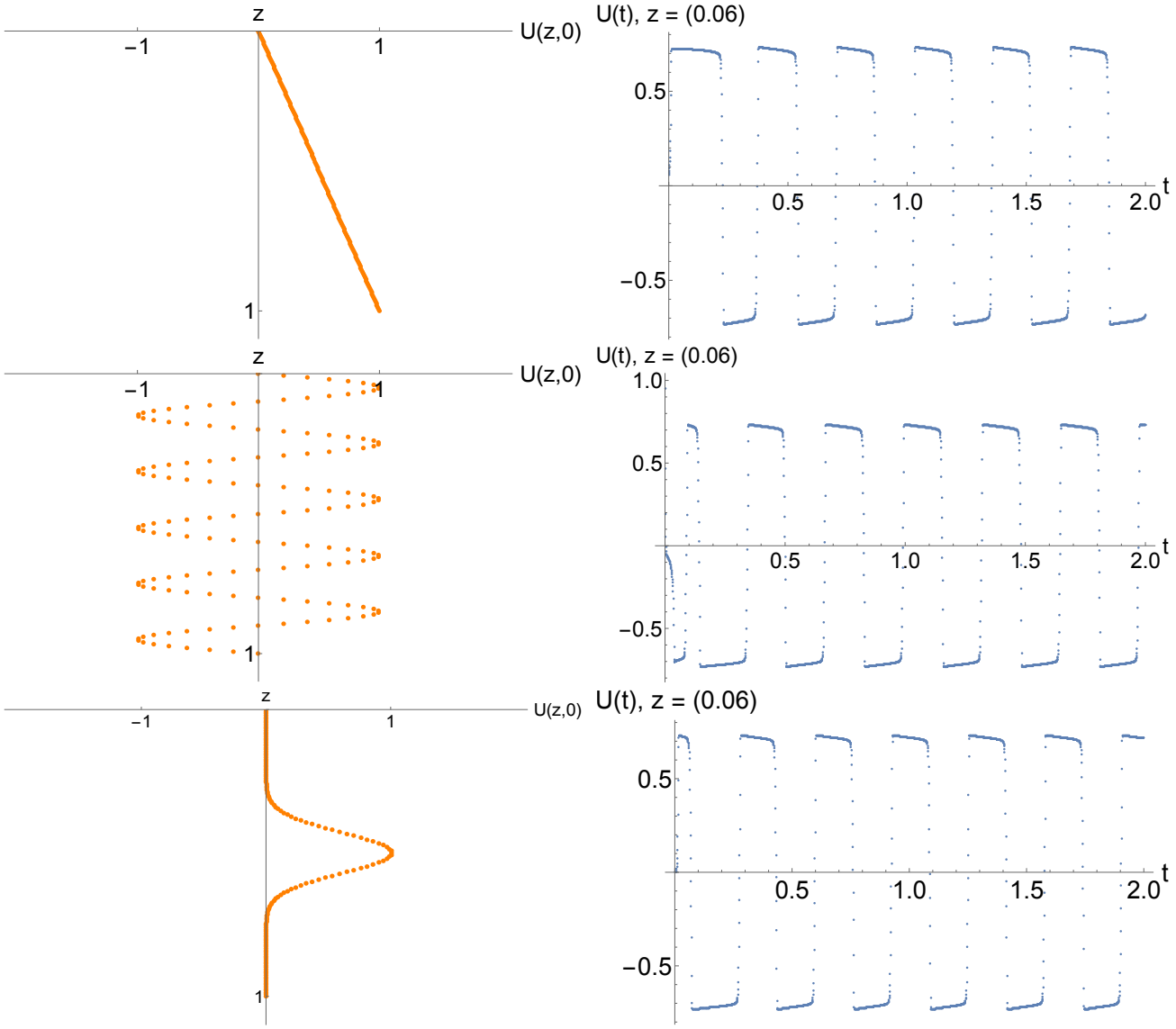

Figure 5.6 – Impact of the initial shape of the rotation profile on the SLO. The initial functions used are the following: $f(z) = z$, $f(z) = \sin(10z)$ and $f(z) = exp(-(10[z - 0.5])^2)$.

5.4 The stationary solution

In the previous sections, we have just seen that the appearance of the SLO does not depend on the conditions we impose on the initial rotation profile. Furthermore, we always observe the formation

of a hook representing the equilibrium between the gradient of the prograde wave flux and the diffusion term. Therefore, we expect that the stationary solution can describe the characteristics of the hook such as its amplitude or its occurrence depth. To do so, we can use Eq. 4.5 in which we neglect the partial time derivative (the problem becomes stationary[2]) as well as the gradient of the retrograde wave flux (negligible at the depth of the first hook). The equation describing the SLO is thus reduced to:

$$\frac{d^2U(z)}{dz^2} = R\frac{d}{dz}\left(\exp\left[-\int_0^z \frac{1}{[1-U(z')]^4}dz'\right]\right). \tag{5.3}$$

for which the variable $U(z)$ does no longer depend on the time, which makes the problem simpler. We can rewrite the latter equation under the following form:

$$\begin{aligned}\frac{d^2U(z)}{dz^2} &= -\frac{1}{[1-U(z)]^4}R\left(\exp\left[-\int_0^z \frac{1}{[1-U(z')]^4}dz'\right]\right)\\ &= \frac{1}{[1-U(z)]^4}F_{WP}(z)\end{aligned} \tag{5.4}$$

where F_{WP} is the prograde wave flux. Then, we can compute the first integral of Eq. 5.3 and we obtain:

$$\frac{dU}{dz} - K = -(R + F_{WP})$$

where $K = dU/dz\ (0)$ is an integration constant and represents the gradient of U at $z = 0$ once the hook is established. We can therefore write:

$$-F_{WP}(z) = \frac{dU}{dz} + (R - K) \tag{5.5}$$

and inserting this result in Eq. 5.4, we finally obtain:

$$\frac{d^2U}{dz^2} = -\frac{1}{[1-U]^4}\left(\frac{dU}{dz} + (R-K)\right) \tag{5.6}$$

where we impose the conditions $U(0) = 0$ and $dU(0)/dz = K$. This equation is easier to solve than Eq. 5.3 because we have got rid of the integral and we directly see that it is an ordinary differential equation. There is no analytical solution, but once again we can use numerical solution as shown in the Figure 5.7. It is very important to note that K is computed numerically by simulating the whole SLO over time and then injected in the latter equation in order to extract the stationary solution. One can clearly see that the orange curve (SLO) fits fairly well to the hook of the grey curve corresponding to the stationary solution. Hence, one can expect that studying the effects of the control parameter R on the stationary solution will give us an indication about the shape of the SLO.

[2]In the frame of any hydrodynamical problem, it is always very interesting to study the stationary case (if it is possible) in order to decompose the dynamics of the problem is several simple steps.

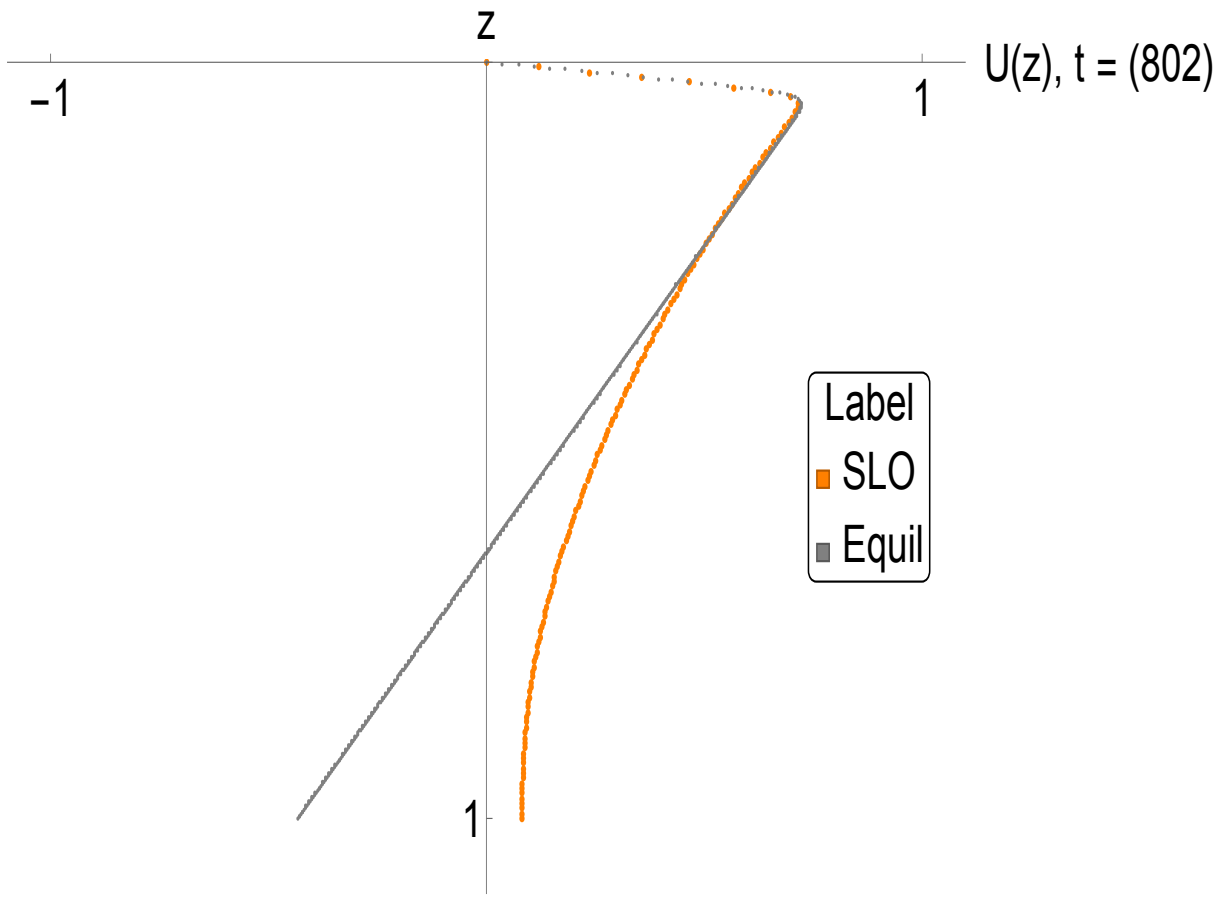

Figure 5.7 – Stationary solution (Equil) between the gradient of the prograde wave flux and the viscosity term (diffusion term). The grey curve represents the solution of Eq. 5.6 and the orange curve is the SLO computed numerically and frozen at a given time $t = (802)$.

5.5 The effects of control parameters on the SLO

In this section, we are going to find an approximative analytical expression for the main properties of the SLO which are the depth of the upper hook, its amplitude and its period. It is important to keep in mind that the main task is to understand the tendency of the SLO properties with respect to R and not to find accurate mathematical laws.

5.5.1 The effects on the shape of the hook

In this subsection, we are going to consider D as a free control parameter. At the end of this subsection, it will allow us to justify analytically the choice to put its value equal to one. Since the physical meaning of R is the competition between the waves and the flow, it is easy to determine its impact. Indeed, if we fix D and let R vary, we can see that the amplitude of the hook and the location of its depth will be proportional and inversely proportional to R, respectively as shown in the figure 5.8. This parameter is, in some way, the amplitude of the wave flux and it is not surprising to find such a dependence.

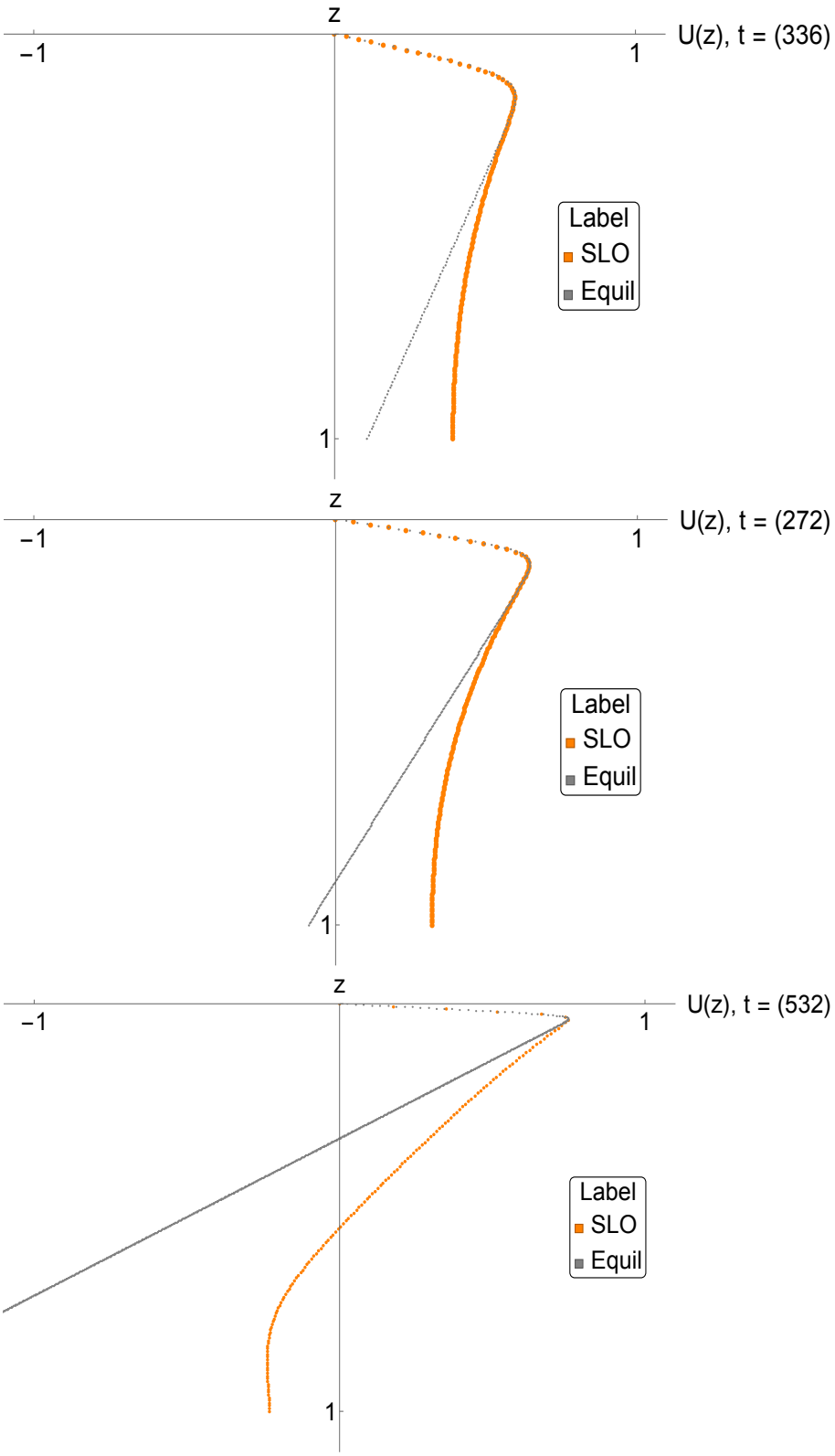

Figure 5.8 – Stationary profile of the SLO at $D = 1$ for three values of R. The top picture is for $R = 7$, the middle picture is for $R = 10$ and the bottom picture is for $R = 30$. The stationary solution is still superimposed on the SLO computed numerically and frozen at a given time.

One way to determine an analytical expression for the depth (expressed as a function of the problem parameters R and D), at which the hook appears, is to consider that at this depth the gradient of the prograde waves flux reaches its maximum (this is what we see in the simulations). Hence, we have to solve the following equation:

$$\frac{d}{dz}\left(\frac{dF_{WP}}{dz}\right) = \frac{d}{dz}\left(-\frac{R}{[1-DU(z)]^4}\exp\left[-\int_0^z \frac{1}{[1-DU(z')]^4}dz'\right]\right) = 0 \tag{5.7}$$

Developing this equation gives:

$$-R\left(4D\frac{dU}{dz}(1-DU)^{-5} - (1-DU)^{-8}\right)\exp\left[-\int_0^z \frac{1}{[1-DU(z')]^4}dz'\right] = 0$$

which is totally equivalent to write:

$$\begin{aligned} 4D\frac{dU}{dz}(1-DU)^{-5} - (1-DU)^{-8} &= 0 \\ \Leftrightarrow 4D\frac{dU}{dz} &= \frac{1}{(1-DU)^3} \end{aligned} \tag{5.8}$$

If we want to find a solution, we have to express U as a function of z. To do so, we need to make an approximation on U by considering the following expression: $U(z) \approx Kz$ because we can see in the simulations that the rotation profile seems more or less like a straight line having a slope equal to K on the considered domain below the base of the convective zone. As a matter of fact, when we reach the maximal value of the hook, $\frac{dU}{dz}(z_{Hook}) \approx 0$ and the approximation we have made on U is no more valid. Inserting this rotation profile in Eq. 5.8 allows us to find:

$$z_H \approx \frac{1}{DK}\left(1 - \frac{1}{(4DK)^{1/3}}\right), \tag{5.9}$$

corresponding to the depth where the hook, more precisely the rotation profile, reaches its maximum ($U(z_H) = U_{max}$). Moreover, we note that multiplying z_H by K allows us to find the corresponding value of the rotation speed at this depth given by the following expression:

$$U_{max} = U(z_H) \approx Kz_H \approx \frac{1}{D}\left(1 - \frac{1}{(4DK)^{1/3}}\right) \tag{5.10}$$

Moreover, we can see that the expression for z_H does not depend on the control parameter R. In fact, this is not the case because K depends itself on R and D. Indeed, if we compute approximatively Eq. 5.5 at $z = z_H$, we can write:

$$K \approx (F_{WP}(z_H) + R) \tag{5.11}$$

where we have considered that $\frac{dU}{dz}(z_H) \approx 0$ because U reaches its maximum. Developing the latter relation allows us to write:

$$K \approx R\left(1 - \exp\left[\frac{1}{3DK}\left(1 - \frac{1}{(1-DKz_H)^3}\right)\right]\right) \tag{5.12}$$

and replacing z_H by Eq. 5.9, we obtain:

$$\begin{aligned} K &\approx R\left(1 - \exp\left[\frac{1}{3DK}(1-4DK)\right]\right) \\ \Leftrightarrow R &\approx \frac{K}{\left(1 - \exp\left[\frac{1}{3DK}(1-4DK)\right]\right)} \end{aligned} \tag{5.13}$$

and if $DK \gg 1$, we can write the asymptotic behaviour:

$$R \approx \frac{K}{(1 - e^{-4/3})} \tag{5.14}$$

The latter equation gives a rather good tendency for K with respect to R. We can observe that for $D = 1$, K grows with R. Indeed, this tendency is verified with the numerical simulations as we can see in the figure 5.9. However, the error made on K is more or less the same than for z_H ($\sim 20 - 30\%$).

To conclude this subsection, we can note that the expression found for U_{max} shows an asymptotic behaviour for a fixed D. Indeed, since K grows with R, we can see that this expression tends towards $1/D$ while R tends towards infinity. This saturation tendency is also observed through the numerical simulations (as we can see in the figure 5.10) but the saturation value is overestimated with Eq. 5.10. For instance, taking 0.2 as a value for D will lead to a saturation value of 4 (with numerical simulations) against a value of 5 (with the latter approximation[3]). In fact, it is the latter equation that has led us to choose $U_0 = v_{\phi,h}$ as a characteristic velocity. Indeed, if we work with the notations of the beginning of Chapter 4, we can write:

$$\begin{aligned} \tilde{U}_{max} \sim \frac{1}{D} &\Leftrightarrow \tilde{U}_{max} = \frac{U_{max}}{U_0} \sim \frac{v_{\phi,h}}{U_0} \\ &\Leftrightarrow U_{max} \sim v_{\phi,h} \end{aligned} \tag{5.15}$$

This is why it is very interesting and physically-grounded to choose this velocity as a characteristic velocity of the problem and to put the value of D equal to one. In this way, the problem is no more degenerated and its physical interpretation becomes simpler since it is reduced to only one control parameter (R).

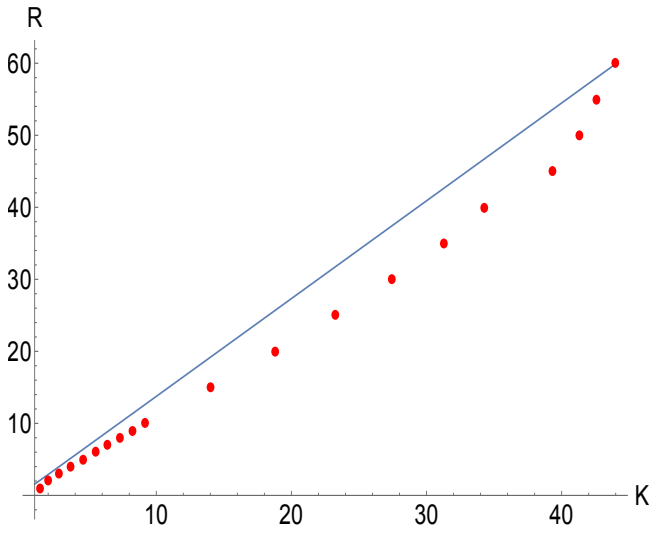

Figure 5.9 – Evolution of the control parameter R as a function of K. The blue curve represents the approximation given by Eq. 5.14 and the red dots are the real values obtained through the simulations ($D = 1$).

[3]This approximation is not perfect because we have made a strong assumption on the expression of U. We can therefore expect that a multiplicative factor could allow us to be in line with the simulations.

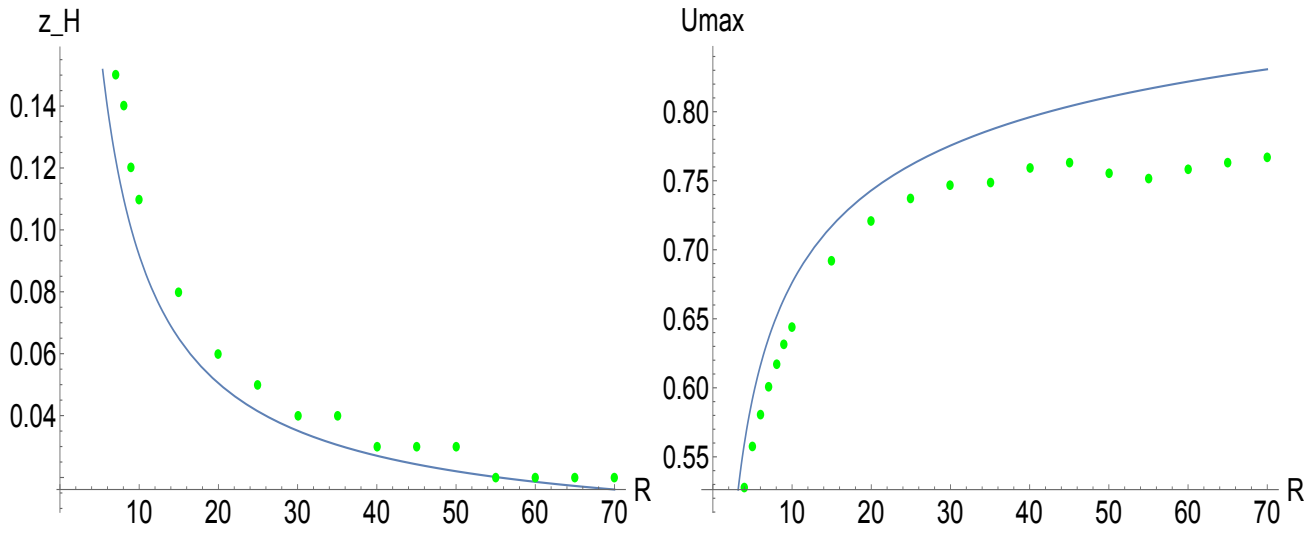

Figure 5.10 – Evolution of the depth of the hook (z_H) and the corresponding maximum value of the rotation profile (U_{max}) as a function of K. The blue curve represents the approximation given by Eq. 5.9 and the green dots are the real values obtained through the simulations ($D = 1$).

5.5.2 The effects on the period

The control parameter R has also an impact on the characteristic times of the SLO. From the simulations, we can observe that there are two main characteristic times that we are going to express analytically as a function of R.

First, we have the equilibration time (the fastest time) between the gradient of the prograde wave flux and the diffusion term. For the purpose of obtaining an order of magnitude of this time, we will use Eq. 4.5 evaluated at $z = z_H$ in which we only keep the diffusion term. The idea is to consider the characteristic time needed to allow the hook to pass on the other side. To do so, we can write:

$$\left(\frac{\partial U}{\partial t}\right)_{z_H} \approx \left(\frac{\partial^2 U}{\partial z^2}\right)_{z_H} \tag{5.16}$$

which is more or less equivalent to write in order of magnitude:

$$\frac{\Delta U_{z_H}}{\Delta t_{z_H}} \approx \left(\frac{d^2 U}{dz^2}\right)_{z_H}$$
$$\Leftrightarrow \Delta t_{z_H} \approx \frac{2U_{max}}{\left(\frac{d^2 U}{dz^2}\right)_{z_H}}$$

and using Eq. 5.6, we obtain (for $R \gg 1$):

$$|\Delta t_{z_H}| = |\Delta t_H| \approx \frac{2U_{max}}{R-K}[1-U_{max}]^4 \approx \frac{2U_{max}}{R} e^{4/3}[1-U_{max}]^4 \tag{5.17}$$

Second, we have the characteristic time for a full cycle of the SLO associated with the action of retrograde waves (the slowest time). This time can be estimated by using once again Eq. 4.5 but in this case, we are going to consider the gradient of the retrograde wave flux evaluated at $z = 1$. The idea is to consider the characteristic time needed to allow the retrograde waves to

switch the whole profile on the other side (considering a profile $U = U_{max}$). This is done once the point located at $z = 1$ has completed a full cycle. To do so, we can write the following equation:

$$\begin{aligned}\left(\frac{\partial U}{\partial t}\right)_{z=1} &\approx (\partial_z F_{WR})_{z=1} \\ &\approx R\frac{1}{[1+U_{max}]^4}\exp\left[-\int_0^1 \frac{1}{[1+U_{max}]^4}dz'\right] \\ &\approx R\frac{1}{[1+U_{max}]^4}\exp\left[-\frac{1}{[1+U_{max}]^4}\right]\end{aligned}$$

We can thus write:

$$|\Delta t_{z=1}| \approx \frac{U_{max}}{R}[1+U_{max}]^4 \exp\left[\frac{1}{[1+U_{max}]^4}\right] \tag{5.18}$$

and finally, the total period of the SLO can be written:

$$|\Delta t_{SLO}| = |\Delta t_H| + |\Delta t_{z=1}| \tag{5.19}$$

The two characteristic times we have just derived give the good tendency of the oscillation period as a function of R, as we can see in the tables 5.1 and in the figure 5.11. Indeed, this figure shows that the equilibration time Δt_H (the vertical doted lines) and the cycle time Δt_{SLO} (the blue plateau) are inversely proportional to the parameter R. Finally, the ratio between the two characteristic times gives:

$$\frac{|\Delta t_H|}{|\Delta t_{z=1}|} \approx 2e^{4/3}\frac{[1-U_{max}]^4}{[1+U_{max}]^4}\exp\left[-\frac{1}{(1+U_{max})^4}\right] \ll 1 \tag{5.20}$$

for $U_{max} \to 1$ (i.e., $R \gg 1$). In this case, the period of the SLO Δt_{SLO} is given in good approximation by $\Delta t_{z=1}$.

R	$\lvert\Delta t_H(R)\rvert$	Measurements
10	0.02	0.04
15	0.01	0.02
20	6×10^{-3}	8×10^{-3}
25	3×10^{-3}	7×10^{-3}
30	2×10^{-3}	5×10^{-3}

R	$\lvert\Delta t_{z=1}(R)\rvert$	Measurements
10	0.57	0.72
15	0.45	0.47
20	0.37	0.34
25	0.32	0.27
30	0.28	0.23

Table 5.1 – Tables showing the comparison between the two characteristic times (Δt_H and $\Delta t_{z=1}$) and the measurements made with the simulations for different values of R.

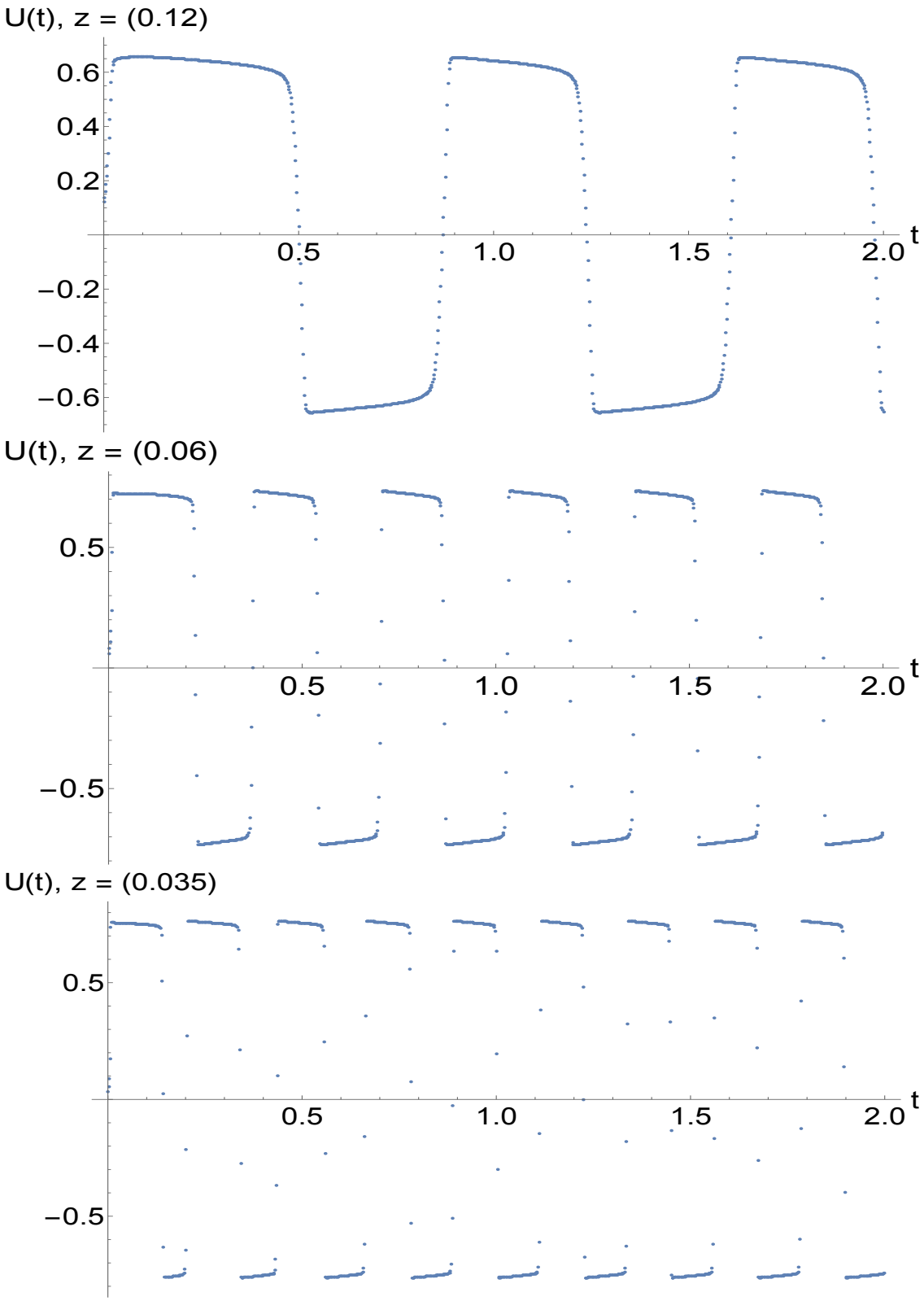

Figure 5.11 – Evolution of the SLO as a function of time at a depth corresponding to the location of the hook for $R = 10,\ 20$ and 30 from the picture of the top towards the bottom, respectively

Chapter 6

Conclusion

This work has aimed at studying the Shear Layer Oscillation (SLO) in order to give simple prescriptions to include in a stellar evolution code. To do so, we have used a small box located just below the convective zone of a Sun-like star in which we have applied the laws of hydrodynamics in a two dimensional plan parallel model. These laws have been used in the frame of the mean flow theory allowing us to split the variables between a mean quantity slowly evolving with time and another small quantity (the perturbation) quickly evolving with time (i.e., the IGW). We have obtained the transport equation describing the interaction between the mean flow and the IGW (i.e., governing the SLO). Considering only one frequency for the waves, we have shown that the dynamics of the SLO is entirely described by two control parameters R and D. R represents the ratio between the wave flux and the turbulent viscosity and D is the measure of the magnitude of the Doppler effect. Then, the dimensionless equation has been solved numerically thanks to a C++ code made entirely by us to have the full control on the problem. Thanks to simulations, we have observed that the dynamics of the SLO does not depend on the characteristics of the initial rotation profile we have used (i.e., its amplitude and its shape). Trough this outcome, we have understood that the characteristic velocity of the problem (denoted U_0) could be associated to the horizontal phase velocity of waves (denoted $v_{\phi,h}$) meaning that the control parameter D is fixed to one and that this choice is physically-grounded. In this way, the physical interpretation of the problem is simpler since the only remaining parameter is R. Therefore, the whole physics of the SLO is contained in only one control parameter allowing us to better understand the whole phenomenon. From this, two distinct regimes have been discovered. A first regime for which R is smaller that one characterizing a diffusion regime where no SLO could be established and a second regime for which we have considered R larger than one and where we could observe an oscillation of the rotation profile. Once we have observed the SLO, we have managed to characterize it in three steps. First, we have looked for a stationary solution allowing us to describe the equilibrium position between the wave fluxes and the diffusion term (the upper 'hook'). Second, we have found simple and approximative analytical relations between the properties of the hook and the control parameter R. Third, we have found approximative analytical laws governing the oscillation cycles of the SLO as a function of R. In this manner, we have carried out a first investigation which has led us to a fairly good understanding of the global characteristics of the SLO which are its amplitude, depth of the upper hook and period.

Concerning the outlooks, all this work has allowed us to have a first qualitative description of the SLO. Nonetheless, many realistic aspects have been intentionally neglected in order to make the physical interpretation, the numerical resolution as well as the analysis of the results simpler. As a matter of fact, having taken a single frequency for waves is far from being sufficient since it is known that the wave excitation mechanism generates waves with various frequencies. In addition, the effective viscosity we have used in the simulations is supposed to be a constant over the all integration domain. However, this is definitively not the case since this viscosity stems from a stability analysis and acts only where the shear of the flow reaches a large enough value to allow the growing of instabilities and thus the appearance of the turbulence. A viscosity depending on the gradient of the flow would have been a better description of the phenomenon. Finally, the whole problem has been studied through the control parameters. Nevertheless, physical conditions of Sun-like stars should be contemplated through the physical parameters of the problem in order to reproduce the physical environment inside this type of stars.

To conclude, even if in the frame of this work we could reach a rather good understanding of this oscillation of the rotation profile, a lot of researches still need to be conducted in order to obtain as much as possible a realistic model of this phenomenon, the so-called Shear Layer Oscillation in order to progressively include its effect in a stellar evolution code.

Appendix A

Basics of fluid mechanics

A.1 The continuity equation

The first equation we need to use is the continuity equation. This equation expresses the mass conservation which implies that the total derivative of the mass M in a given volume V with respect to time is equal to zero. Under its integral form, this equation is written :

$$\int\int\int_V \frac{\partial \rho(\vec{r},t)}{\partial t} dV = -\int\int_S \rho(\vec{r},t)\ \vec{v}.\vec{n}\ dS \tag{A.1}$$

where $\frac{\partial}{\partial t}$ is the partial derivative with respect to time, $\rho(\vec{r},t)$ is the density of the fluid, $\vec{v}$ is the velocity field and $\vec{n}$ is the unitary vector normal to the surface S corresponding to the volume V. This equation states that the time variation of the density is balanced by the flux of particules incoming or outgoing from the volume V through its surface S. However, under this form, this equation counts for the entire volume V but we can also write this equation under its local form thanks to the Ostrogradski Theorem[1].

$$\frac{\partial \rho(\vec{r},t)}{\partial t} + \vec{\nabla}.(\rho\vec{v}) = 0 \tag{A.2}$$

where the operator nabla $\vec{\nabla} = (\partial_x, \partial_y, \partial_z)$ is the partial derivative with respect to the space coordinates x, y, z. This is the most common form of the continuity equation. As a matter of fact, it is mere to use it in physical context because this equation is valid for any part of the fluid we want to study.

A.2 The momentum equation

The second equation we need to use is the momentum equation in the frame of the fluid mechanics. This equation comes directly from the conservation of momentum in classical mechanics but involves some additional concepts like density forces or viscous constraints. The most common form of this equation is called the Navier-Stokes equation and is written :

$$\frac{\partial \vec{v}}{\partial t} + (\vec{v}.\vec{\nabla})\vec{v} = -\frac{1}{\rho}\vec{\nabla}p + \nu\Delta\vec{v} + \vec{f_V} \tag{A.3}$$

[1]The Ostrogradski theorem allows us to change a surface integral into a volume integral with a differential operator called divergent and noted $\vec{\nabla}$. Indeed, for all vector $\vec{u}$, we have : $\int\int_S \vec{u}.\vec{n}\ dS = \int\int\int_V \vec{\nabla}.\vec{u}\ dV$

where $\vec{v}$ is the velocity field, $\vec{\nabla}$ is the nabla operator, ρ is the density, ν is the kinematic viscosity, $\Delta \equiv \vec{\nabla}^2 = (\partial_x^2 + \partial_y^2 + \partial_z^2)$ is the Laplace operator and $\vec{f_V}$ represents the density forces which has the dimensions of an acceleration. The left hand side of this equation states for the acceleration and is composed of two terms. The first term is the partial derivative of the velocity field with respect to time and is called the Eulerian derivative because it represents the fact that we measure the variation of the velocity of the flow at a given place. The second term is the advection term and added to the first one, they represent the total derivative with respect to time noted $\frac{d}{dt}$ and means that we observe a small fluid element moving in the flow. This derivative is also called Lagrangian derivative. The right hand side of the equation states for the different forces acting on the fluid through the pressure, viscosity and external forces like the gravity. As the second law of motion, this equation is a vector equation which means that there are three different components following the $\vec{e}_x, \vec{e}_y$ and $\vec{e}_z$ directions.

In some cases, it is more convenient to rewrite the Navier-Stokes equation in another form. From the combination of A.2 and A.3, we can write:

$$\frac{\partial \rho \vec{v}}{\partial t} + \vec{\nabla}.(\rho\ \vec{v} \otimes \vec{v}) = -\vec{\nabla} p + \eta \Delta \vec{v} + \rho \vec{f_V} \tag{A.4}$$

where η is the dynamic viscosity and the symbol $\otimes$ defines the tensor product ($\vec{v} \otimes \vec{v}$ is a 3×3 matrix having $v_i v_j$ as components). Indeed, if we develop (in term of its components) the left hand side of the equation A.4 we get[2] :

$$\begin{aligned}
\partial_t(\rho v_i) + \partial_j(\rho v_i v_j) &= \rho\partial_t(v_i) + v_i\partial_t(\rho) + \rho\partial_j(v_i v_j) + v_i v_j \partial_j(\rho) \\
&= \rho\partial_t(v_i) + v_i\partial_t(\rho) + \rho[v_i\partial_j(v_j) + v_j\partial_j(v_i)] + v_i v_j\partial_j(\rho) \\
&= \rho\partial_t(v_i) + v_i\partial_t(\rho) + v_i[\rho\partial_j(v_j) + v_j\partial_j(\rho)] + \rho v_j\partial_j(v_i) \\
&= \rho\partial_t(v_i) + v_i\partial_t(\rho) + v_i\partial_j(\rho v_j) + \rho v_j\partial_j(v_i)
\end{aligned}$$

Thus, in a tensor form, this expression is written:

$$\begin{aligned}
\partial_t(\rho\vec{v}) + \vec{\nabla}.(\rho\ \vec{v} \otimes \vec{v}) &= \rho(\partial_t\vec{v}) + \vec{v}(\partial_t\rho) + \vec{v}\ \vec{\nabla}.(\rho\vec{v}) + \rho(\vec{v}.\vec{\nabla})\vec{v} \\
&= \rho\left[\partial_t\vec{v} + (\vec{v}.\vec{\nabla})\vec{v}\right] + \vec{v}\underbrace{\left[\partial_t\rho + \vec{\nabla}.(\rho\vec{v})\right]}_{=0} \\
&= \rho\left[\partial_t\vec{v} + (\vec{v}.\vec{\nabla})\vec{v}\right]
\end{aligned}$$

which is similar to the first term of the Navier-Stokes equation A.3 and where the second term of the second line vanishes thanks to the continuity equation A.2.

[2]Here, $\partial_t \equiv \frac{\partial}{\partial t}$, but in general, $\partial_q \equiv \frac{\partial}{\partial q}$, with $q = x, y, z, t$

Appendix B

Gravity waves in a simple model

In order to introduce internal gravity waves, it is interesting to consider a simple case with a medium stratified in the vertical direction z with a density $\rho(z)$ and at the hydrostatic equilibrium, as shown in figure B.1. The gravitational acceleration is denoted $\vec{g} = -g\vec{e_z}$.

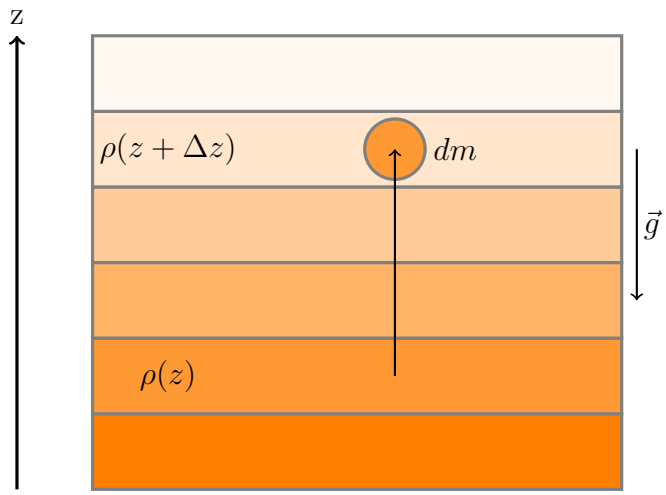

Figure B.1

We consider a small fluid element having a volume dV and a mass dm initially at a level z that we move in an other layer at $z + \Delta z$ keeping its initial density and thus its volume. At this moment, the forces acting on this fluid element is the buoyancy force $\vec{B}$ and the weight $\vec{W}$. By applying the Newton's second law ($\vec{F} = m\vec{a}$), we obtain

$$\vec{B} + \vec{W} = dm\ \vec{a} \tag{B.1}$$

and projected along the z axis, the latter equation gives

$$\rho(z + \Delta z)gdV - g\ dm = dm\frac{d^2\Delta z}{dt^2} \tag{B.2}$$

where Δz is the displacement of dm along the z axis.

Then, the mass element dm can be expressed by $dm = \rho(z)dV$ and equation B.2 becomes

$$\begin{aligned}
&\rho(z+\Delta z)gdV - g\ \rho(z)dV = \rho(z)dV\frac{d^2\Delta z}{dt^2} \\
\Leftrightarrow\ &\rho(z+\Delta z)g - g\ \rho(z) = \rho(z)\frac{d^2\Delta z}{dt^2} \\
\Leftrightarrow\ &g[\rho(z+\Delta z) - \rho(z)] = \rho(z)\frac{d^2\Delta z}{dt^2}
\end{aligned}$$

Now if we consider that $\Delta z \to 0$ then we can replace $[\rho(z+\Delta z) - \rho(z)]$ by $\frac{d\rho}{dz}\Delta z$ and we get, renaming $\Delta z = h$,

$$g\frac{d\rho}{dz}h = \rho(z)\frac{d^2h}{dt^2}$$

By renaming $\rho(z) \equiv \rho_0$ and $N^2 = -\frac{g}{\rho_0}\frac{d\rho}{dz}$ with N the Brunt-Väisälä frequency, we finally obtain

$$\frac{d^2h}{dt^2} + N^2h = 0 \tag{B.3}$$

Thera are two cases which can be envisaged. The first case is the one where $N^2 > 0 \Rightarrow \frac{d\rho}{dz} < 0$ which means that $\rho(z+\Delta z) < \rho(z)$, the acceleration of the fluid element dm points toward the negative z and equation B.3 is the harmonic oscillator equation and its solution is given by

$$h(t) = H_0\cos(Nt + \phi) \tag{B.4}$$

where H_0 is the initial amplitude of the motion and ϕ is just a phase term which is not very important here. We can clearly see in this solution that the Brunt-Väisälä frequency is the motion frequency of the fluid element dm through the stably-stratified medium. Moreover, the motion of the small fluid element dm is an oscillating motion that is only due to the buoyancy force. The second case is the one for which $N^2 < 0 \Rightarrow \frac{d\rho}{dz} > 0$ meanning that $\rho(z+\Delta z) > \rho(z)$, the acceleration points toward the positive z and the solution of equation B.3 is no longer a periodic function but a sum of exponential functions, i.e., as $A\exp(Nt) + B\exp(-Nt)$, which means that the motion is itself exponential and we can deduce that the medium is not stably-stratified in density, that is, convectively unstable.

Appendix C

Temporal mean for the fluxes

Internal gravity waves are excited in the overlying convective zone by turbulent motions of matter. The excitation process is supposed random, uniform in the horizontal direction, stationary and ergodic. The characteristic time scale associated with this process is noted τ_c. One therefore assume that over a time interval τ_c around the moment $t = 0$, the convection generates a wave packet with an amplitude $A_{\tau_c}(t)$ and a 'lifetime' of the order of τ_c (by means of correlation between the 'exciting' convection and the 'excited' waves). The stationarity implies that over an interval $k\tau_c$, with $k \gtrsim 1$, the field associated with waves can be represented by a succession of wave trains each generated over a time interval τ_c and each of them with a mean amplitude $A_{\tau_c}(t - t_i)$, where t_i represents the time shift associated with the i-th wave train with respect to the one generated at $t = 0$. We also note that the convection generates waves efficiently in the domain $\tau_\omega \lesssim \tau_c$ to which we limit ourselves.

For the following, we will define the temporal mean of a physical quantity $X(x, z, t)$ as:

$$\langle X \rangle_{k\tau_c}(x, z, t) = \frac{1}{k\tau_c} \int_{t-k\tau_c/2}^{t+k\tau_c/2} X(x, z, t')dt' \tag{C.1}$$

In order to continue, we assume that $\tau_U \gg k\tau_c \gg \tau_\omega$. Under this hypotheses, the temporal mean filters the waves effect and thus varies over large time scales τ_U. Moreover, as the excitation does not depend on the horizontal position, it makes sense to assume that the temporal mean does not depend on the variable x. By correspondence, since $\overline{X}$ varies over time scales τ_U and X' varies over $\tau_\omega \lesssim \tau_c$, one obtains:

$$\langle X \rangle_{k\tau_c} = \overline{X} \tag{C.2}$$

$$\langle X' \rangle_{k\tau_c} = \overline{X'} = 0 \tag{C.3}$$

Using the above properties and noting that for any quantity Z representing average values of perturbations or perturbation products, we can write:

$$\langle \partial_t Z \rangle_{k\tau_c} = \partial_t \langle Z \rangle_{k\tau_c} \tag{C.4}$$

$$\langle \partial_x Z \rangle_{k\tau_c} = \partial_x \langle Z \rangle_{k\tau_c} = \partial_x \overline{Z} = 0 \tag{C.5}$$

It is then possible to derive in an equivalent way the same evolution equations of the mean flow by taking this time the temporal mean for the equations of dynamics instead of the horizontal mean. Therefore, the wave angular momentum flux can be rewritten in two different ways and we have:

$$\overline{u'w'} = \langle u'w' \rangle_{k\tau_c} \tag{C.6}$$

From the properties of the exciting source (stationarity) described above, we can write:

$$\overline{u'w'} = \langle u'w' \rangle_{k\tau_c} = \frac{1}{k\tau_c} \int_{t-k\tau_c/2}^{t+k\tau_c/2} u'_{\tau_c} w'_{\tau_c} dt' \tag{C.7}$$

$$\approx k \, \frac{1}{k\tau_c} \int_{t-\tau_c/2}^{t+\tau_c/2} u'_{\tau_c} w'_{\tau_c} dt' \tag{C.8}$$

$$\approx \frac{1}{\tau_c} \int_{-\infty}^{+\infty} u'_{\tau_c} w'_{\tau_c} dt' \tag{C.9}$$

where u'_{τ_c} and w'_{τ_c} are associated with the wave train generated at $t = 0$ over a time interval τ_c with an amplitude A_{τ_c} and where we have considered that the lifetime of the wave train was of the order of τ_c allowing us to extend the integration limits to infinity. Using the Parseval-Plancherel theorem and relations derived on the chapter **??**, one find:

$$\overline{u'w'} \approx \int_{-\infty}^{+\infty} F_J(l, \omega) e^{\tau(z)} d\omega \tag{C.10}$$

where F_J is the angular momentum flux emitted at the top of the considered radiative domain.

Appendix D

Extract of the C++ code

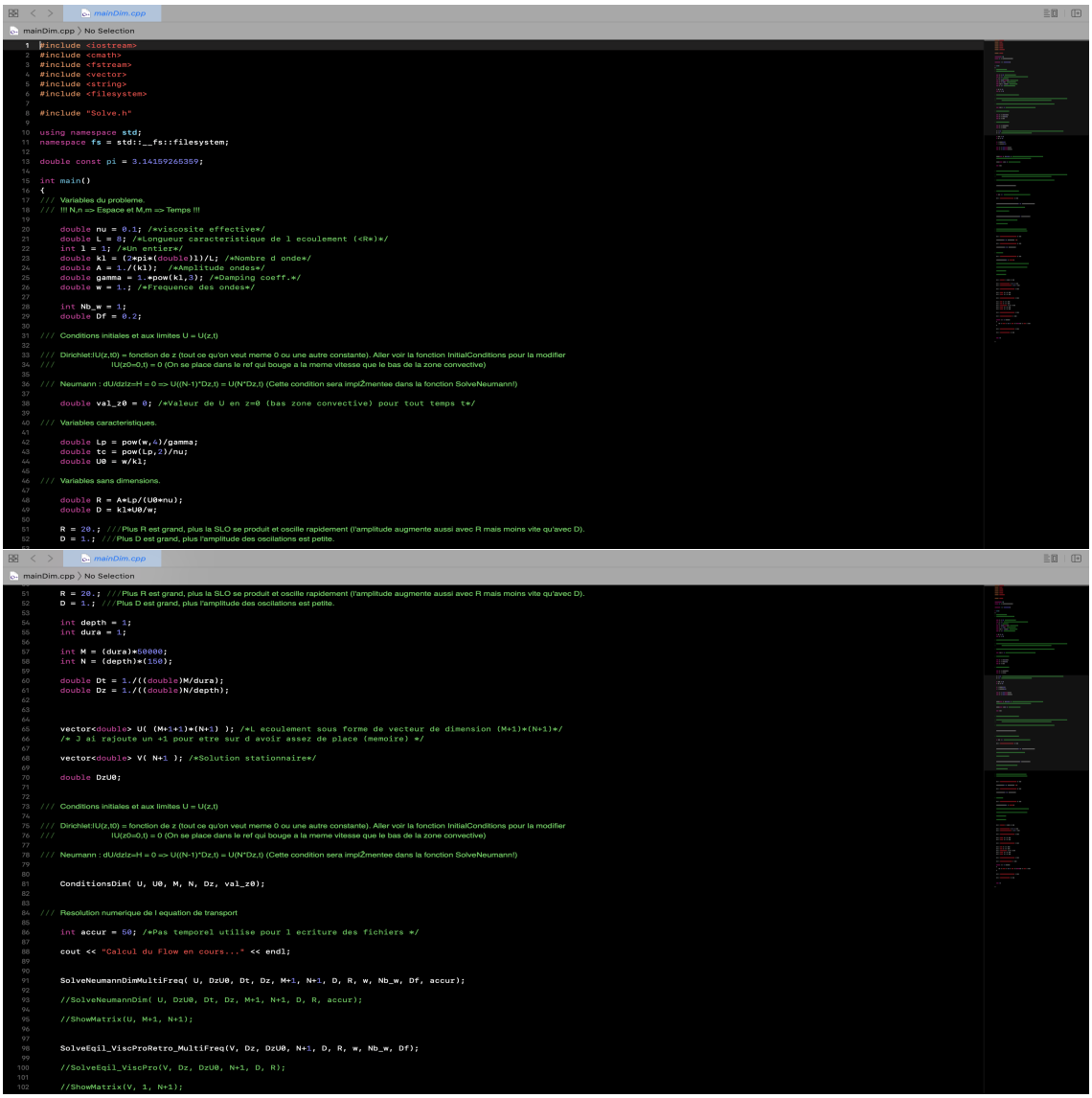

```cpp
#include <iostream>
#include <cmath>
#include <fstream>
#include <vector>
#include <string>
#include <filesystem>

#include "Solve.h"

using namespace std;
namespace fs = std::__fs::filesystem;

double const pi = 3.14159265359;

int main()
{
/// Variables du probleme.
/// !!! N,n => Espace et M,m => Temps !!!

    double nu = 0.1; /*viscosite effective*/
    double L = 8; /*Longueur caracteristique de l ecoulement (<R*)*/
    int l = 1; /*Un entier*/
    double kl = (2*pi*(double)l)/L; /*Nombre d onde*/
    double A = 1./(kl);  /*Amplitude ondes*/
    double gamma = 1.*pow(kl,3); /*Damping coeff.*/
    double w = 1.; /*Frequence des ondes*/

    int Nb_w = 1;
    double Df = 0.2;

/// Conditions initiales et aux limites U = U(z,t)

/// Dirichlet:U(z,t0) = fonction de z (tout ce qu'on veut meme 0 ou une autre constante). Aller voir la fonction InitialConditions pour la modifier
///             U(z0=0,t) = 0 (On se place dans le ref qui bouge a la meme vitesse que le bas de la zone convective)

/// Neumann : dU/dz|z=H = 0 => U((N-1)*Dz,t) = U(N*Dz,t) (Cette condition sera impl?mentee dans la fonction SolveNeumann!)

    double val_z0 = 0; /*Valeur de U en z=0 (bas zone convective) pour tout temps t*/

/// Variables caracteristiques.

    double Lp = pow(w,4)/gamma;
    double tc = pow(Lp,2)/nu;
    double U0 = w/kl;

/// Variables sans dimensions.

    double R = A*Lp/(U0*nu);
    double D = kl*U0/w;

    R = 20.; ///Plus R est grand, plus la SLO se produit et oscille rapidement (l'amplitude augmente aussi avec R mais moins vite qu'avec D).
    D = 1.; ///Plus D est grand, plus l'amplitude des oscillations est petite.

    int depth = 1;
    int dura = 1;

    int M = (dura)*50000;
    int N = (depth)*(150);

    double Dt = 1./((double)M/dura);
    double Dz = 1./((double)N/depth);


    vector<double> U( (M+1+1)*(N+1) ); /*L ecoulement sous forme de vecteur de dimension (M+1)*(N+1)*/
    /* J ai rajoute un +1 pour etre sur d avoir assez de place (memoire) */

    vector<double> V( N+1 ); /*Solution stationnaire*/

    double DzU0;


/// Conditions initiales et aux limites U = U(z,t)

/// Dirichlet:U(z,t0) = fonction de z (tout ce qu'on veut meme 0 ou une autre constante). Aller voir la fonction InitialConditions pour la modifier
///             U(z0=0,t) = 0 (On se place dans le ref qui bouge a la meme vitesse que le bas de la zone convective)

/// Neumann : dU/dz|z=H = 0 => U((N-1)*Dz,t) = U(N*Dz,t) (Cette condition sera impl?mentee dans la fonction SolveNeumann!)


    ConditionsDim( U, U0, M, N, Dz, val_z0);


/// Resolution numerique de l equation de transport

    int accur = 50; /*Pas temporel utilise pour l ecriture des fichiers */

    cout << "Calcul du Flow en cours..." << endl;


    SolveNeumannDimMultiFreq( U, DzU0, Dt, Dz, M+1, N+1, D, R, w, Nb_w, Df, accur);

    //SolveNeumannDim( U, DzU0, Dt, Dz, M+1, N+1, D, R, accur);

    //ShowMatrix(U, M+1, N+1);


    SolveEqil_ViscProRetro_MultiFreq(V, Dz, DzU0, N+1, D, R, w, Nb_w, Df);

    //SolveEqil_ViscPro(V, Dz, DzU0, N+1, D, R);

    //ShowMatrix(V, 1, N+1);
```

Figure D.1 – Extract of the C++ code made in the frame of this work. These pictures come from the main file but each function has been implemented in an other file.

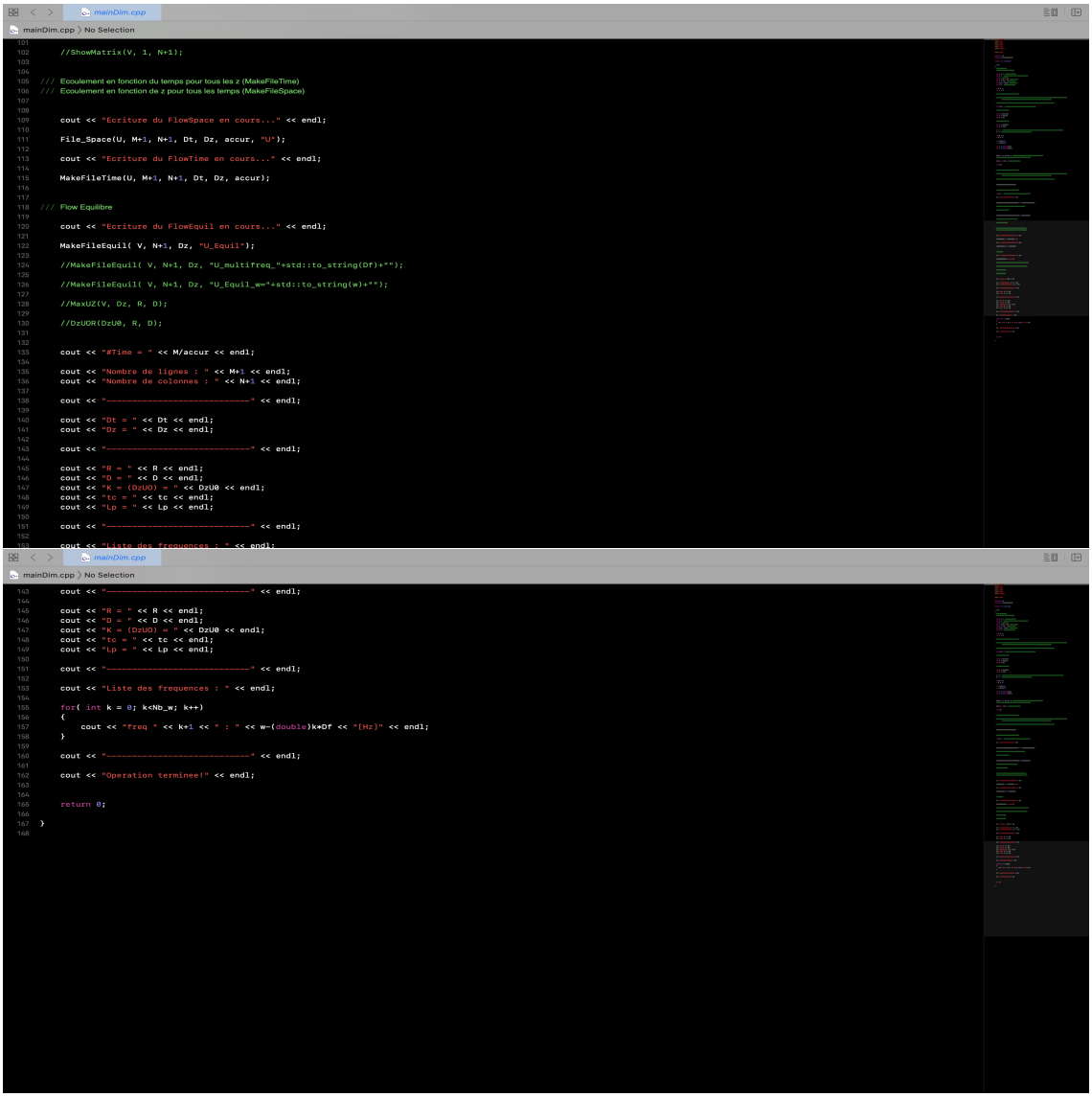

Figure D.2 – Extract of the C++ code made in the frame of this work. These pictures come from the main file but each function has been implemented in an other file.

Bibliography

Amard, L., Palacios, A., Charbonnel, C., Gallet, F., and Bouvier, J. (2016). Rotating models of young solar-type stars. Exploring braking laws and angular momentum transport processes. A&A, 587:A105.

Benomar, O., Takata, M., Shibahashi, H., Ceillier, T., and García, R. A. (2015). Nearly uniform internal rotation of solar-like main-sequence stars revealed by space-based asteroseismology and spectroscopic measurements. MNRAS, 452(3):2654–2674.

Cantiello, M., Mankovich, C., Bildsten, L., Christensen-Dalsgaard, J., and Paxton, B. (2014). Angular Momentum Transport within Evolved Low-mass Stars. ApJ, 788(1):93.

Ceillier, T., Eggenberger, P., García, R. A., and Mathis, S. (2013). Understanding angular momentum transport in red giants: the case of KIC 7341231. A&A, 555:A54.

Cowling, T. G. (1941). The non-radial oscillations of polytropic stars. MNRAS, 101:367.

Deheuvels, S., García, R. A., Chaplin, W. J., Basu, S., Antia, H. M., Appourchaux, T., Benomar, O., Davies, G. R., Elsworth, Y., Gizon, L., Goupil, M. J., Reese, D. R., Regulo, C., Schou, J., Stahn, T., Casagrande, L., Christensen-Dalsgaard, J., Fischer, D., Hekker, S., Kjeldsen, H., Mathur, S., Mosser, B., Pinsonneault, M., Valenti, J., Christiansen, J. L., Kinemuchi, K., and Mullally, F. (2012). Seismic Evidence for a Rapidly Rotating Core in a Lower-giant-branch Star Observed with Kepler. ApJ, 756(1):19.

Dintrans, B. and Rieutord, M. (2001). A comparison of the anelastic and subseismic approximations for low-frequency gravity modes in stars. MNRAS, 324(3):635–642.

Eggenberger, P. (2013). Rotation and stellar evolution. In European Physical Journal Web of Conferences, volume 43 of European Physical Journal Web of Conferences, page 01005.

Eggenberger, P., Maeder, A., and Meynet, G. (2005). Stellar evolution with rotation and magnetic fields. IV. The solar rotation profile. A&A, 440(1):L9–L12.

Fuller, J., Piro, A. L., and Jermyn, A. S. (2019). Slowing the spins of stellar cores. MNRAS, 485(3):3661–3680.

García, R. A., Turck-Chièze, S., Jiménez-Reyes, S. J., Ballot, J., Pallé, P. L., Eff-Darwich, A., Mathur, S., and Provost, J. (2007). Tracking Solar Gravity Modes: The Dynamics of the Solar Core. Science, 316(5831):1591.

Kim, E.-j. and MacGregor, K. B. (2003). Gravity Wave-driven Flows in the Solar Tachocline. II. Stationary Flows. ApJ, 588(1):645–654.

Maeder, A. (2009). Physics, Formation and Evolution of Rotating Stars.

Mosser, B., Goupil, M. J., Belkacem, K., Marques, J. P., Beck, P. G., Bloemen, S., De Ridder, J., Barban, C., Deheuvels, S., Elsworth, Y., Hekker, S., Kallinger, T., Ouazzani, R. M., Pinsonneault, M., Samadi, R., Stello, D., García, R. A., Klaus, T. C., Li, J., Mathur, S., and Morris, R. L. (2012). Spin down of the core rotation in red giants. A&A, 548:A10.

Nielsen, M. B., Gizon, L., Schunker, H., and Schou, J. (2014). Rotational splitting as a function of mode frequency for six Sun-like stars. A&A, 568:L12.

Pinçon, C., Belkacem, K., Goupil, M. J., and Marques, J. P. (2017). Can plume-induced internal gravity waves regulate the core rotation of subgiant stars? A&A, 605:A31.

Press, W., Teukolsky, S., Vetterling, W., and Flannery, B. (2007). Numerical Recipes: The Art of Scientific Computing. Cambridge University Press.

Press, W. H. (1981). Radiative and other effects from internal waves in solar and stellar interiors. ApJ, 245:286–303.

Rogers, T. M., Glatzmaier, G. A., and Jones, C. A. (2006). Numerical Simulations of Penetration and Overshoot in the Sun. ApJ, 653(1):765–773.

Roisin, B. and Beckers, J.-M. (2010). Introduction to Geophysical Fluid Dynamics : Physical and Numerical Aspects. Academic Press.

Talon, S. and Charbonnel, C. (2005). Hydrodynamical stellar models including rotation, internal gravity waves, and atomic diffusion. I. Formalism and tests on Pop I dwarfs. A&A, 440(3):981–994.

Talon, S., Kumar, P., and Zahn, J.-P. (2002). Angular Momentum Extraction by Gravity Waves in the Sun. ApJ, 574(2):L175–L178.

Zahn, J. P. (1992). Circulation and turbulence in rotating stars. A&A, 265:115–132.